SYNTHESIS OF GREEN CALCIUM SULFOALUMINATE CEMENTS USING AN INDUSTRIAL SYMBIOSIS APPROACH

A THESIS SUBMITTED TO
THE GRADUATE SCHOOL OF NATURAL AND APPLIED SCIENCES
OF
MIDDLE EAST TECHNICAL UNIVERSITY

BY

MELTEM TANGÜLER BAYRAMTAN

IN PARTIAL FULFILLMENT OF THE REQUIREMENTS
FOR
THE DEGREE OF DOCTOR OF PHILOSOPHY
IN
CIVIL ENGINEERING

SEPTEMBER 2022

Approval of the thesis:

SYNTHESIS OF GREEN CALCIUM SULFOALUMINATE CEMENTS USING AN INDUSTRIAL SYMBIOSIS APPROACH

submitted by **MELTEM TANGÜLER BAYRAMTAN** in partial fulfillment of the requirements for the degree of **Doctor of Philosophy in Civil Engineering, Middle East Technical University** by,

Prof. Dr. Halil Kalıpçılar
Dean, Graduate School of **Natural and Applied Sciences** _____

Prof. Dr. Erdem Canbay
Head of the Department, **Civil Engineering** _____

Prof. Dr. İsmail Özgür Yaman
Supervisor, **Civil Engineering, METU** _____

Examining Committee Members:

Prof. Dr. Sinan Turhan Erdoğan
Civil Engineering, METU _____

Prof. Dr. İsmail Özgür Yaman
Civil Engineering, METU _____

Assoc. Prof. Dr. Can Baran Aktaş
Civil Engineering, TED University _____

Asst. Prof. Dr. Güzide Atasoy Özcan
Civil Engineering, METU _____

Asst. Prof. Dr. Derya Över
Civil Engineering, Eskişehir Technical University _____

Date: 01.09.2022

I hereby declare that all information in this document has been obtained and presented in accordance with academic rules and ethical conduct. I also declare that, as required by these rules and conduct, I have fully cited and referenced all material and results that are not original to this work.

Name Last name : Meltem Tangüler Bayramtan

Signature :

ABSTRACT

SYNTHESIS OF GREEN CALCIUM SULFOALUMINATE CEMENTS USING AN INDUSTRIAL SYMBIOSIS APPROACH

Tangüler Bayramtan, Meltem
Doctor of Philosophy, Civil Engineering
Supervisor: Prof. Dr. İsmail Özgür Yaman

September 2022, 150 pages

Portland cement (PC), the main binder of concrete, is an energy- and emission-intensive construction material. Calcium sulfoaluminate (CSA) cement can be seen as a sustainable alternative to PC because its production uses less energy and emits less CO_2 to the environment. A potential problem facing the production of CSA cement is the cost and availability of alumina-bearing raw materials like bauxite. In this study, it was aimed to synthesize environmentally friendly CSA cement using an industrial symbiosis approach. In addition to the natural raw materials limestone and gypsum, the wastes/by-products from different industries i.e., Serox, ladle furnace slag, ceramic waste, and glass waste were used as raw materials for CSA production in the laboratory. The characterization of the CSA cements, their hydration behavior, and long-term performance were evaluated by various test techniques. As a result, three different CSA cements were successfully synthesized using at least 40% waste/by-product and it was determined that their main compounds were ye'elimite, anhydrite, merwinite, and fluorellestadite. Ettringite formation was detected as the main hydration product in all CSA cements and a

compressive strength of over 30 MPa was obtained within one day. The ettringite that was formed seemed to carbonate in the long term. In addition, using Monte Carlo simulation technique, the CO_2 emission of CSA cements were compared with that of PC, and considering all CSA cements, it was found out that the reductions up to 48% can be achieved.

Keywords: CSA Cement, Ye'elimite, Waste/By-product, Environmental Assessment, Industrial Symbiosis

ÖZ

ENDÜSTRİYEL SİMBİYOZ YAKLAŞIMI İLE YEŞİL KALSİYUM SÜLFOALUMİNAT ÇİMENTOLARININ SENTEZİ

Tangüler Bayramtan, Meltem
Doktora, İnşaat Mühendisliği
Tez Yöneticisi: Prof. Dr. İsmail Özgür Yaman

Eylül 2022, 150 sayfa

Betonun ana bağlayıcısı olan Portland çimentosu (PÇ), enerji ve emisyon yoğun bir yapı malzemesidir. Kalsiyum sülfoalüminat (KSA) çimentosu ise, üretiminde daha az enerji kullanıldığı ve çevreye daha az CO_2 salındığı için PÇ' ye alternatif sürdürülebilir bir bağlayıcı olarak görülebilir. KSA çimentosu üretiminde karşılaşılması muhtemel bir sorun ise, boksit gibi alümina içeren hammaddelerin maliyeti ve bulunabilirliğidir. Bu çalışmada, endüstriyel simbiyoz yaklaşımı kullanılarak çevre dostu KSA çimentosu sentezi amaçlanmıştır. Doğal hammaddeler olan kalker ve alçıtaşının yanı sıra Serox, pota fırını cürufu, seramik atıkları ve cam atıkları gibi farklı endüstrilerden gelen atıklar/yan ürünler laboratuvarda sentezlenen KSA çimentolarında hammadde olarak kullanılmıştır. KSA çimentolarının karakterizasyonu, hidratasyon davranışları ve uzun dönem performansları farklı deneysel yöntemlerle değerlendirilmiştir. Sonuç olarak, üç farklı KSA çimentosu en az %40 atık/yan ürün kullanılarak başarıyla sentezlenmiş ve ana bileşenler olarak ye'elimit, anhidrit, mervinit ve florellestadit oluşumu saptanmıştır. Tüm KSA çimentolarında ana hidratasyon ürünü olarak etrenjit oluşumu tespit edilmiş ve bir gün içinde 30 MPa'nın üzerinde bir basınç dayanımı elde edilmiştir. Oluşan bu

etrenjitin, uzun dönemde karbonatlaşma eğiliminde olduğu da saptanmıştır. Ayrıca, Monte Carlo simülasyon tekniği kullanılarak KSA çimentolarının CO_2 emisyonu PÇ ile karşılaştırılmış ve sentezlenen tüm KSA çimentoları göz önüne alındığında emisyon değerlerinde %48'e varan azalmalar görülmüştür.

Anahtar Kelimeler: KSA Çimentosu, Ye'elimit, Atık/Yan Ürün, Çevresel Değerlendirme, Endüstriyel Simbiyoz

To my family & my love, Görkem

ACKNOWLEDGMENTS

First, I would like to express my deep appreciation to my supervisor Prof. Dr. İsmail Özgür Yaman, for his great support, encouragement, and guidance throughout my Ph.D. study. I am truly grateful to him for his patience against my endless questions and for the support he gave me to find a way out when I could not clearly see my next step.

I would also thank my thesis committee members, Prof. Dr. Sinan Turhan Erdoğan and Assoc. Prof. Dr. Can Baran Aktaş, for their valuable suggestions, constructive discussions, and feedback. Moreover, I wish to express my thanks to the other jury members, Asst. Prof. Dr. Güzide Atasoy Özcan and Asst. Prof. Dr. Derya Över, for their valuable comments.

During this thesis, I am also grateful to have the support of Prof. Dr. Mustafa Tokyay, who did not spare for once his valuable advice and guidance throughout my education at METU.

I would also like to thank my brother Dr. Burhan Alam, whose support I have always felt since the first day I came to METU. I will always remember that rather than the destination what really matters is the journey itself. Thank you very much for all the knowledge and experience you have shared with me and for your endless motivational support on this long journey.

There is also the Materials of Construction Division team, of which I am very glad to be part of. My special thanks to Sahra Shakouri, Dr. Mehmet Kemal Ardoğa, Sepehr Seyedian Choubi, Dr. Mahdi Mahyar, Muhammet Atasever, Aykut Bilginer, Cuma Yıldırım, and Gülşah Bilici for their support, help, and motivation.

I would like to thank TürkÇimento for material supply and their technical support.

My great appreciation to my friends Pınar Karataş, Dr. Yalçın Karakaya, Sema Melek Kasapgil, Tümay Çelikkol Koçak, Merve Zorlu, Aslan Alam, Beyhan

İpekyüz, Asst. Prof. Dr. Funda Türe Kibar, Asst. Prof. Dr. Ayhan Öner Yücel for their great friendship, moral support, and motivation.

Along with people I have me in METU, I would certainly like to thank my parents Gönül and Ali Tangüler, my brothers İlyas and Caner, and my entire extended family for their endless support, encouragement, and motivation.

In addition, I am happy to express my gratitude to Assoc. Prof. Dr. Cansu Dağsuyu for being there for me, not only during my thesis study, but whenever I needed her, regardless of time and place. She is one of my greatest chances in my life.

The one thanks that my English is not enough to express, is to my beloved husband Görkem Bayramtan, with whom I have shared my life with great pleasure. I want to thank him for his understanding, patience, constant support, and for sharing all my joys, sorrows, and many stresses during this time.

Last but not least, many thanks to my amazing prince Viki, who made me smile even in my most tense moments with his various strange movements, despite all his scratching, biting, and even trying to sabotage my studies.

TABLE OF CONTENTS

LIST OF TABLES

TABLES

LIST OF FIGURES

FIGURES

LIST OF ABBREVIATIONS

ABBREVIATIONS

CE	CO_2 emission
CSA	Calcium sulfoaluminate
DTA	Differential thermal analysis
EAF	Electric arc furnace
EC	Energy consumption
EDX	Energy dispersive X-ray spectroscopy
ICP-OES	Inductively Coupled Plasma-Optical Emission Spectroscopy
IS	Industrial symbiosis
LFS	Ladle furnace slag
LOI	Loss on ignition
PC	Portland cement
PSD	Particle size distributions
SEM	Scanning electron microscope
TGA	Thermogravimetric analysis
XRD	X-ray diffraction
XRF	X-ray fluorescence

CEMENT CHEMISTRY NOTATIONS

A:	Al_2O_3	M:	MgO
C:	CaO	N:	Na_2O
$\overline{C}$:	CO_2	S:	SiO_2
F:	Fe_2O_3	$\overline{S}$:	SO_3
H:	H_2O	T:	TiO_2
K:	K_2O		

CHAPTER 1

INTRODUCTION

1.1 General

While global warming threatens our present and future, a general environmental consciousness has emerged, and the study of the sustainability of construction materials, in general, has become a priority. As concrete is known as the most widely used construction material, and its main binder, Portland cement (PC), is known to have a high energy and raw material consuming process, researchers in the field of cement and concrete technology are seeking solutions for alternative binders. Calcium sulfoaluminate (CSA) cements are considered as one of such alternative binders. However, a potential problem facing the production of CSA cements is the cost and availability of alumina-bearing raw materials like bauxite. Therefore, researchers are looking for alternative raw materials to produce CSA cements.

At this point, industrial symbiosis, which can be defined as the mutually beneficial exchange of waste and by-products between industries, allows materials to be used in a more sustainable way and contributes to the creation of a circular economy. This new economic model is identified as a novel approach to sustainability and has rapidly gaining momentum worldwide.

The broad aim of this thesis was to utilize the wastes/by-products of various industries and to develop a novel and sustainable binder, namely a green calcium sulfoaluminate cement. The wastes/by-products used in the production of the CSA cement were obtained through the FISSAC (Fostering Industrial Symbiosis for a Sustainable Resource Intensive Industry across the extended Construction Value Chain) project. This Horizon 2020 funded project aimed to develop and demonstrate a new industrial symbiosis model that steers the material process towards a zero-

waste approach in the resource-intensive sectors of the construction value chain, leading to closed material loops and enabling the transition to a circular economy.

1.2 Objective and Scope

The objective of this study is threefold, as listed below:

- Synthesis of an environmentally friendly CSA cement using an industrial symbiosis approach in the laboratory
- Evaluation of the hydration behavior and the long-term mechanical performance of the CSA cement through paste and mortar testing
- Investigation of the environmental performance of CSA cement using a life cycle perspective

This thesis consists of six chapters, the first of which is the introduction. In the second chapter, the literature research on CSA cements and industrial symbiosis are presented. In the third chapter, the CSA cement manufacturing process and the experimental methods are explained. In the fourth chapter, the experimental results of CSA cements, cement pastes and cement mortars are given. In the fifth chapter, the environmental performance of the CSA cements is evaluated with a life cycle perspective, and the CSA cement's energy consumption and CO_2 emission results calculated using a Monte Carlo simulation is presented. Finally, the conclusions of the study and recommendations are listed in Chapter 6.

CHAPTER 2

LITERATURE REVIEW

2.1 General

Cement is a finely ground, dry material that has no binding property on its own but becomes a binder as a result of its reaction with water known as hydration. A cement is named hydraulic when its hydration products remain stable in an aqueous medium (Mehta & Monteiro, 2006).

The development of cement in history dates to the 1800s. Joseph Aspdin received the patent for the hydraulic binder called "portland cement" in 1824. This binder was later developed further and kept the name "portland." In 1845, Isaac Johnson produced modern portland cement, whose physical and chemical properties have not changed significantly since its manufacture (Chen, 2009; Erdoğan, 2016).

ASTM C219 defines portland cement (PC) as "a hydraulic cement produced by pulverizing clinker, consisting essentially of crystalline hydraulic calcium silicates, and usually containing one or more of the following: water, calcium sulfate, up to 5% limestone, and processing additions" (ASTM C219 - 20a, 2020).

Because calcium silicates are the main components of PC, the raw material used for its production must contain calcium and silica in appropriate forms and amounts. Calcium carbonate materials such as limestone and chalk are the common source of calcium, while clays and shales are the preferred sources of silica. The raw meal, a mixture of calcareous and clayey minerals in certain proportions, is burned to a temperature of around 1450°C in a rotary kiln, yielding clinker nodules. The clinker is then ground with 3-6% of gypsum, and portland cement is obtained (Taylor, 1997; Mehta & Monteiro, 2006). During the cement grinding stage, the cement temperature must be controlled to avoid excessive dehydration of the gypsum. This can be

accomplished using a cold air circulation system and/or water diffusers (García-Maté, 2014).

According to the 2019 Cement Industry "Getting the Numbers Right" database, the annual worldwide PC production is about 4.1 billion tons (WBCSD, 2019). PC is used as the main binder of concrete, and it is the product of an industry which is both energy-intensive and a significant emitter of CO_2 (Mehta, 2002). The cement industry uses 12-15% of the worldwide industrial energy (Ali et al., 2011) and emits about 5-8% of global anthropogenic CO_2, making it a significant source of greenhouse gases (Huntzinger & Eatmon, 2009; Ali et al., 2011; Flatt et al., 2012; Salas et al., 2016). The average global CO_2 emissions are about 0.83 tons per ton of PC clinker (WBCSD, 2019). CO_2 emissions in the cement industry are primarily caused by the combustion of fossil fuels and the decomposition of limestone into CaO as a result of calcination. The combustion of fuels accounts for around half of CO_2 emissions, while the calcination of limestone accounts for the other half (Ali et al., 2011; Gursel et al., 2014).

Apart from these environmental drawbacks, PC is not the best binder for all construction applications because of its durability issues, especially in aggressive environments (Juenger et al., 2011). In addition, binders based on PC alone may not wholly fulfill needs like rapid setting, rapid hardening, and dimensional stability (Pelletier-Chaignat et al., 2011; Bizzozero et al., 2014). As a result, there is an increasing interest in discovering, characterization and using alternative concrete binders (García-Maté, 2014). In this scope, calcium sulfoaluminate (CSA) cement is one of the promising alternatives to the ordinary PC, considering its technical advantages and lower CO_2 emissions from the manufacturing process (Gartner, 2004; Martín-Sedeño et al., 2010; Juenger et al., 2011; Aranda & De la Torre, 2013).

This chapter will first look at the existing literature on CSA cements and later will explain industrial symbiosis to facilitate circular economy.

2.2 Calcium Sulfoaluminate (CSA) Cements

2.2.1 A Historical Perspective and the Types of CSA Cements

The calcium sulfoaluminate phase, also known as ye'elimite, was first synthesized by Ragozina in 1957, but its correct chemical composition was identified by Fukuda in 1961 as $3CaO{\cdot}3Al_2O_3{\cdot}CaSO_4$ (Fukuda, 1961; Andac & Glasser, 1994; Hargis et al., 2014). In the 1960s, Alexander Klein defined the ye'elimite compound as a cementitious phase and patented it as an expansion additive for cementitious binders; therefore, ye'elimite is also referred to as Klein's compound (Klein, 1964; Juenger et al., 2011).

Initially, CSA was mainly used as an expansive binder to compensate shrinkage (Mehta, 1973), and then, in the middle of 1970s, CSA cements were developed by the China Building Materials Academy (Zhang et al., 1999; Glasser & Zhang, 2001; Shi et al., 2011; Telesca et al., 2013) and launched as the "third cement series" following the first cement series and the second cement series, PC and calcium aluminate cements, respectively (Juenger et al., 2011; Hargis et al., 2014).

In fact, this third cement series includes two main types of CSA: sulfoaluminate cements, "SAC", and ferroaluminate cements, "FAC." The first standard for SAC was published in China in 1981, while the one for FAC was published in 1987. Both standards were revised in 1996 and then came into effect in 1997. The related standards show that different cement matrices were formed with calcium sulfate and other mineral additive modifications in the SAC and FAC series, as presented in Table 2.1 (Zhang et al., 1999).

Table 2.1 CSA types in China (Zhang, 2000)

Cement series	clinker	Cement type	Interground calcium sulfate	Content	Other mineral additives
SAC	$C\bar{S}A$	Rapid hardening	Gypsum or anhydrite	Low	Limestone or others
		High strength	Gypsum or anhydrite	Low	Limestone
		Expansive	Gypsum	Medium	None
		Self-stressing	Gypsum	High	None
		Low alkalinity	Anhydrite	Low	Limestone
FAC	Fe-rich $C\bar{S}A$	Rapid hardening	Gypsum or anhydrite	Low	Limestone or others
		High strength	Gypsum or anhydrite	Low	Limestone
		Expansive	Gypsum	Medium	None
		Self-stressing	Gypsum	High	None

Partly because of the main mineral phase in SAC and FAC clinkers is $C_4A_3\bar{S}$, these two types show mostly similar properties such as rapid hardening, high early strength, and controllable expansion. However, due to the different content of the ferrite phase, differences in their performance occur, e.g., in their alkalinity. Since the durability of glass fibers is affected by alkalinity, SAC is more suitable for use in glass fiber reinforced cement products due to its lower alkalinity compared to FAC (Zhang et al., 1999).

According to the last revision of the SAC standard in 2006 (GB/T 20472-2016, 2006), the SAC series is divided into three:

- Rapid hardening sulfoaluminate cement (R·SAC)
- Low alkaline sulfoaluminate cement (L·SAC)
- Self-stress sulfoaluminate cement (S·SAC)

As can be seen from the cement designations, features such as rapid setting, high early strength, low alkalinity, expansive or self-stressing can be achieved with CSA cements, depending on the calcium sulfate amount ground with clinker. Due to their distinctive features, CSA cements have been used in various applications in China,

such as precast and prestressed concrete, cold weather applications, shotcreting applications, fiberglass-reinforced cement products, concrete pipes, waterproof structures, bridges, leakage and seepage prevention projects (Sharp et al., 1999; Zhang et al., 1999; Zhang, 2000; Juenger et al., 2011). However, their use outside of China has been relatively limited to special cements and non-structural applications for many years (Zhang, 2000).

The total production capacity of 15 cement factories producing various types of CSA cements in China in 1997 was reported to be nearly 1 million tons per year (Zhang, 2000). And today, China's annual CSA cement production is thought to be over 1 million tons. Besides China, CSA cements are now commercially produced both in Europe and the United States. In the United States, they are mostly used for pavement applications, thanks to their rapid strength gain and low shrinkage features (Thomas et al., 2018; Bescher & Kim, 2019).

The cost and availability of raw materials can be considered as one of the barriers to the widespread manufacture and use of CSA cements. Calcium oxide and silica deposits exist all over the world. Thus, PC can be produced inexpensively in most places using local resources. CSA cements, on the other hand, require a higher aluminum content than PC. Bauxite deposits, mostly reserved for alumina and aluminum production, are not extensive, and alumina extraction can be costly. The problems in cost and availability of raw materials may hinder the widespread production of CSA cements on an industrial basis. On the other hand, the use of alternative raw materials can offer an effective solution to overcome these problems (Chen, 2009).

In recent years, CSA cements have once again attracted the interest of industry and scientific community due to their lower CO_2 emissions and lower energy requirements compared to PC during production, as well as offering some special technical advantages to the mortars and concretes made from them (Aranda & De la Torre, 2013; Hargis et al., 2014). At the same time, the economic challenges have prompted research on using industrial by-products/waste materials such as fly ash,

blast furnace slag, phosphogypsum, baghouse dust, or scrubber sludge in the production of CSA cements (Juenger et al., 2011). Thus, while trying to overcome the economic issues of CSA cements by utilizing by-products/wastes, environmental benefits are also provided.

2.2.2 Importance of CSA Cements: CO_2 Emissions and Energy Savings

Concerns about global warming have made research on cements with lower CO_2 emissions more attractive. In this regard, CSA cement can be seen as a sustainable alternative to PCs because its production uses less energy and emits less CO_2 to the environment. In cement production, the primary sources of CO_2 emissions are related to the raw materials and production processes. CO_2 emissions that come from the raw materials can be theoretically computed by using the stoichiometry of the chemical reactions that take place during cement production. For example, during the formation of the C_3S and the $C_4A_3\bar{S}$ phases, which are the main phases for PC and CSA cements, CO_2 is released as shown below (Aranda & De la Torre, 2013):

$$3C\overline{C} + S \rightarrow C_3S + 3\overline{C} \quad (1)$$

$$3C\overline{C} + 3A + C\bar{S} \rightarrow C_4A_3\bar{S} + 3\overline{C} \quad (2)$$

The amount of CO_2 emitted during the formation of pure anhydrous phases of PC and ye'elimite is given in Table 2.2.

Table 2.2 CO_2 emitted during the formation of clinker phases

Phase	CO_2 released (t/t of phase)
C_3S	0.578
C_2S	0.511
C_3A	0.488
C_4AF	0.362
$C_4A_3\bar{S}$	0.216

As seen in Table 2.2, the amount of CO_2 emissions from ye'elimite formation is less than that of the PC phases. Moreover, while the enthalpy of C_3S formation is 1848 kJ/ kg of phase, the enthalpy of ye'elimite formation is about 800 kJ/ kg of phase (Sharp et al., 1999; Glasser & Zhang, 2001). That is, the formation of ye'elimite requires temperatures 200-300°C below those required for forming C_3S (Beretka et al., 1996). Based on the raw meal composition, the burning temperature for CSA clinkering is between 1250°C and 1350°C. This temperature is lower than the temperature needed for PC manufacturing (Sharp et al., 1999). The decrease in clinkering temperature results in a reduction in the energy demand and correspondingly lower CO_2 emissions. Additionally, CSA clinker requires less energy to grind than PC due to its more friable nature (Beretka et al., 1996).

2.2.3 Production of CSA Cements

CSA cement production technology on an industrial scale is rarely reported outside of China. Chinese technology can be considered in three stages: raw meal preparation, clinker burning, and cement finishing. The main raw materials used in CSA clinker production are bauxite, limestone, and calcium sulfate, and the raw materials should meet some chemical requirements that vary with the cement types. Gypsum or anhydrite can be added to the clinker to obtain CSA cement, depending on their SO_3 content. The fuel normally used in CSA clinker production is bituminous coal. The clinker burning and cement finishing processes of CSA cements production in China is given in Figure 2.1 (Zhang, 2000).

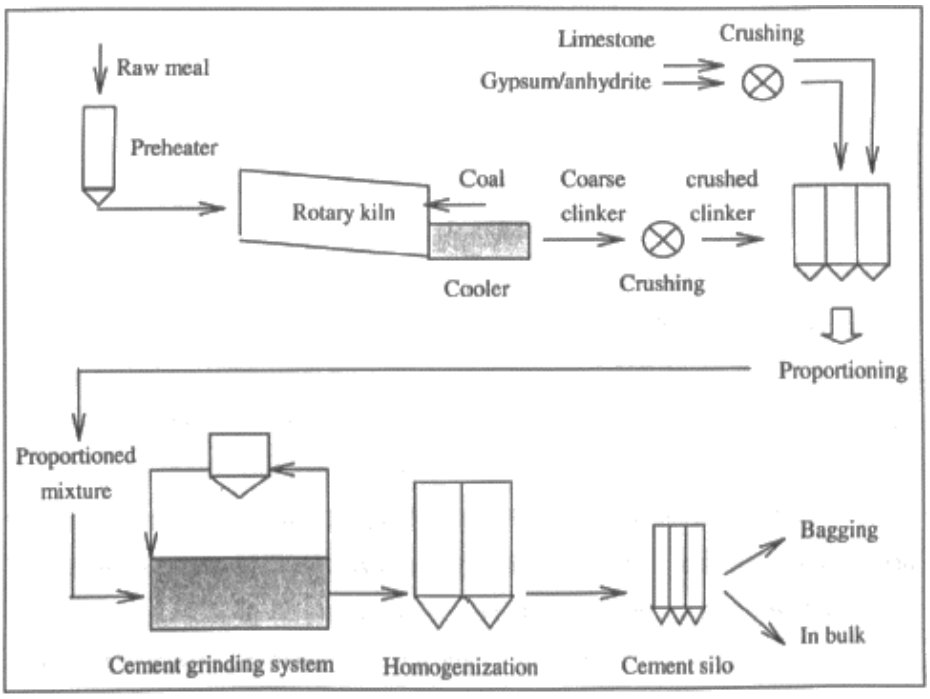

Figure 2.1 Clinker burning and cement finishing processes of CSA cements production (Zhang, 2000)

A formula has been developed in China for calculating the optimum sulfate content for the different types of CSA cements, based on stoichiometric calculations.

$$C_T = 0.13\ M\ \frac{A}{\bar{S}} \qquad (3)$$

where C_T is the molar ratio of gypsum/clinker, A is the wt.% of ye'elimite in clinker, $\bar{S}$ is the wt.% of SO_3 in gypsum and M is the molar ratio of gypsum/ye'elimite, and 0.13 is the stoichiometric factor related to mass-mole conversion.

M value refers to the type of CSA cement. Cements show different properties according to the M value. Rapid hardening or high strength properties are achieved with M=0-1.5, expansive properties are achieved with M=1.5-2.5, and self-stressing properties are achieved with M=2.5-6 (Zhang, 2000; Winnefeld & Barlag, 2010).

2.2.4 Chemical Composition of CSA Cements

CSA cement distinctively has a different chemical composition when compared to PC and other common supplementary cementitious materials (SCM) as shown in a ternary diagram (see Figure 2.2).

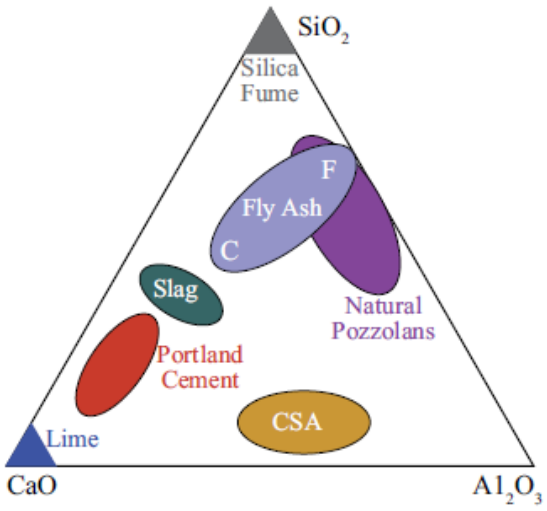

Figure 2.2 Oxide composition of PC, CSA cement and other SCMs (% mass) (Thomas et al., 2018)

Compared to PC, CSA cements contain more Al_2O_3 and less CaO and SiO_2; they are also richer in sulfate. These oxides are mostly found in the form of ye'elimite ($C_4A_3\bar{S}$) belite (C_2S), ferrite (C_4AF), and calcium sulfate ($C\bar{S}H_2$ or $C\bar{S}$) (Thomas et al., 2018). Different phases can also form based on the raw materials' composition, e.g., free lime, calcium aluminates, perovskite or gehlenite (Juenger et al., 2011). The terminology of CSA cements is slightly confusing. Throughout the years, CSA cements have been referred to by various names and abbreviations, leading to different classifications (Odler, 2000). For example, according to Aranda & De la Torre (2013), CSA cements can be classified based on the main compounds they contain (see Table 2.3), while according to Bescher et al. (2018), CSA binders can be classified according to their properties as shown in Table 2.4.

Table 2.3 A classification proposed by Aranda & De la Torre (2013)

Definition	**Acronym**	**Main compound**	**Secondary and other compounds**
Calcium sulfoaluminate cement	CSA	$C_4A_3\bar{S}$	C_2S (C_4AF, $C\bar{S}$, CT, …)
Iron-rich belite calcium sulfoaluminate cement	BCSAF	C_2S	$C_4A_3\bar{S}$ (C_4AF, CT, …)
Aluminum-rich belite calcium sulfoaluminate cement	BCSAA	C_2S	$C_4A_3\bar{S}$ ($C_{12}A_7$, CA, …)
Alite calcium sulfoaluminate cement	ACSA	$C_4A_3\bar{S}$	C_3S (C_2S, …)

Table 2.4 A classification proposed by Bescher et al. (2018)

	$C_4A_3\bar{S}$ (%)	**C_2S (%)**	**$C\bar{S}$ (%)**	**Other (%)**
Type A - Accelerating additive	35-45	0-20	10-30	5-55
Type B - Belitic calcium Sulfoaluminate cement	20-30	40-60	5-25	0-35
Type C - Expansive additive	10-20	10-30	40-60	0-40
Type K - Shrinkage compensating cement	1-10	30-50	1-20	20-70

Based on the oxide compositions of the raw materials, a set of Bogue equations was adapted to estimate the phase composition of the CSA clinker (Majling et al., 1993; Chen, 2009):

$$\%C_4AF = 3.043(\%Fe_2O_3) \quad (4)$$

$$\%\ C_4A_3\bar{S} = 1.995(\%Al_2O_3) - 1.273(\%Fe_2O_3) \quad (5)$$

$$\%C_2S = 2.867(\%SiO_2) \quad (6)$$

$$\%C\bar{S} = 1.700(\%SO_3) - 0.445(\%Al_2O_3) + 0.284(\%Fe_2O_3) \quad (7)$$

$$\%C = 1.000(\%CaO) - 1.867(\%SiO_2) - 1.054(\%Fe_2O_3) - 0.550(\%Al_2O_3) - 0.700(\%SO_3) \quad (8)$$

However, these equations ignore the impurities present in the system and assume that the cement phases are in their stoichiometric form, so the modified Bogue equations may not apply to all types of CSA cements, especially CSA cements containing wastes like this study.

While there are definite specifications for PC and its types (EN 197-1), this is not the case for CSA cements. Since there is no standard other than Chinese standards and its features are affected by many factors, it is not easy to establish a clear framework for classifying this type of cements. However, the European Technical Assessment Organization issued two evaluation documents about "CSA based cement" (EOTA, 2017a) and "rapid hardening sulfate resistant CSA based cement" (EOTA, 2017b). According to the European Assessment Document (EAD) related to CSA based cement; CSA clinker generally contains more than 45 wt% $C_4A_3\bar{S}$, and the remaining part is composed of C_2S and other compounds. According to EAD related to rapid hardening sulfate resistant CSA based cement; this cement has rapid setting and sulfate resistance features. At least 50 wt% of the clinker consists of $C_4A_3\bar{S}$ and the remaining part is formed of C_2S and other compounds. This type of cement may additionally contain CEM I cement clinker (0-50 wt%). CSA cements show a great diversity in their composition. There are several CSA clinkers/cements available in the market along with many others synthesized in laboratory conditions.

2.2.4.1 Commercially Available CSA Cements

Commercial CSA cements with a high proportion of ye'elimite have been produced and used extensively in China since the 1970s for special applications (Aranda & De la Torre, 2013). In addition, there are CSA clinkers/cements commercially available in Europe and America, albeit in limited numbers. The oxide ranges and phase

compositions of the CSA clinkers in the market compiled from the literature is summarized in Table 2.5 and Table 2.6, respectively.

Table 2.5 Oxide composition range of commercially available CSA clinkers

Oxide %	
CaO	36.2% - 45.3%
Al_2O_3	27.3% - 47.4%
SiO_2	3.6% - 11%
SO_3	6.5% - 13.9%
Fe_2O_3	0.9% - 8.6%
Na_2O	0.04% - 1.4%
K_2O	0.1% - 0.5%
MgO	0.3% - 4.1%
TiO_2	0.4% - 2.2%

Table 2.6 Phase composition of commercially available CSA clinkers

Brand/ Producer	**Phases**	**Reference**
CS10 BELITH [1]	72.3% $C_4A_3\bar{S}$; 14.5% C_2S; 6.8% CT; 2.5% C_4AF; 1.6% M; 1.4% C_2MS_2; 0.9% $C\bar{S}$	(García-Maté et al., 2012)
ALIPRE (2009)[2]	69.5% $C_4A_3\bar{S}$; 17.1% C_2S; 9% $C\bar{S}$; 3.5% CT; 0.52% M	(Álvarez-Pinazo et al., 2012)
Mirae C&C Corp., South Korea	69.4% $C_4A_3\bar{S}$; 20% C_2S; 4.2% $C_{12}A_7$; 3.8% CT; 1.5% C_2AS; 1% M	(Jeong et al., 2018)
KTS 100-Belitex	68.5% $C_4A_3\bar{S}$; 15.9% C_2S; 9.5% $C_{12}A_7$; 2.9% CT; 1.5% M; 1.2 % Fe_2O_3; 0.5% $C\bar{S}$; 0.5% quartz	(Berger et al., 2011)
ALI PRE GREEN[3]	68.4.5% $C_4A_3\bar{S}$; 16.9% C_2S; 7.40% C_7MS_4 3.67% M; 1.90% C_2AS; 1.75% C_3A	(Padilla-Encinas et al., 2020)
No brand specified	68.1% $C_4A_3\bar{S}$; 14.8% C_2AS; 7.8% CA; 3.6% CT; 3.4% C_3A; 1.2% CA_2; 1% M	(Pelletier et al., 2010)
ALIPRE[4]	65% $C_4A_3\bar{S}$; 9% C_2S; 11% $C_{10}S_3\bar{S}_3F_2$; 5% M; 3% $C\bar{S}$	(Trauchessec et al., 2015)

Table 2.6 Continued

Brand/ Producer	**Phases**	**Reference**
No brand specified	64.3% $C_4A_3\bar{S}$; 10.6% C_2S; 7.4% $C_{10}S_3\bar{S}_3F_2$; 3.8% C_7MS_4; 3.3% M, 2.8% C_3MS_2; 2.3% $C_{12}A_7$; 2% $C\bar{S}$; 1.5% C_3S; 0.9% CT; 0.9% C_2AS	(Martin et al., 2017)
42.5R CSAC[5]	58.68% $C_4A_3\bar{S}$; 28% C_2S; 13.35% C_4AF	(Gao et al., 2021)
R.SAC 42.5[6]	57.37% $C_4A_3\bar{S}$; 25.55% C_2S; 6.56% C_4AF; 1.92% f-SO_3	(Chang et al., 2009)
Rockfast 450[7]	57% $C_4A_3\bar{S}$; 16% C_2AS; 15% CA; 4% C_4AF; 4% CT; 1% $C_{12}A_7$; 0.5% $C\bar{S}$; 0.3% f-CaO	(Zhou et al., 2006)
Chinese CSAC[8]	57% $C_4A_3\bar{S}$; 17% C_2S; 7% C_2AS; 7% CA; 6% CT; 3% $C_{12}A_7$; 2% C_3A; 1% $C\bar{S}$	(Galan et al., 2016)
S.A.Cement[9]	56.2% $C_4A_3\bar{S}$; 31.1% C_2S; 6.3% $C\bar{S}$; 3.5% CT; 1.9% CA; 1.1% M	(Álvarez-Pinazo et al., 2012)
Grade 72.5 belite-CSAC[10]	53.6% $C_4A_3\bar{S}$; 20.6% C_2S; 11.7% C_2AS; 4.8% CT; 4.2% C_3MS_2; 3.3% $C_{12}A_7$	(Jen et al., 2017)
TS-Belitex[11]	53.5% $C_4A_3\bar{S}$; 21.2% C_2S; 16.5% C_4AF; 9% CT	(Cau Dit Coumes et al., 2009)
Italian CSAC	52.1% $C_4A_3\bar{S}$; 23.8% C_2S; 9.4% C_3A; 4.9% $C\bar{S}$; 4.7% C_4AF; 1.6% C_2AS; 1.4% M; 1.2% $C_{12}A_7$; 0.9% $C_5S_2\bar{S}$	(Telesca et al., 2014)

[1] produced in China and marketed in Europe by BELITH S.P.R.L.
[2] produced by Italcementi, Italy
[3]supplied by HeidelbergCement Hispania, Spain
[4]produced by Italcementi with recycled materials, Italy
[5]produced by Dengfeng Electric Power Group Cement Co. Ltd., Henan, China
[6]obtained from Zibo Jinhu Highwater Material Co. Ltd., China
[7]provided by Lafarge Cement, UK
[8]obtained from Shenzhen Chenggong Building Materials Co. Ltd., China
[9] produced by Buzzi Unicem, Italy
[10]obtained from China
[11]produced by Carrie`res du Boulonnais, France (Péra & Ambroise, 2004)

As shown in Table 2.6, CSA clinkers on the market consist mainly of ye'elimite and C_2S. The Rockfast CSA clinker does not contain belite. Instead, it mostly contains gehlenite (C_2AS) and calcium aluminate (CA) phases. Fluorellestadite ($C_{10}S_3\bar{S}_3F_2$), merwinite (C_3MS_2), bredigite (C_7MS_4), akermanite (C_2MS_2), periclase, perovskite, and calcium aluminate phases such as CA, CA_2, C_3A, $C_{12}A_7$, were also observed.

The main oxide range for the products reported as commercial CSA cement in the studies in the literature is as follows; CaO: 40.5%-49.5%, Al_2O_3:14.7%-34.2%, SiO_2: 3.4%-14.3%, SO_3: 11.02%-19.5%. The main phases contents are $C_4A_3\bar{S}$: 27.4%-62.7%, C_2S: 19%-48%, $C\bar{S}$: 4.8%- 22%. As minor phases, C_4AF, $C_{12}A_7$, CT, C_3A, C_2AS, and MgO phases can be found, one or more of them together.

2.2.4.2 Laboratory Synthesized CSA Cements

CSA cements are not a commonly used cement type worldwide. Although production on an industrial scale is limited, laboratory-scale production studies are not few. Existing literature demonstrates that CSA cements can be produced by using reagent grade chemicals such as CaO, Al_2O_3, SiO_2, Fe_2O_3, $CaSO_4 2H_2O$ (Chen & Juenger, 2011, 2012; Galan et al., 2014) or by using raw materials consisting of bauxite, limestone and gypsum in different proportions (Marroccoli et al., 2009; Gastaldi et al., 2011; Telesca et al., 2019; Canbek & Erdoğan, 2020; Paul et al., 2021). Clay was also used in the raw meal along with these raw materials (Álvarez-Pinazo et al., 2012; Telesca et al., 2020).

The availability of raw materials and the high cost of bauxite form economic challenges for the CSA cements. One of the reasons for laboratory research in this field is to reduce the cost of CSA cement production using locally available materials. By-products/wastes that can be sources of CaO, SiO_2, Al_2O_3, and SO_3 needed for CSA cement production were often utilized. By-products/wastes used in CSA clinker production compiled from the literature can be listed as follows: red mud (Senff et al., 2011; Wu et al., 2019; Canbek et al., 2020), aluminum slag (Wu et al., 2019), alumina powder (Marroccoli et al., 2010), aluminium anodising sludge (Pace et al., 2011; da Costa et al., 2016), fly ash (Živica, 2000; Marroccoli et al., 2010; Chen & Juenger, 2012; Ma et al., 2013; Bullerjahn et al., 2015; Borštnar et al., 2020; Canbek et al., 2020; Dolenec et al., 2020; Huang et al., 2020), granulated blast furnace slag (Bullerjahn et al., 2015), electric arc furnace slag (Iacobescu et al., 2013; Ukrainczyk et al., 2013), desulfurization gypsum (Marroccoli et al., 2010; Ma et al.,

2013), phosphogypsum (Ukrainczyk et al., 2013), fluidized bed ash (Chen & Juenger, 2012), fluorogypsum**,** water potabilization sludge (Telesca et al., 2019), titanogypsum (Telesca et al., 2019; Borštnar et al., 2020; Dolenec et al., 2020), bottom ash (Marroccoli et al., 2010; Ukrainczyk et al., 2013; Borštnar et al., 2020; Dolenec et al., 2020), jarosite–alunite precipitate (Katsioti et al., 2005), and pyrite-rich cyanide tailings (Dong et al., 2020).

Table 2.7 shows the range of oxide and phase compositions for CSA clinkers synthesized in the laboratory. In addition to the phases listed in that table, ternesite, periclase, calcium aluminate phases (CA, CA_2, C_3A), bredigite, merwinite, fluorellestadite, perovskite, free lime, and quartz phases were also encountered.

Table 2.7 Oxide and phase composition range of laboratory- synthesized CSA clinkers

Oxide %		Phase %	
CaO	22.0% - 56.8%	$C_4A_3\bar{S}$	10% - 84%
Al_2O_3	5.7% - 37.4%	C_2S	1.2% - 72%
SiO_2	4.7% - 27.1%	C_4AF	0.0% - 42.7%
SO_3	1.3% - 22.3%	$C\bar{S}$	0.0% - 22.8%
Fe_2O_3	0.0% - 10.0%	$C_{12}A_7$	0.0% - 15.2%
Na_2O	0.0% - 1.0%	C_2AS	0.0% - 18.0%
K_2O	0.1% - 1.0%		
MgO	0.1% - 5.6%		
TiO_2	0.1% - 1.7%		

Both commercial and laboratory synthesized CSA clinkers reveal that ye'elimite and belite are mostly the two main phases of these clinkers. Figure 2.3 shows the range of CSA clinkers gathered from the literature. In the same graph, the ye'elimite and belite contents of the CSA clinkers in the market are also presented. As seen in Figure 2.3, there is a wide distribution for CSA clinkers. While some of the synthesized clinkers are close to the commercial ones, some are quite different. When the main phase, ye'elimite, has been replaced by belite, these clinkers can be called belite-rich CSA clinkers.

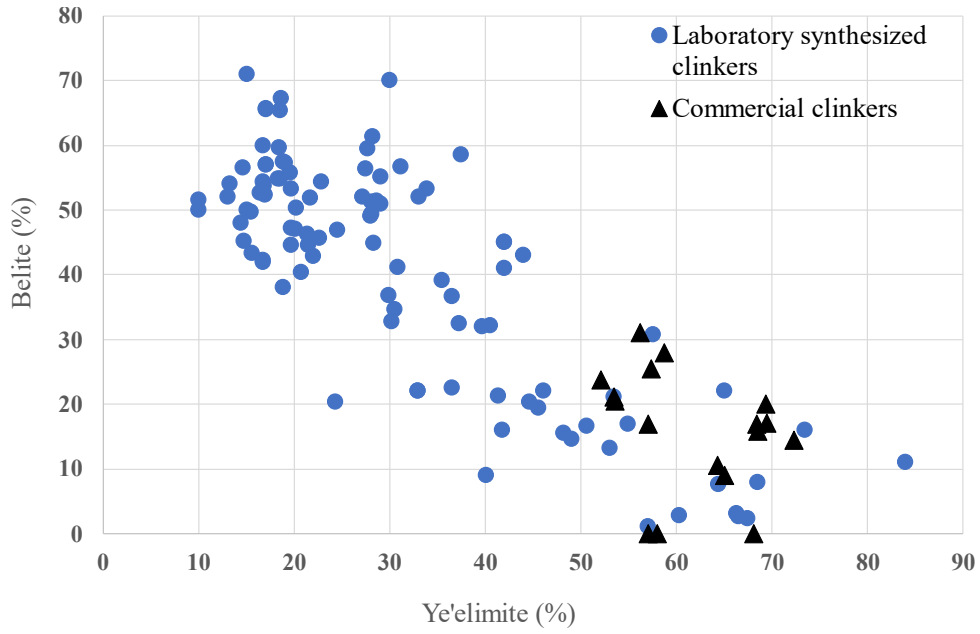

Figure 2.3 Ye'elimite vs. C_2S content of CSA clinkers compiled from the literature

2.2.5 Hydration Behavior of CSA Cements

Zajac et al. (2016) stated that the hydration mechanism of CSA cements is mainly affected by the composition of clinker (Winnefeld & Lothenbach, 2010; Bullerjahn et al., 2015), the quantity and reactivity of calcium sulfate added (Winnefeld & Barlag, 2009; García-Maté et al., 2015) and production process parameters (Bullerjahn et al., 2014).

The hydration of ye'elimite depends on the presence of calcium sulfate and calcium hydroxide (Odler, 2000). As seen in Equation 9, the hydration of ye'elimite alone results in monosulfate ($C_4A\bar{S}H_{12}$) and aluminum hydroxide (AH_3) formation. This hydration kinetics is quite slow, and its dormant period takes several hours (Juenger et al., 2011).

$$C_4A_3\bar{S} + 18H \rightarrow C_4A\bar{S}H_{12} + 2AH_3 \quad (9)$$

If calcium sulfate (gypsum or anhydrite) is present together with ye'elimite, the hydration kinetics are accelerated. Furthermore, the products formed vary depending on the amount of calcium sulfate in the medium; for example, if the molar ratio of gypsum to ye'elimite is at least 2, ettringite ($C_6A\bar{S}_3H_{32}$) and aluminum hydroxide (AH_3) are formed, as shown in Equation 10. On the other hand, less gypsum in the medium causes the reaction to proceed as in Equation 11; in this case, monosulfate is also formed besides ettringite and aluminum hydroxide. When enough gypsum and calcium hydroxide are present together, the reaction occurs only to form ettringite, as shown in Equation 12.

$$C_4A_3\bar{S} + 2C\bar{S}H_2 + 34H \rightarrow C_6A\bar{S}_3H_{32} + 2AH_3 \quad (10)$$

$$2C_4A_3\bar{S} + 2C\bar{S}H_2 + 52H \rightarrow C_6A\bar{S}_3H_{32} + C_4A\bar{S}H_{12} + 4AH_3 \quad (11)$$

$$C_4A_3\bar{S} + 8C\bar{S}H_2 + 6CH + 74H \rightarrow 3C_6A\bar{S}_3H_{32} \quad (12)$$

In general, CSA cements consist of several hydraulic compounds, but the reactions are similar. $C_4A_3\bar{S}$ (ye'elimite) reactivity is higher compared to other minor phases such as C_2S, C_4AF or CA (Juenger et al., 2011). The minor phases also react with water or calcium sulfate and contribute in some way to rapid hardening, as given by the following reactions (Equation 13, 14, 15). In the absence of calcium sulfate, these phases are directly hydrated (Equation 16, 17, 18) (Aranda & De la Torre, 2013).

$$C_4AF + 3C\bar{S}H_2 + 30H \rightarrow C_6A\bar{S}_3H_{32} + FH_3 + CH \quad (13)$$

$$C_{12}A_7 + 12C\bar{S}H_2 + 113H \rightarrow 4C_6A\bar{S}_3H_{32} + 3AH_3 \quad (14)$$

$$3CA + 3C\bar{S}H_2 + 32H \rightarrow C_6A\bar{S}_3H_{32} + 2H_3 \quad (15)$$

$$C_4AF + 16\,H \rightarrow 2C_2(A_{0.5}F_{0.5})H_8 \quad (16)$$

$$C_{12}A_7 + 51H \rightarrow 6C_2AH_8 + AH_3 \quad (17)$$

$$2CA + 11H \rightarrow C_2AH_8 + AH_3 \quad (18)$$

As seen from the above equations, aluminum hydroxide is also formed in most of the hydration reactions as a product. Since AH_3 is amorphous at first, it cannot be directly identified with X-ray diffraction, but its existence can be approved with thermogravimetric analysis. This amorphous phase may later crystallize and acquire the gibbsite form (Aranda & De la Torre, 2013).

C_2S hydration is of particular interest, especially in CSA cements with high C_2S content. The coexistence of C_2S with amorphous AH_3 hydrates promotes the formation of strätlingite (C_2ASH_8), as shown in Equation 19, which helps in increasing the strength development. If AH_3 is totally consumed, direct hydration of C_2S, the same as that of PC, may occur at later ages (Equation 20) (Aranda & De la Torre, 2013).

$$C_2S + AH_3 + 5H \rightarrow C_2ASH_8 \quad (19)$$

$$C_2S + (x+2-y)H \rightarrow C_ySH_x + (2-y)CH \quad (20)$$

In summary, early-age hydration products are ettringite, monosulfate, and amorphous aluminum hydroxide. Based on the clinker and cement composition, different other hydrates such as strätlingite, C-S-H, monocarboaluminate or hydrogarnet may also occur in later ages (Winnefeld & Barlag, 2009; Zajac et al., 2016).

Compared to PC, CSA cements react faster, and most of the heat of hydration evolves between the 2^{nd} and 12^{th} hours of hydration (Zhang & Glasser, 2002). Based on isothermal calorimetry measurements, the typical values for the 3-day heat of hydration are around 400 J/g of cement (Lura et al., 2010; Winnefeld & Lothenbach, 2010; Juenger et al., 2011). Aranda & De la Torre (2013) reported a heat flow profile for an iron-rich belite CSA cement (BCSAF) containing ~45 wt.% of C_2S, ~27 wt.% of $C_4A_3\bar{S}$, ~18 wt.% of C_4AF, and ~10 wt.% of gypsum, and with a 0.5 of w/c (see Figure 2.4)

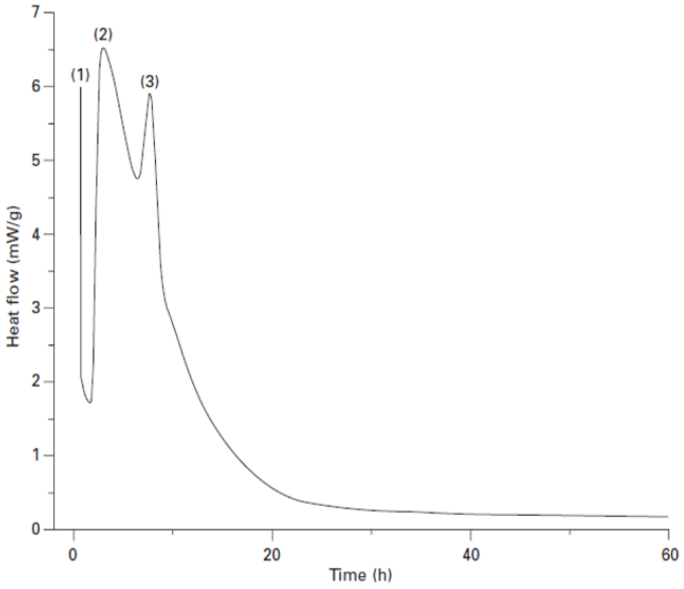

Figure 2.4 Heat flow curve of a BCSAF cement (Aranda & De la Torre, 2013)

According to Aranda & De la Torre, when water is added to cement, the ye'elimite dissolution starts, corresponding to peak (1). Due to the time needed for the mixing process, just a part of the exothermic process is generally recorded in a calorimeter. Immediately after wetting, ettringite starts to form by the reaction between ye'elimite and calcium sulfate, corresponding to peak (2). This peak is also associated with the heat release of reactions of minor phases. When calcium sulfates are consumed, ye'elimite hydration results in monosulfate formation that corresponds to peak 3 (see Figure 2.4).

2.2.6 General Properties of CSA Cements

The properties of CSA cements are influenced by many factors, such as the chemical and mineralogical composition of the clinker, the type and amount of sulfate source, the water/cement ratio, and the presence of other binders, e.g., PC (Aranda & De la Torre, 2013). Depending on these factors, CSA cements can be obtained with different properties such as rapid setting, high strength, expansive, shrinkage

compensating and self-stressing (Cau Dit Coumes et al., 2009; Winnefeld & Barlag, 2010; Juenger et al., 2011; Hargis et al., 2017).

2.2.6.1 Setting Time

The setting time of the cement paste refers to the beginning of solidification and subsequent hardening (Ma et al., 2014). CSA cements have a faster initial and final setting time than PCs. Ettringite, the hydration product of ye'elimite, crystallizes rapidly, resulting in fast setting (Thomas et al., 2018). According to Chinese standard, the minimum initial setting time should be 25 minutes and the maximum final setting time should be 3 hours for rapid hardening sulfoaluminate cements (Zhang et al., 1999).

Juenger et al. (2011) stated that setting time is directly affected by the amount of ye'elimite, the presence and quantity of other minor compounds, the amount of calcium sulfate added and its reactivity, and the setting time values can range from 30 minutes to 4 hours. Increased water/cement (w/c) ratio and lower temperatures can lead to an extension in setting time, just as with PCs. CSA cements can set in 10 minutes or less, especially at lower w/c ratios (Thomas et al., 2018). Li et al. (2018) measured the initial and final setting times of a CSA paste containing mainly ye'elimite (45.7%), anhydrite (19.7%), belite (11.9%) as 5 minutes and 11 minutes, respectively. These measurements were made at 20 °C at a w/c of 0.29. In such cases, workability issues may arise; however, this can be avoided by utilizing a specific retarding superplasticizer (Zhang et al., 1999; Quillin, 2001). Citric acid, tartaric acid, gluconate, carboxylic acids, and borax can be used as retarder (Chang et al., 2009; García-Maté et al., 2016; Zajac et al., 2016; Burris & Kurtis, 2018). In addition, although chloride salts are effective accelerators in PC, they have a retarding impact in CSA cements which depends on the dosage and the temperature (Zajac et al., 2016).

2.2.6.2 Compressive Strength

During hydration, increased precipitation of ettringite crystals forms a denser matrix, and considerable strength is attained at an early age. Compared with PC, the CSA cements' early-age and later-age strengths are generally higher (Lan & Glasser, 1996; Zhang et al., 1999; Sharp et al., 1999; Glasser & Zhang, 2001; Quillin, 2001; Winnefeld & Barlag, 2010; Juenger et al., 2011). Thomas et al. (2018) showed the compressive strength development of concretes cast with CSA cement, Type I cement, and Type III-high early strength cement (see Figure 2.5).

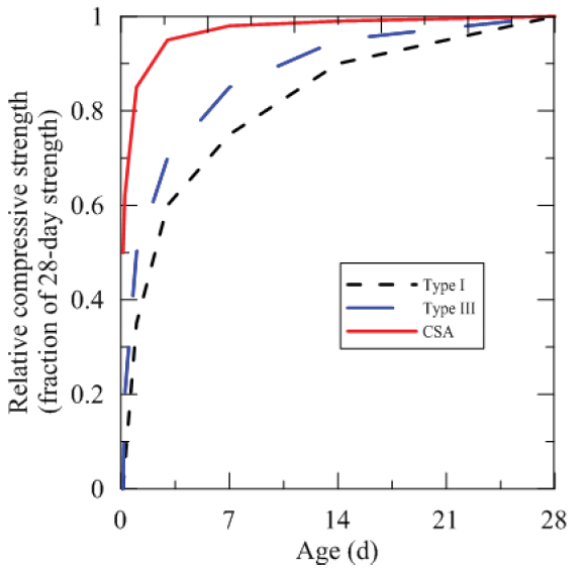

Figure 2.5 Compressive strength development of CSA and PC concretes (normalized to 28-day compressive strength) (Thomas et al., 2018)

As seen in Figure 2.5, the strength of CSA-based concrete increases very rapidly, even in comparison with Type III-based concrete. Within a few hours, CSA-based concrete samples reached almost half of their ultimate strength, and within the first three days, they reached almost 90% of their ultimate strength. According to some authors, the reason why a high early strength and relatively low or even no additional increase in strength is that free water is quickly consumed, and voids are filled with hydrates. Consequently, considerable amounts of unreacted phases such as C_2S,

C_4AF, $C\bar{S}$, and even $C_4A_3\bar{S}$ remain as mixed components in the hydrated structure (Bullerjahn, 2018).

The strength development is mainly influenced by the composition and the quantity of the phases contained in the cement. At appropriate calcium sulfate levels, an increasing proportion of the ye'elimite phase in the cement increases the early strength. However, the belite phase has an impact on the later strength of the cement primarily (Odler, 2000). In addition, the production parameters of cements, such as burning temperature and residence time in the kiln, impact the clinker phases significantly and thus the compressive strength of the cement. The w/c ratio and the admixture usage such as retarders are other relevant factors (Canbek & Erdoğan, 2020).

2.2.6.3 Durability

Field and laboratory studies on the durability of materials made from CSA-based cements have shown that these materials generally perform well when compared to the durability of PC-based materials (Sherman et al., 1995; Zhang et al., 1999; Glasser & Zhang, 2001; Quillin, 2001; Zhang & Glasser, 2005). However, the literature is quite limited on this topic, and further studies are needed to draw clear conclusions about their long-term behavior.

Generally, during the hydration of CSA cements, the available water is consumed within a short time. Furthermore, a high amount of hydration products is formed. This provides a dense microstructure with low porosity and permeability (Aranda & De la Torre, 2013; Thomas et al., 2018), and this well-made microstructure can show high resistance against freezing-thawing and chemical attacks by seawater, sulfates, chlorides, magnesium and ammonium salts (Bernardo et al., 2006; Juenger et al., 2011). The pore solution alkalinity of CSA cements is lower, compared to PC. However, it is still enough to form a passive layer on the embedded steel reinforcement, and this can protect steel from corrosion. Due to both the absence of

lime and the reduced alkalinity, CSA cements are advantageous in term of alkali-silica reaction (Juenger et al., 2011; Thomas et al., 2018). CSA cements are also shown to be highly resistant to sulfate attack (Glasser & Zhang, 2001; Aranda & De la Torre, 2013; Thomas et al., 2018).

While some studies on carbonation have indicated that PC-based and CSA-based concretes have similar carbonation rates (Glasser & Zhang, 2001; Winnefeld & Lothenbach, 2010), some studies have shown that the carbonation resistance of mortars and concretes made by CSA cement is lower than that of those made by PC (Ioannou et al., 2010; Juenger et al., 2011; Aranda & De la Torre, 2013; Hargis et al., 2017). The carbonation reaction of ettringite is as follows:

$$C_6A\bar{S}_3H_{32} + 3\bar{C} \rightarrow 3C\bar{C} + AH_3 + 3C\bar{S}H_2 + 23H \quad (21)$$

During carbonation, ettringite decomposes into gypsum, calcium carbonate, and aluminum hydroxide, which leads to solid volume reduction. This could result in strength losses, particularly in CSA-based products with higher w/c (Hargis et al., 2017).

2.3 Industrial Symbiosis

Industrial symbiosis (IS) is a notion that emerged by taking inspiration from nature. The term "symbiosis" is based on the concept of a biological symbiotic relationship in nature (Chertow, 2000). It is described as the association of different species providing mutual benefit to each other. Regarding the industrial environment, it means providing mutual networking and mutual benefits through the cooperation of different sectors (Schwarz & Steininger, 1997).

Approaches to basing organic relationships among industries on ecological science date back to the late 1940s (Renner, 1947). Over time, the term "industrial metabolism" (Ayres, 1989), "industrial ecosystem", and "industrial ecology" (Frosch & Gallopoulos, 1989) have been put forward by different researchers based on the

similarity of industrial activities to biological or ecological systems (Zhang et al., 2015).

Industrial metabolism represents the flow of materials and energy in an industrial system, from the extraction of resources to the disposal of waste. Industrial ecosystem is a term based on the cyclical use of resources in biological ecosystems. In an industrial ecosystem, the wastes of one industry process become raw materials for another industry and form the basis of industrial ecology (Frosch & Gallopoulos, 1989; Connelly & Koshland, 2001). Industrial ecology, which was frequently used synonymously with industrial metabolism in the early days, has overtaken industrial metabolism over time (Johansson, 2002). Industrial ecology is a concept that deals with the working mechanism of the industrial system, how it is regulated, and its interactions with the environment and the other industrial systems. Then it seeks how it can be redesigned to harmonize with the way natural ecosystems based on existing ecosystem knowledge (Erkman, 2001; Johansson, 2002). With this concept, the linear flow of the industrial system has been tried to transform into a more closed flow similar to that of ecological systems (Garner & Keoleian, 1995). This flow change in production systems was defined by Braden Allenby as the evolution from a Type I system to a Type III system, as indicated in Figure 2.6.

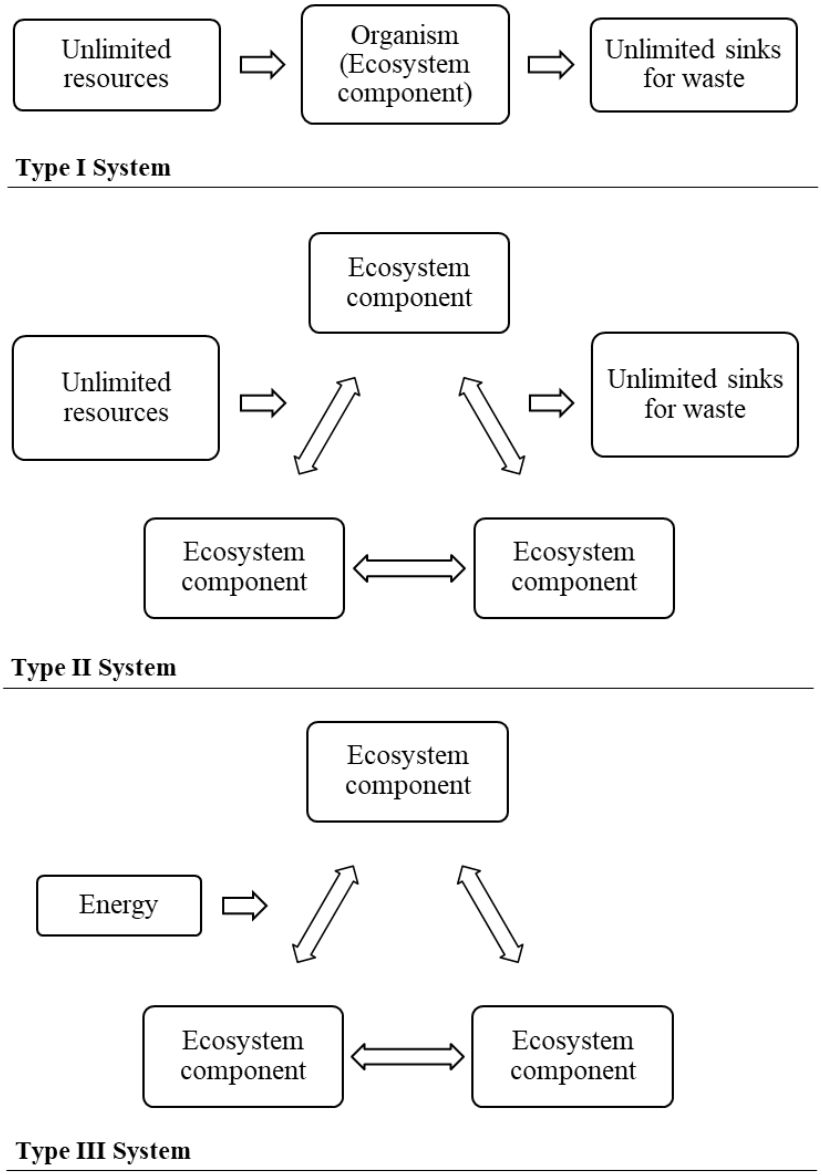

Figure 2.6 Types of production systems (adapted from Allenby, 1992)

A Type I system is a linear system in which raw materials and energy are consumed, products are manufactured, and then generated by-products/wastes are released to the environment. This system depends on a large and continuous supply of resources because by-products/wastes are not recycled or reused. This system is not sustainable unless the supply of materials and energy is infinite. A Type II system, which is more visible in most of today's industrial systems, represents a system in which part of the

waste is recycled or reused, and another part is disposed of. However, a Type II system is not yet truly sustainable since resource usage is necessary, albeit limited. A Type III system, on the other hand, is a highly integrated, closed system in which all materials and energy are in a complete cycle. In a completely closed system, the only thing coming from the outside is the solar energy, and all other materials are continuously reused and recycled in the system, representing true sustainability or circular economy (Garner & Keoleian, 1995).

Industrial ecology has three focuses at different scales: the firm level, the inter-firm level and the regional or global level (see Table 2.8) (Chertow, 2000). Briefly, it not only covers pollution and environmental issues but also addresses equally at technologies, process economics, business interrelationships, finance, general government policy, and the related issues involved in managing business enterprises (Erkman, 2001).

Table 2.8 Industrial ecology levels (Chertow, 2000)

Sustainability ⇩		
Industrial Ecology ⇩		
<u>Facility or Firm</u>	<u>Inter-Firm</u>	<u>Regional/Global</u>
•design for environment •pollution prevention •green accounting	•**industrial symbiosis** (eco-industrial parks) •product life cycles •industrial sector initiatives	•budgets and cycles •materials and energy flow studies (industrial metabolism)

As shown in Table 2.8, industrial symbiosis is a subfield of industrial ecology that includes the physical exchange of materials, energy, and by-products at the inter-firm level, where the firm operates in collaboration with other firms, preferably in geographic proximity, rather than as a stand-alone entity (Chertow, 2000; Ehrenfeld

& Chertow, 2002; Martin et al., 2015; Zhang et al., 2015; Petríková et al., 2016; Fraccascia et al., 2017). Industrial symbiosis closes loops by converting by-products/wastes into valuable materials that can be used as raw materials for another product or process in an industrial system to achieve a natural closed ecosystem (Morales et al., 2019).

The real-life application areas of industrial symbiosis concept can be observed in eco-industrial parks (Şenlier & Albayrak, 2011; Verguts et al., 2016). According to the US Environmental Protection Agency (EPA) Fieldbook,

> "an eco-industrial park is a community of manufacturing and service businesses seeking enhanced environmental and economic performance through collaboration in managing environmental and resource issues including energy, water, and materials. By working together, the community of businesses seeks a collective benefit that is greater than the sum of the individual benefits each company would realize if it optimized its individual performance only" (Lowe et al., 1996).

Evaluating the examples of industrial symbiosis networks can reveal that environmental, economic, business and social benefits have been provided. These benefits are listed in Table 2.9 (Mirata & Emtairah, 2005).

Table 2.9 Potential benefits of industrial symbiosis systems (Mirata & Emtairah, 2005)

Environmental benefits	• More efficient use of resources • Minimization of the use of non-renewable resources • Diminished emissions of pollutant
Economic benefits	• Lowering the cost of resource use in production • Lowering the cost of waste management • Additional revenue thanks to higher values of by-product and waste streams
Business benefits	• Advanced relationship with external parties • Development of a green vision, new products, and new markets
Social benefits	• Improving the quality of existing jobs • Creating new employment area • Obtaining a cleaner, safer, natural, and working environment

2.3.1 Industrial Symbiosis Examples around the World

The most well-known example related to the concept of industrial symbiosis is the Kalundborg Eco-Industrial Park in Denmark (Schwarz & Steininger, 1997; Chertow, 2000; Jacobsen, 2006; Neves et al., 2019). The Kalundborg network evolved spontaneously from a self-organized attempt of firms in the early 1970s and has grown over the years, both in terms of the number of symbioses and the number of partners. Today it is still considered as a successful-living example (Neves et al., 2019). The main collaborators of Kalundborg are an oil refinery, a power plant, a

gypsum board factory, a pharmaceutical plant, and the municipality of Kalundborg. They share groundwater, surface water, wastewater, steam, and electricity, and also exchange a variety of residues that serve as feedstock for other processes (Chertow, 2000). This symbiosis network has led to considerable savings of resources such as water, fuel, avoided wastes through with exchanges, and led to significant reductions in SO_2 and CO_2 emissions (Ehrenfeld & Chertow, 2002).

The National Industrial Symbiosis Programme (NISP), launched as a program in the UK, has also been one of the successful examples of industrial symbiosis, where significant environmental and economic gains have been achieved (Mirata, 2004).

In addition, there are many examples of industrial symbioses with various synergistic networks in many countries around the world, such as Europe, China, the USA, Canada, the United Kingdom, Japan, South Korea, Brazil, Australia, Algeria, and Morocco, as summarized by Neves et al. (2019).

2.3.2 Industrial Symbiosis in Türkiye

Studies on industrial symbiosis in Türkiye were initiated with "Industrial Symbiosis Project in Iskenderun Bay." Between 2011 and 2014, the implementation phase of the project was carried out in the Iskenderun Bay region covering Adana, Iskenderun, Mersin, and Osmaniye. The general aim of the project was to introduce industrial symbiosis in the Iskenderun Bay region as a mechanism to strengthen cooperation and unity between firms in order to improve both the environment and the economy in the region and to provide the background for a national industrial symbiosis program. The potential environmental, social, and economical gains achieved with the eight pilot projects implemented in Iskenderun Bay are summarized in Table 2.10 (Alkaya et al., 2014).

Table 2.10 Potential gains of the industrial symbiosis project in Iskenderun Bay

Environmental						
Landfill diversion	Water saving	Natural resource substitution	Workforce saving	Energy saving	CO_2 reduction	Land recovery
327 250 tons/year	6 500 m^3/year	276 250 tons/year	3 500 man-day year	33 580 000 kWh/year	36 700 tons/year	45 000 m^2
Social						
New employment		New initiative		Organizations participated		Universities contributed
21		6		27		5
Economic						
New product	Amount of new products		Investment cost	Annual net earnings		Pay-back period
10	283 000 tons/year		6 965 000 $	6 370 500 $		1.1 year

Other reported industrial symbiosis projects in Türkiye are the "Trakya Industrial Symbiosis Program" (2014-1016), "Bursa Eskisehir Bilecik Industrial Symbiosis Program" (2014-2015) and "Industrial Symbiosis and Eco-efficiency Project in Antalya Organized Industrial Zone" (2015-2017), "Gaziantep Industrial Symbiosis Program" (2015-2016), "Green Organized Industrial Zone Framework Development for Türkiye" (2016-2018), "Eco-Industrial Park Transformation in Izmir: Green IAOSB" (2019), "Eco-Industrial Park Transformation Project in Tire Organized Industrial Zone" (2019-2020) (Dolgen & Alpaslan, 2020).

2.3.3 The FISSAC Project

The FISSAC project called "Fostering Industrial Symbiosis for a Sustainable Resource Intensive Industry across the extended Construction Value Chain" is a Horizon 2020 research project involving 26 collaborators from 9 countries, including

8 EU member states and Türkiye. The general goal of the FISSAC project is to develop and demonstrate a new industrial symbiosis model that steers the material process towards a zero-waste approach in the resource-intensive sectors of the construction value chain, leading to closed material loops and enabling the transition to a circular economy. The targeted innovative construction products within the scope of the FISSAC project and the wastes/by-products of the various industries used in these productions are illustrated in Figure 2.7 (FISSAC, 2020).

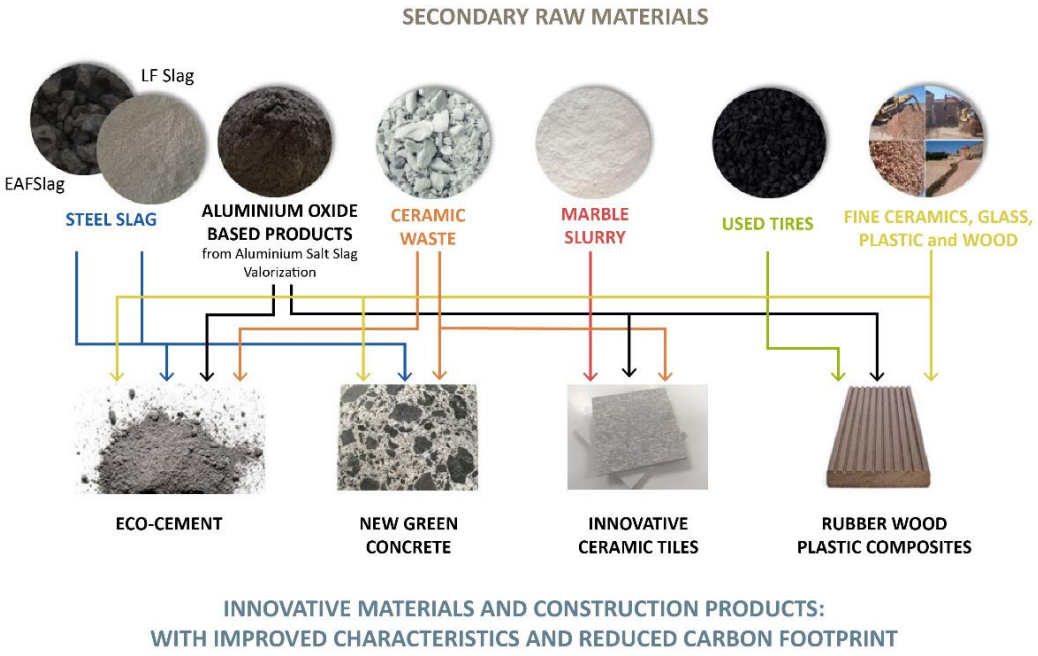

Figure 2.7 FISSAC industrial symbiosis network (FISSAC, 2020)

The collaborators in the Turkish leg of the FISSAC project were "TürkÇimento" and "Ekodenge." The materials utilized within the experimental program of this thesis study were obtained via the FISSAC project. As part of the FISSAC project, industrial production of a blended cement was also conducted, which was later utilized in a concrete road.

Under the scope of this thesis, the following wastes/by-products (which were obtained through FISSAC project) were utilized to produce CSA cements under

laboratory conditions. A general description for each of these materials is presented in the following sections.

2.3.3.1 Aluminum Salt Slag and "Serox"

Aluminum is one of the much-used non-ferrous metals obtained from natural ores mining and used in a wide variety of products (Liu & Müller, 2012). Unlike most other metals, aluminum can be repeatedly recycled into new aluminum products. In other words, aluminum can be obtained in two different ways, from primary and secondary aluminum production, depending on the raw materials used. Bauxite ore is used for primary aluminum production, while aluminum scrap is recycled and remelted for secondary aluminum production. The process of recycling aluminum consumes about 5% of the energy needed to produce primary aluminum and emits scarcely 5% of greenhouse gasses from primary aluminum production. It is obvious that secondary production brings economic and environmental benefits both by saving raw materials and energy, and recycling waste products instead of sending them to a landfill (Tsakiridis, 2012; Tolaymat & Huang, 2015).

The aluminum production processes generate various types of wastes. One of the main wastes created in the production of secondary aluminum is salt slag, also known as saline slag or salt cake (Tolaymat & Huang, 2015; Gil & Korili, 2016; Yoldi et al., 2019). These salt slags come from salt fluxes used in smelting furnaces to lower the melting temperature, prevent oxidation, and promote the removal of certain impurities such as Mg, Ca, Li. Proprietary salt flux contains NaCl, KCl, and small quantities of calcium fluoride (CaF_2). Up to 5% additional fluoride can also be added. The salt slag consists of metallic aluminum, various impurities separated from the molten metal by flux, and large amounts of aluminum oxides (see Table 2.11). The typical components of salt slag's insoluble, non-metallic part are also shown in Table 2.12 (Cusano et al., 2017).

Table 2.11 Typical contents of the aluminum salt slag (Cusano et al., 2017)

Contents	Typical Value (%)	Range (%)
Al, metallic	6	4-10
Water-soluble salts	37	20-55
Metal oxides, unrecovered metal, and insoluble salts	55	35-75

Table 2.12 Typical contents of the insoluble non-metallic part of the aluminum salt slag (Cusano et al., 2017)

Contents	Weight (%)	Contents	Weight (%)
Al_2O_3	60-75	TiO_2	0.5-1.5
MgO	3-14	MnO	<0.3
SiO_2	3-12	Na_2O	<1
CaO	1.5-5.0	K_2O	<1.2
Fe_2O_3	1.5-3.0	Cl^-	<0.8
Bound water	7-16		

However, the chemical and mineralogical content of salt slag varies depending on the type of aluminum scrap recycled and the recycling processes used, such as furnace type, salt composition, etc. Based on these factors, fluorides (CaF_2, NaF, AlF_3, Na_3AlF_6, etc.), nitrides (AlN), carbides (Al_4C_3), phosphides (AlP), sulfites (Al_2S_3), etc. may be present in addition to metallic aluminum, metal oxides (Al_2O_3, MgO, SiO_2, CaO, etc.), and chlorides ($AlCl_3$, NaCl, KCl) (Gil & Korili, 2016; Padilla et al., 2022).

Because of its content, salt slag is categorized in the "European Waste Catalogue and Hazardous Waste List" as a hazardous waste requiring proper disposal methods (EPA, 2002). Salt slag is regarded as "highly flammable", "irritant", "harmful" and "leachable", and improper disposal is a critical issue that can lead to serious

environmental problems. In such a case, toxic metal ions in its content may leach into groundwater around the disposal area. Since their reactivity is high, when in contact with water or even with the moisture in the air, such reactions may cause the release of toxic, harmful, explosive, poisonous, and unpleasant-smelling gases such as CH_4, NH_3, PH_3, H_2, H_2S (Tsakiridis, 2012).

Several million tons of salt slag are generated annually, and this number is increasing with the growing use of aluminum, especially recycled aluminum. An estimated 95% of these are disposed of, and the disposal costs amount to around 80 million euros (Gil & Korili, 2016). The amount of salt slag formed, as well as its content, varies depending on factors such as scrap mix, furnace type use, the operation mode (Tsakiridis, 2012; Gil & Korili, 2016). The 2012 review study by Tsakiridis states that one ton of secondary production yields between 200-500 kg of salt slag, and the 2016 review study by Grill & Korili states that this ratio is 300-600 kg.

Since landfilling of salt slag raises an environmental concern, recycling salt slag instead of its disposal eliminates the need for landfills. In this way, a significant environmental problem is solved, and also new economic opportunities are generated (Yoldi et al., 2019). Partial recovery of aluminum salt slag, e.g., aluminum only or KCl only, or full recovery, in which the three main components are recovered, is possible. In 2014, it was reported that one million tons of salt slag are produced and processed annually in the EU-28 countries (Cusano et al., 2017).

The conventional recovery involves three phases: grinding-sieving, dissolution-reaction, and filtration-evaporation. First, the salt slag is ground and sieved to recover the metallic portion. In the second phase, the residual part is treated by water leaching at room temperature or higher temperature and pressure to dissolve the salts. In the last phase, the salt is recovered by filtration and evaporation technology (Tsakiridis, 2012).

Salt slag treatment, which minimizes landfill challenges, is generally carried out in Europe, Canada, and the USA. The non-metallic oxide part obtained from the salt slag recovery, which mainly contains alumina and minor amounts of other oxides,

can be used as an alternative alumina source in various industries such as ceramic, cement, and construction (Tsakiridis, 2012). Alumina, which turns into a commercial by-product from waste with this recovery, is marketed as BFA or other brand names such as Serox, and Paval (Befesa, 2019), Valoxy, Noval, and Oxiton (Gil & Korili, 2016). The salt slag recovery process at the Befesa Aluminio S.L. plant (Valladolid, Spain), which is one of the partners of the FISSAC project, is shown in Figure 2.8. It is seen that recycling one ton of salt slag yielded 500 kg of Al_2O_3-based new by-product, called Paval, in the market.

In this study, another commercial product of Befesa Aluminum Salt Slag Recycling Plant (Spain), Serox, was used as the alumina source. Befesa reported that in 2020, 426 thousand tons of aluminum salt slag were recycled, and about 368 thousand tons of aluminum oxide and others were obtained (Befesa, 2020). It should be noted that Serox is one of the trademarks of the alumina obtained in this recycling process and that in this thesis, the term Serox was used instead of alumina raw material.

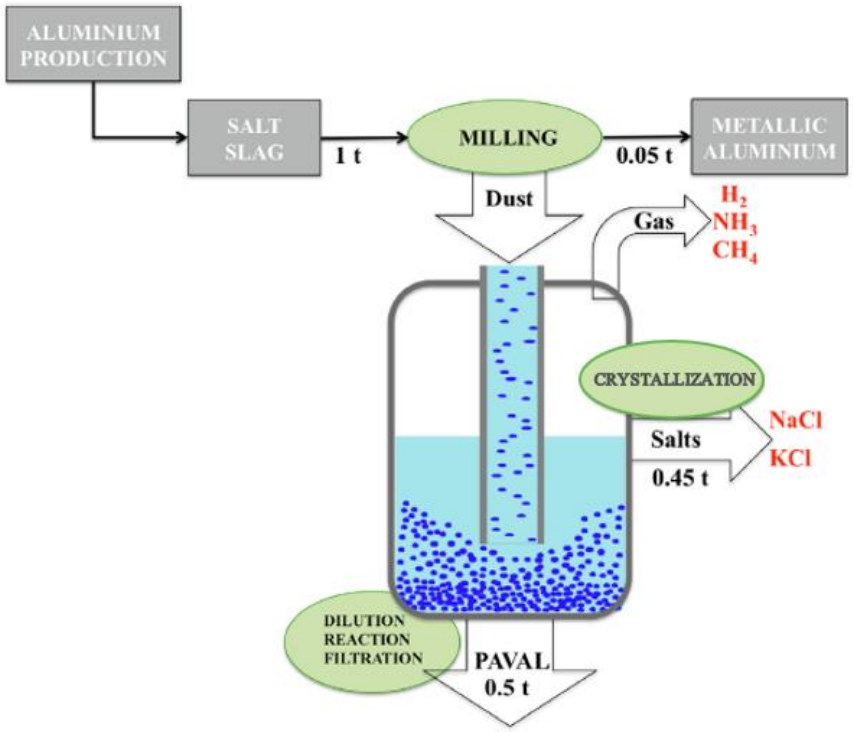

Figure 2.8 Full recovery scheme of aluminum salt slag (Font et al., 2020)

2.3.3.2 Ladle Furnace Slag

The iron and steel industry uses two main routes to produce steel: primary and secondary steel production. The former route, also known as integrated steel production, uses iron ore as the raw material, whereas the latter uses steel scrap. A typical integrated steelmaking plant is blast furnace/basic oxygen furnace (BF/BOF) based. Secondary steelmaking, on the other hand, melts steel scrap directly in an electric arc furnace (EAF) (Pardo et al., 2012).

Depending on the technology used in production, different types of slags are generated as wastes (which are also considered by-products), such as blast furnace slag, basic oxygen furnace slag, electric arc furnace slag, argon oxygen decarburization slag, and ladle furnace slag (Adolfsson et al., 2007).

Ladle furnace slag (LFS) is formed during further refinement of molten steel that has gone through initial refinement in a BOF or an EAF. In the refinement stages, the fluxes used to separate impurities from the steel affect the chemical composition of the resulting slags (Shi & Hu, 2003). LFS is also known as white slag, reducing slag, basic slag or refining slag (Skaf et al., 2016).

The chemical composition of LFS might vary from batch to batch because scrap melting is done in batches. Local conditions, production processes, and scrap metal differences can all have an impact on the chemical composition of the slag formed. CaO and MgO typically account for more than 60% of the LFS by weight. The remaining less than 40% of the entire weight is composed of SiO_2, Al_2O_3 and Fe_2O_3. Other compounds, involving manganese and titanium oxides, sulfur from the steel desulfurization stage, and calcium fluoride, are also present at minor amounts (Vilaplana et al., 2015).

Dicalcium silicate (C_2S), generally γ polymorph, merwinite ($Ca_3Mg(SiO_4)_2$), bredigite ($Ca_7Mg(SiO_4)_4$), and periclase (MgO) are the primary minerals found in LFS (Kriskova et al., 2014). During cooling, based on the temperature zones, C_2S undergoes a series of polymorph transformations such as from α-C_2S to β-C_2S and

from β-C_2S to γ-C_2S. The transformation β to γ polymorph causes a volume increase of almost 10%, and the crystals to shatter into dust. The fine portion less than 75 μm in LFS can be as much as 20-35% (Shi & Hu, 2003).

LFS is usually around a third of the slag produced in an EAF, and the annual production in Europe is anticipated to be about 4 million tons (Murri et al., 2013). A significant amount of LFS is disposed of in landfills near manufacturing centers, leading to environmental and visual issues (Skaf et al., 2016). The major problems caused by the landfilling of LFS are the decomposing of LFS into a fine-grained material, causing dust to spread, and hexavalent chromium (Cr(VI)) leaching, as well as the release of some other toxic elements (Serjun et al., 2015). For every ton of steel refined, around 60-80 kg of LFS is recovered. Different amounts of LFS are frequently reintroduced into the steelmaking process (Skaf et al., 2016). LFS are also currently utilized in fields such as agriculture and environmental engineering (Vilaplana et al., 2015). Unlike EAF slags, which are widely used in construction applications, the use of LFS is limited, especially because of its high CaO content which causes volume stability issues upon hydration. However, LFS appears to be a promising alternative as a raw material in cement manufacture due to its high CaO content (40-50%) and comparatively high silica content (20-35%) (Mancio et al., 2011).

Vilaplana et al. (2015) investigated the usability of LFS as a raw material in PC production. A raw meal with a limestone / shale / LFS / mill sludge content of 45.1% / 14.4% / 39.2% / 1.3% by weight was prepared, formed into square plates, and fired in a laboratory kiln at 1550°C. The clinker was rapidly cooled by blowing cool air and ground with 5 wt.% gypsum. They revealed that adding LFS to the raw meal affects cement properties positively, especially in terms of compressive strength and dimensional stability. However, the initial setting time of the produced cement was measured to be 120 minutes, which is quite high when compared to ordinary PC.

In another work, Nguyen et al. (2019) indicated that a binder based on ettringite can be developed as a result of hydrations between an LFS, which has self-reactive

properties, and gypsum. Thus, they showed that LFS could be used as a good alternative raw material for an ettringite-based binder that could be employed in various construction applications.

In this study, LFS was obtained from Ekinciler Iron and Steel Industry as part of the FISSAC project.

2.3.3.3 Ceramic Waste

In general, the term "ceramics" refers to inorganic materials (possibly with some organic content) consisting of non-metallic compounds, which are permanently hardened by firing. The ceramic industry offers a wide range of products, and it is divided into sub-sectors such as bricks and roof tiles, wall and floor tiles, refractory products, vitrified clay pipes, sanitary ware, and inorganic bonded adhesive, depending on the products manufactured. Ceramic products are manufactured by firing mainly of clays and other raw materials such as quartz, feldspar etc. at high temperatures (European Comission, 2007).

According to the Ceramic World Report, the global production of ceramic tiles in 2019 is about 12.67 billion square meters, and Türkiye ranks 10th among the leading producing countries with 296 million square meters (CRW, 2020). In the production of ceramic tiles, a great deal of waste is generated at various stages of production due to broken pieces or inferior products. A significant percentage becomes unusable due to changes in the composition of the ceramic material (such as color and glaze) during the production process (Poyraz & Yılmaz, 2018). Awoyera et al. (2017) stated that approximately 30% of the materials used in the production of ceramic tiles end up as waste. The share of non-standard tiles in the total production of the ceramic tile industry can be up to 7%, and they are mostly discarded due to the high-quality control (Meena et al., 2022). In Türkiye, ceramic tile wastes are disposed of directly in landfills that are usually close to the plants. In addition, waste storage creates a

significant environmental problem, particularly in the cities where there is a lack of disposal sites (Elçi, 2016).

On the other hand, ceramic wastes may have properties that make them suitable for use as pozzolans since heat-treated clays are known to have pozzolanic properties (Sánchez de Rojas et al., 2009; Zimbili et al., 2014). As shown in the review study by Meena et al. (2022), many studies reveal that ceramic wastes can be used as a cement or aggregate replacement material in concrete. Therefore, with the use of ceramic wastes in the cement and concrete industry, a good alternative recycling route for these wastes can be obtained.

In this study, the ceramic wastes of wall and floor tiles were obtained from Çanakkale Ceramic as part of the FISSAC project.

2.3.3.4 Glass Waste

Glass, a highly transparent material, is generally manufactured by melting a mixture of substances such as silica, soda ash, and $CaCO_3$ at high temperatures and then cooling it. During cooling, solidification takes place without crystallization. Glass is widely used in our lives in various products such as flat glass, bottles, glassware, and vacuum tubes (Park et al., 2004). Glass is not a biodegradable material. Therefore, storing glass waste in landfills does not offer an environmental solution. Nevertheless, an environmental solution is achieved by evaluating the waste rather than disposing it (Shao et al., 2000).

Due to its high silica content and highly amorphous structure, glass waste shows pozzolanic properties. For this reason, just like the ceramic wastes, glass wastes can also be used by the cement and concrete industry, which will be a good alternative recycling route for these wastes. Fine and coarse aggregates, blended cement, bricks, blocks, ceramics and concrete are listed as construction materials in which glass waste can be used (Safiuddin et al., 2010)

In this study, glass wastes were obtained from Trakya Cam, a subsidiary company of Şişecam, as part of the FISSAC project.

2.4 Point of Departure and Existing Literature Gap

As the literature shows, PC production consumes a large amount of energy and raw materials and is a significant CO_2 emitter. Compared to PC, the sintering temperature of CSA cements is about 200°C lower, and the limestone requirement is less. Due to less energy consumption and less CO_2 emissions, CSA seems to be a promising alternative binder to PC. On the other hand, the availability and high cost of the raw material, bauxite, form economic challenges for CSA cement. The economic challenges have prompted research on using industrial wastes/by-products in CSA cement production. In this context, various industrial wastes/by-products have been used together with natural raw materials in CSA cement production as summarized in Section 2.2.4.2.

The starting point of this thesis is to produce CSA cement with an industrial symbiosis approach. In this symbiosis, ceramic waste from the ceramic industry, LFS from the secondary steel industry, Serox from the secondary aluminum (non-ferrous metals) industry, and glass waste from the glass industry will simultaneously be used as raw materials for CSA cement production. More than 40% of the CSA cement raw meal produced will consist of waste/by-products of four different resource-intensive industries. One of the most important points is that instead of bauxite, aluminum oxide (Serox) obtained from the recycling of aluminum salt slag, which is the waste of the secondary aluminum sector, will be used. Thus, a more sustainable CSA production will be achieved by considering the zero-waste approach in the resource-intensive sectors of the construction value chain.

CHAPTER 3

EXPERIMENTAL PROGRAM

3.1 Materials

In this thesis, CSA cements were synthesized using an industrial symbiosis approach, i.e. the waste of one industry would be the raw material of another industry. All materials used in the experimental program were obtained by the FISSAC project that was briefly mentioned in Chapter 2. The wastes, which are the raw materials for CSA cement synthesis, come from the non-ferrous metals, steel, ceramic, and glass industries. In addition to industrial waste materials, some raw materials were also used due to the lack of sulfate and calcium oxide required to synthesize the CSA cement.

3.1.1 Natural Materials

Limestone and gypsum were obtained from Hasanoğlan region. The oxide compositions of the materials were determined through X-ray fluorescence (XRF) analysis in TürkÇimento. The main oxide compositions of the materials are given in Table 3.1. The mineralogical composition of the materials was determined through X-ray diffraction (XRD) analysis in METU Central Laboratory. The XRD patterns of the natural resources are given in Figure 3.1. As seen in Figure 3.1 (a), the dolomite phase ($CaMg(CO_3)_2$) was also identified besides calcite ($CaCO_3$) in limestone.

Table 3.1 Main oxide composition of natural materials used

Main oxides (%)	Limestone	Gypsum
SiO_2	0.99	2.02
Al_2O_3	0.34	0.29
Fe_2O_3	0.19	0.29
CaO	50.59	32.22
MgO	4.06	0.29
Na_2O	<0.01	0.05
K_2O	0.09	0.08
TiO_2	-	0.04
MnO	-	0.01
SO_3	0.04	43.90
Cl^-	0.0086	0.0057
LOI	43.60	20.77

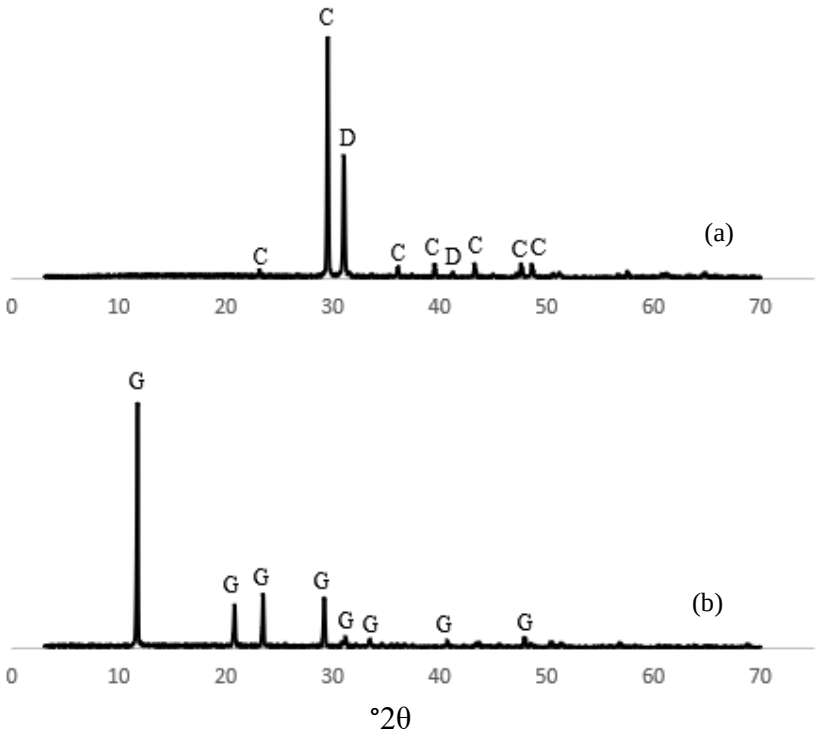

Figure 3.1 XRD patterns of natural materials used: (a) limestone (b)gypsum (C: Calcite, D: Dolomite, G: Gypsum)

3.1.2 Waste Materials

In addition to natural raw materials, Serox, ladle furnace slag (LFS), ceramic waste and glass waste were used for the synthesis of CSA cements. Detailed information on these materials is provided in Section 2.3.3. Briefly, Serox is a by-product of recycling aluminum salt slag from secondary aluminum production. It is a commercially available secondary mineral, primarily alumina, and has similar characteristics to bauxite. LFS is a waste that can be also considered as a by-product generated in the final stages of steelmaking. In this study, LFS from an EAF steel production, ceramic waste from wall and floor tiles, and glass waste from flat glass production were used. Serox was supplied by Befesa, Spain, while the other materials were provided by local suppliers in Türkiye; LFS from Ekinciler Iron and Steel Industry, ceramic waste from Çanakkale Ceramic, and glass waste from Trakya Cam, a subsidiary company of Şişecam. The oxide composition of the industrial wastes was analyzed with the ICP-OES instrument (Spectro Ciros Vision) in TürkÇimento, and the analysis results are presented in Table 3.2.

Table 3.2 Main oxide composition of industrial wastes used

Main oxides (%)	Serox	LFS	Ceramic waste	Glass waste
SiO_2	8.62	22.40	63.29	71.46
Al_2O_3	66.40	6.34	19.63	0.84
Fe_2O_3	1.83	2.35	2.34	0.12
CaO	1.49	52.44	7.49	8.52
MgO	8.38	6.78	0.72	4.46
Na_2O	1.05	0.75	0.87	13.11
K_2O	0.72	0.09	2.82	0.40
TiO_2	1.18	0.34	1.43	<0.01
P_2O_5	0.13	0.03	0.23	0.02
SO_3	0.14	2.85	0.09	0.04
Cl^-	0.4700	0.0326	0.0152	0.0050
F^-	0.30	1.16	0.39	0.03
Free CaO	0.03	2.43	0.05	0.16
LOI	6.90	3.49	0.62	0.13

The mineralogical composition of the waste materials was determined through XRD analysis in TürkÇimento. The XRD patterns of the waste materials are given in Appendix A. The identified phases as a result of XRD analysis are as follows:

- Corundum (Al_2O_3), spinel ($MgAl_2O_4$), tobermorite ($Ca_5Si_6O_{16}(OH)_2$), quartz (SiO_2), boehmite (AlO(OH)), and calcium titanium oxide ($Ca(TiO_3$) for Serox
- Larnite (β-C_2S), calcio-olivine (γ-C_2S), mayenite ($Ca_{12}Al_{14}O_{33}$), bredigite ($Ca_{14}Mg_{12}(SiO_4)_8$), pargasite ($K_{0.1}Na_{0.9}Ca_{1.7}Mg_{2.65}Ti_{0.2}Fe_{1.6}Al_{2.5}Si_{6.2}O_{22}$) for LFS
- Quartz (SiO_2), albite ($NaAlSi_3O_8$), and mullite ($Al_{2.32}Si_{0.68}O_{4.84}$) for ceramic waste
- An amorphous structure only for glass

3.2 Synthesis

After the chemical analysis of the raw materials, different formulations for the production of CSA cement were created considering the CSA cements in the literature, and preliminary trials were carried out, and accordingly, three different formulations with high waste content (>40%) were formed. The mixtures were labeled as Mix A, B, and C. The percentages of raw materials in the mixtures are shown in Table 3.3. As seen in Table 3.3, the total percentage of waste materials was 45%, 42%, and 52% for Mix A, Mix B, and Mix C, respectively.

Table 3.3 Composition percentages of raw meals

(%)	Limestone	Gypsum	Serox	LFS	Ceramic waste	Glass waste
Mix A	28	27	23	14	7	1
Mix B	29	29	16	19	4	3
Mix C	12	36	16	33	1.5	1.5

The raw materials were ground in a laboratory ball mill down to 90 μm size. The raw meals were prepared according to the ratios given in Table 3.3 and homogenized using a mixer. For the uniform clinkerization, the raw meals were mixed with distilled water with a water-to-cement ratio (w/c) of 0.30 in the mixer. After preparation of the raw meal paste, it was formed into small rods, placed on a refractory plate and burned in an electric furnace (Protherm MoS–B 160/8). All the manufacturing steps are shown in Figure 3.2, and the burning process is illustrated in Figure 3.3 (Arjunan et al., 1999). According to this process, the temperature was first increased to 800 °C in one hour (~13 °C/min) and kept constant at 800 °C for 30 minutes. Then, the temperature was raised to 1250°C (5 °C/min) in 90 minutes. After keeping it stable at this temperature for another 90 minutes, the process was terminated. In order not to damage the furnace heating elements, the clinkers were taken when the furnace temperature reached room temperature without rapid cooling. All clinkers were ground in a ball mill to pass through a 90 μm sieve.

Figure 3.2 Manufacturing process of CSA cements

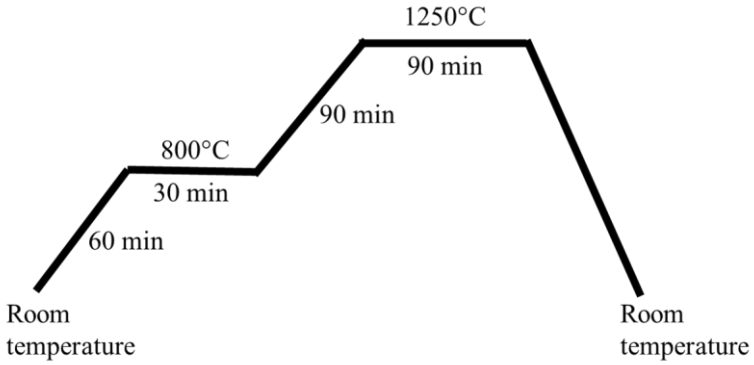

Figure 3.3 The burning process used for CSA cements

3.3 Analyses

The analyses performed were divided into three groups: analyses on CSA cements, pastes, and mortars. First, chemical, physical, mineralogical, and morphological analyses were performed on the synthesized CSA cements. Then, cement pastes and mortars were prepared, and the hydration development of the products was investigated by various test method. Finally, the environmental performance of the cements was evaluated using the Monte Carlo simulation technique. The environmental assessment results are presented in Chapter 5.

3.3.1 Analyses on CSA Cements

3.3.1.1 Chemical Analysis

The chemical analysis was performed on both raw meals and resultant cements. X-ray fluorescence (XRF) spectrometry was used for the quantitative determination of the elemental major oxide composition using the XRF device (ZSX Primus 2) in TürkÇimento.

3.3.1.2 Physical Analysis

Density and Blaine fineness values of the synthesized CSA cements were determined according to EN 196-6. The particle size distributions (PSD) of cements were determined using Malvern Mastersizer 2000 laser diffraction equipment in TürkÇimento.

3.3.1.3 Mineralogical Analysis

The quantitative mineralogical composition of the synthesized CSA cements was determined by X-ray diffraction (XRD) analysis. The analyses were made with the Rigaku Ultima IV XRD device in TürkÇimento. PDXL software with Pdf-4 database was used to identify minerals. Before analysis, the samples were pulverized and sieved through a 45 μm sieve. The analyses were performed in the angle range of 3° to 70° 2θ. Besides, the ground CSA cements were investigated by scanning electron microscope with energy dispersive X-ray spectroscopy (SEM-EDX), "Quanta 400F Field Emission SEM", at the METU Central Laboratory.

3.3.2 Analyses on CSA Cement Pastes

3.3.2.1 Setting time and Soundness

The initial and final setting times and the soundness of the CSA pastes were determined according to EN 196-3.

3.3.2.2 Isothermal Calorimetry

The heat evolution of the CSA cement pastes was measured through TAM AIR isothermal calorimeter, an 8-channel micro-calorimeter located at METU Materials of Construction Laboratory. Each channel consists of two inner channels, one for the

sample and one for the reference. For each mix, 4 g of cement and 2 g of distilled water were used. As the reference material, silica sand was used with the same thermal mass as the sample tested. An in-situ mixing procedure in ASTM C 1702 was applied. In this method, the sample and water are kept in temperature equilibrium and mixed inside the calorimeter channel. Since the in-situ mixing method is used, the heat of hydration data can be measured from the first mixing moment. The mixes' heat flow and cumulative heat curves were obtained for 72 h at a temperature of 23°C.

3.3.2.3 X-ray Diffraction Analysis

Cement pastes containing 4 g of CSA cement and 2 g of distilled water were prepared to monitor the products of the hydration processes. They were kept in a moist room for the first 24 h. After that, the samples were cured in water until testing day. The qualitative XRD analysis of unhydrated CSA cements and hydrated cement pastes at hydration ages of 1 h, 3 h, 6 h, 24 h, 3 d, 7 d, 28 d, 90 d, 180 d, and 360 d were performed at METU Central Laboratory. Before analysis, the samples were pulverized and sieved through No:100 sieve, except for the 1-hour samples. The XRD device used was the Rigaku Ultima IV XRD instrument with CuKα radiation (40 kV/30 mA) in METU Central Laboratory. Samples were scanned in the range of 3° to 70° 2θ. Qualitative information of the crystalline phases was obtained using the X'Pert HighScore software.

3.3.2.4 Thermogravimetric/ Differential Thermal Analysis

Thermogravimetric/ Differential Thermal Analyses (TGA/DTA) were performed simultaneously on the hydrated pastes to investigate the products of the hydration progress of the CSA cements. Setaram Labsys Thermogravimetry Analysis and Differential Thermal Analysis System at METU Central Laboratory were used for analyses. Measurements were made in the temperature between 25°C and 1000°C

with a 10°C/min heating rate. Analyses were made on the samples at the hydration ages of 7 d, 28 d, 90 d, 180 d, and 360 d.

3.3.2.5 Scanning Electron Microscopy

The microstructure of the CSA pastes was investigated by scanning electron microscope with energy dispersive X-ray spectroscopy (SEM-EDX), "Quanta 400F Field Emission SEM", in the METU Central Laboratory. Analyses were made on the samples at the hydration age of 28 d, 90 d, and 360 d. Before analyses, samples in small pieces were kept in a vacuum oven at 40°C and then coated with gold-palladium.

3.3.3 Analyses on CSA Cement Mortars

The compressive strength of the mixes was determined according to the EN 196-1 standard. The prismatic samples of 40*40*160 mm^3 were casted using the CSA cement, tap water, and standard sand, with a water-to-cement ratio (w/c) of 0.5. The compressive strength measurements were done at the hydration ages of 3 h, 6 h, 12 h, 24 h, 3 d, 7 d, 28 d, 90 d and 180 d. The mortars to be tested before 24 hours were cured in a moist room with a temperature of 23±2°C. They were demolded just before the test hour. Other mortar samples were demolded at the end of 24 hours and cured in water at 23±2°C until the test day. The compressive strength of the mixes was measured by a universal testing machine (UTEST UTCM-6420) located at METU Materials of Construction Laboratory with a loading rate of 2.4 kN/s.

CHAPTER 4

RESULTS AND DISCUSSIONS

4.1 Characterization of the Raw Meal

The theoretical oxide compositions of the raw meals were calculated using the oxide composition (Table 3.1, Table 3.2) and the weight percentage (Table 3.3) of each raw material are given in Table 4.1. Table 4.1 also includes the experimentally determined oxide compositions of raw meals. Considering the oxide compositions found by both methods, it can be said that the raw meals prepared are homogeneous.

Table 4.1 Main oxide composition of the raw meals

Oxides (%)	Theoretically computed			Experimentally determined		
	Mix A	Mix B	Mix C	Mix A	Mix B	Mix C
SiO_2	10.99	11.18	11.64	10.13	10.28	10.53
Al_2O_3	17.74	12.82	13.17	16.64	13.48	13.74
Fe_2O_3	1.05	0.98	1.23	1.15	0.90	0.92
CaO	31.27	34.77	35.45	33.63	34.67	36.79
MgO	4.21	4.05	4.25	3.57	4.23	4.21
SO_3	12.28	13.31	16.77	11.92	13.15	16.24
Na_2O	0.55	0.76	0.64	0.39	0.95	0.71
K_2O	0.42	0.31	0.23	0.25	0.50	0.37
LOI	19.89	20.46	14.98	20.02	20.16	16.04

4.2 Characterization of the CSA Cements

4.2.1 Chemical Properties

The oxide compositions of the three CSA cements obtained after the burning of raw meals and the grinding are presented in Table 4.2. It should be noted that in the CSA

cements calcium sulfate was not added during the grinding stage, unlike ordinary portland cement. It can be seen from Table 4.2 that the principal oxides of the CSA cements are CaO, Al_2O_3, SO_3, and SiO_2. As mentioned in Chapter 2, CSA cements have a wide range of oxide compositions. Commercially available CSA cements that are reported in the literature have the following oxide compositions; CaO: 40.5%-49.5%, Al_2O_3:14.7%-34.2%, SiO_2: 3.4%-14.3%, SO_3: 11.02%-19.5%. Considering these ranges specified for each oxide, the cements produced appear compatible with the commercially available CSA cements reported in the literature regarding the chemical composition. The Al_2O_3 content of Mix A, which contains a higher proportion of Serox, and the SO_3 content of Mix C, which includes a higher proportion of gypsum, seem to be slightly higher when all three cements are considered.

Table 4.2 Main oxide composition of the CSA cements

Oxides (%)	Mix A	Mix B	Mix C
SiO_2	13.03	13.26	12.97
Al_2O_3	20.03	17.14	16.13
Fe_2O_3	1.56	1.14	1.21
CaO	43.61	44.41	42.97
MgO	3.83	5.38	5.10
SO_3	15.96	16.68	19.54
Na_2O	0.49	0.77	0.70
K_2O	0.35	0.32	0.26
TiO_2	0.42	0.32	0.40
P_2O_5	0.09	0.06	0.05
LOI	0.18	0.21	0.32

4.2.2 Mineralogical Properties

The XRD patterns of the three CSA cements are presented in Figure 4.1. In addition, quantitative results of the identified mineral phases are also listed in Table 4.3. PDXL software with Pdf-4 database was used to identify minerals.

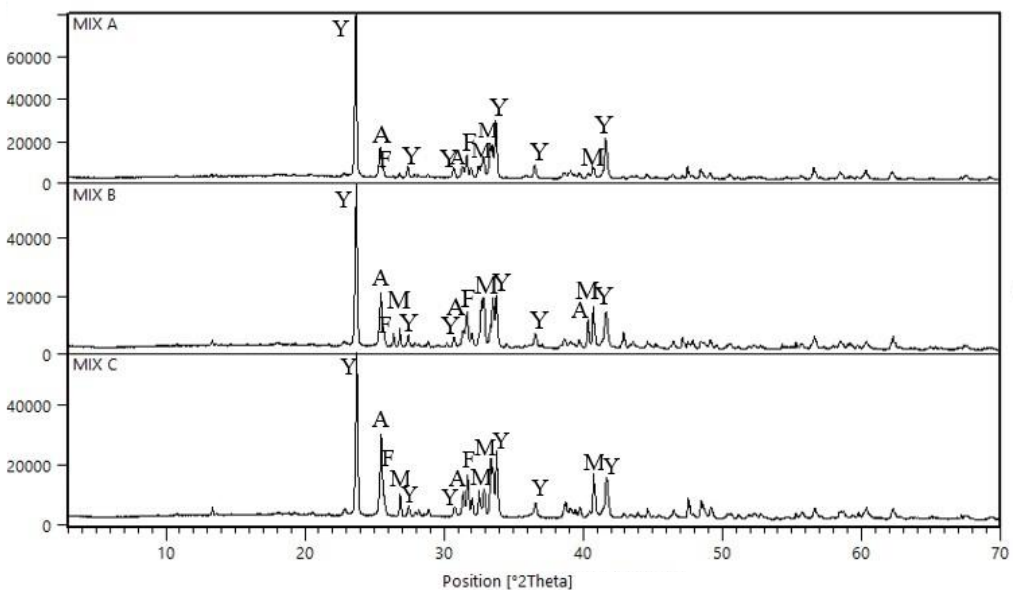

Figure 4.1 XRD patterns of cements (Y: Ye'elimite, A: Anhydrite, M: Merwinite, F: Ellestadite-F)

Table 4.3 Quantitative phase composition of the CSA cements

Minerals (%)	Formula	Mix A	Mix B	Mix C
Ye'elimite	$Ca_4Al_6SO_{16}$	48	35	33
Anhydrite	$CaSO_4$	12.7	13.5	25.3
Merwinite	$Ca_3MgSi_2O_8$	21.4	20	21
Ellestadite-F	$Ca_5(SiO_4)_{1.5}(SO_4)_{1.5}Cl_{0.2}F_{0.8}$	16.6	24	17.8
Belite	Ca_2SiO_4	0.1	2.8	2.1
Perovskite	$CaTiO_3$	1.2	4.7	0.8
R_{wp}		9.31	13.63	7.42

Table 4.3 also includes the R_{wp} value of the analyses. The weighted profile R, denoted R_{wp}, is an index indicating the reliability of the agreement between the observed and calculated patterns (Snellings, 2016; Tsubota & Kitagawa, 2017). An R_{wp} value below 15% generally means that the analysis results are reliable (Huang et al., 2017; Chang et al., 2017). Based on the R_{wp} values of the quantitative XRD

analysis of the mixes, it can be said that the quantitative phase composition analysis results are reliable.

In all mixes, ye'elimite phase was clearly detected. Mix A, whose alumina is the highest, has the highest ye'elimite content at 48%, while Mix B and Mix C contain a similar amount of ye'elimite at 35% and 33%, respectively. Anhydrite phase, the other phase expected to be present, was also identified in all mixes. While the anhydrite content of Mix A and Mix B is close to each other, Mix C contains about twice as much anhydrite as the others. The other phases identified were merwinite, ellestadite, belite, and perovskite. Contrary to the literature, higher amounts of merwinite and ellestadite phases were detected in all mixes. CaO and SiO_2, two important oxides required for the formation of belite, were seen to be involved in the formation of the merwinite and ellestadite phases. The amount of belite and perovskite phases was quite low in all three mixes. Perovskite can be considered a hydraulically inactive mineral (Juenger et al., 2011).

Merwinite, a Ca-, Mg-, Si-, and O-bearing mineral, has been regarded as a non-hydraulic or hydraulically less active mineral at ambient temperature (Qian et al., 1997; Wang et al., 2011; Kriskova et al., 2014; Vlček et al., 2016). Kriskova et al. (2014) tried to increase the hydraulic activity of synthetic mervinite by mechanical and chemical activation. As a result of mechanical activation by increasing the fineness (d_{90} < 4μm), they obtained a strength of 1.5 MPa at 7 days, 2.4 MPa at 28 days, and 5.3 MPa at 90 days. The main hydration products formed were reported as crystalline and amorphous C-S-H and brucite ($Mg(OH)_2$). Portlandite was also observed as a result of chemical activation, i.e., alkali activation.

On the other hand, ellestadite is a mineral belonging to the mineral group of calcium silicate sulfate apatites, whose varieties are distinguished by their end members, e.g., F (fluorellestadite), Cl (chlorellestadite), or OH (hydroxylellestadite) (Rouse & Dunn, 1982). Ellestadite detected in all three mixes is thought to be Cl-bearing fluorellestadite (Avdontceva et al., 2021). It is also referred to as F-ellestadite or Ellestadite-F. In manufacturing Portland clinker, mineralizers and/or fluxes are often

added to the raw mixes to accelerate reactions and improve combustibility. When the mineralization pair $CaF_2/CaSO_4$ is used instead of the traditional fluxes such as Fe_2O_3 and Al_2O_3, this can lead to the formation of fluorellestadite during the clinker phase (Pajares et al., 2002). Haha et al. (2019) also stated that the presence of fluorellestadite in CSA clinkers might be due to the use of a fluorine-containing mineralizing agent or fluorine-containing raw materials such as fluorogypsum. Likewise, Isteri et al. (2020) stated that the formation of fluorellestadite in the CSA clinker they synthesized was due to the fluorine content of argon oxygen decarburization (AOD) slag from stainless steel production, one of the raw components of CSA clinker. Similarly, the formation of ellestadite in the produced CSA cements is thought to be related to the fluorine (F) and chlorine (C) contents in the raw materials used during the production stage.

In the literature, some studies stated that fluorellestadite has no (Pöllman, 2002; Isteri et al., 2020) or poor hydraulic properties (Isteri et al., 2021). Trauchessec et al. (2014) detected that fluorellestadite was not hydraulically active based on XRD analyses performed on one-month hydrated cement blends containing 4-7% fluorellestadite. In white OPC, it was observed to be unreactive during 90 days of hydration (Trauchessec et al., 2015). On the other hand, some other studies stated that fluorellestadite phase is hydraulically active (Martin et al., 2017; Haha et al., 2019). Haha et al. (2019) stated that silicate-bearing phases like belite and fluorellestadite dissolve much more slowly and to a lesser extent, resulting in strätlingite formation. Martin et al. (2017) also observed a decrease in the fluorellestadite peak intensities in XRD analysis of 300-day hydrated CSA cement containing fluorellestadite and estimated the fluorellestadite's hydration level to be 80%. They also noted that the fluorellestadite reactions are expected to be similar to those of belite and provide additional sulfate for the ettringite and/or monosulfate formation. Considering this information, fluorellestadite appears to be reactive in the long term, even if it is hydraulically active. In view of all this, fluorellestadite may be considered as a phase to be minimized or avoided in the clinker because of its no or low hydraulic character. The binding of the valuable oxides in the raw materials

such as CaO, SiO_2, and SO_3 with F prevents the formation of hydraulically more active phases (Isteri et al., 2020, 2021).

4.2.3 Physical Properties

Some physical properties of the three CSA cements are given in Table 4.4 and the particle size distributions (PSD) are shown in Figure 4.2. In terms of physical properties, it can be said that they are similar. The cements have a faster initial and final setting time than PCs, and their setting time values are close to each other. Soundness values are the same.

Table 4.4 Some physical properties of the CSA cements

Property	Unit	Mix A	Mix B	Mix C
Density	g/cm^3	2.94	2.99	3.00
Blaine	cm^2/g	4600	4510	4900
Normal consistency	%	23.5	22.3	23.3
Initial setting time	min	12	15	11
Final setting time	min	25	30	26
Soundness	mm	1	1	1

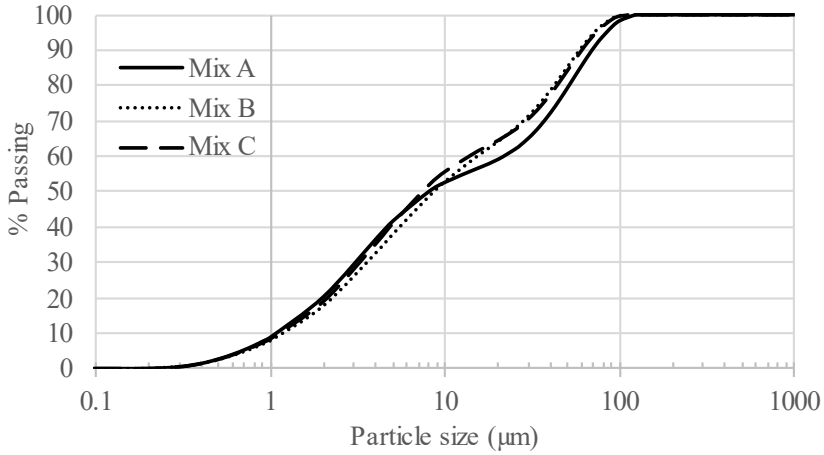

Figure 4.2 Particle size distributions of the CSA cements

The d_{10}, d_{50}, and d_{90} sizes obtained from the PSD analyses of the mixes are presented in Table 4.5. According to the results, 10% of the cement particles are smaller than 1 μm, and 50% of the particles are less than about 8 μm. Whereas 90% of the particles in Mix B and C are smaller than about 60 μm, this value is about 69 μm for Mix A.

Table 4.5 Some PSD parameters of the CSA cements

d	Unit	Mix A	Mix B	Mix C
d_{10}	μm	1.09	1.19	1.14
d_{50}	μm	7.99	8.55	7.32
d_{90}	μm	68.81	58.35	60.11

4.2.4 SEM Images of CSA Cements

Figure 4.3, Figure 4.4, and Figure 4.5 show the SEM images of Mix A, Mix B, and Mix C, respectively. It should be noted that these SEM images were obtained on the ground CSA cements during the COVID-19 pandemic, where our access to the laboratory was quite limited. Therefore, they didn't provide any valuable information other than validating the presence of the oxides by EDX analysis. The EDX analysis results of Mix A, B, and C, taken from the center of the images, are listed in Table 4.6, Table 4.7, and Table 4.8, respectively.

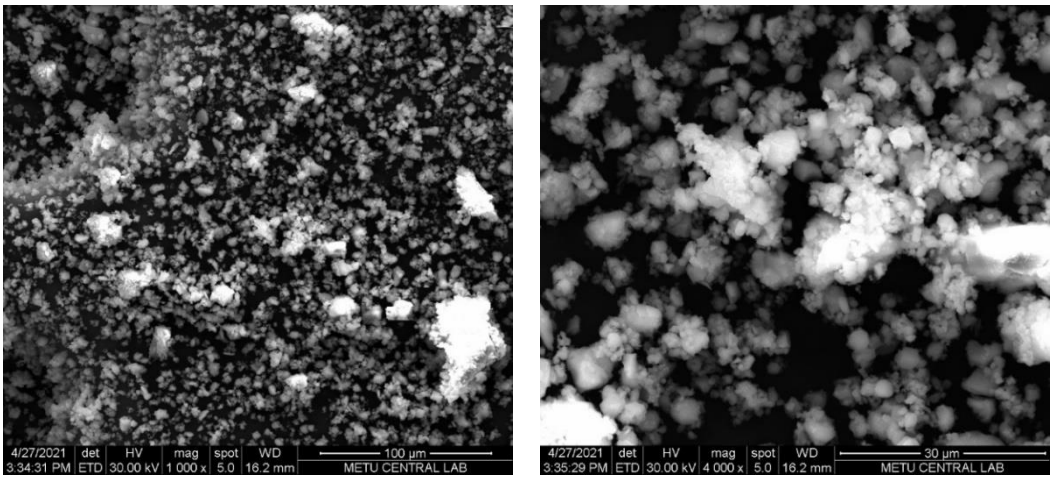

(a) (b)

Figure 4.3 SEM images of Mix A (a) 1000 X (b) 4000 X

Table 4.6 EDX quantitative analysis results of Mix A

Element (wt%)	(a)	(b)
O	35.92	36.59
Ca	35.91	27.24
Al	11.17	16.63
Si	10.39	5.44
S	3.40	5.15
Mg	2.82	1.59
Fe	0.89	1.68
C	-	5.68

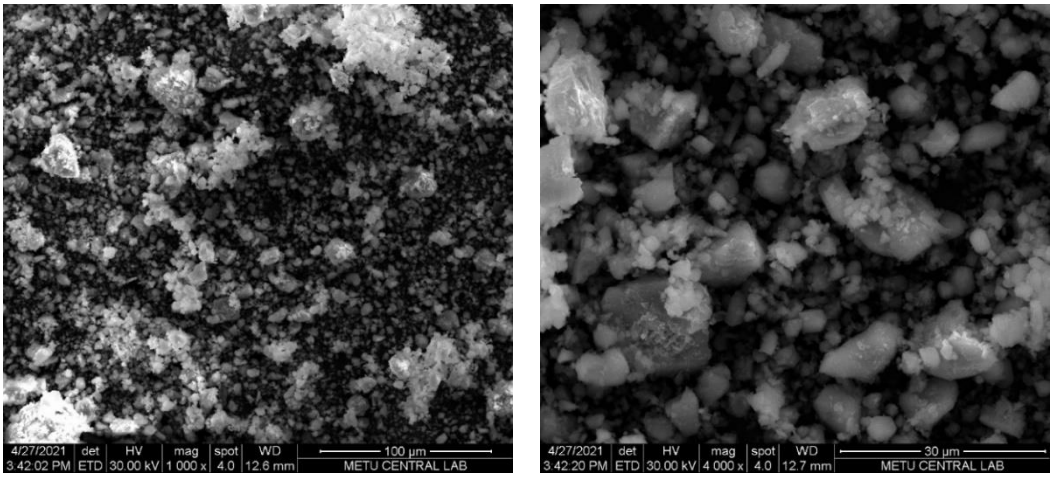

(a) (b)

Figure 4.4 SEM images of Mix B (a) 1000 X (b) 4000 X

Table 4.7 EDX quantitative analysis results of Mix B

Element (wt%)	(a)	(b)
O	36.60	39.04
Ca	26.85	29.39
Al	13.79	11.05
Si	5.05	7.09
S	6.51	6.30
Mg	2.29	1.93
Fe	1.62	0.89
C	7.30	4.30

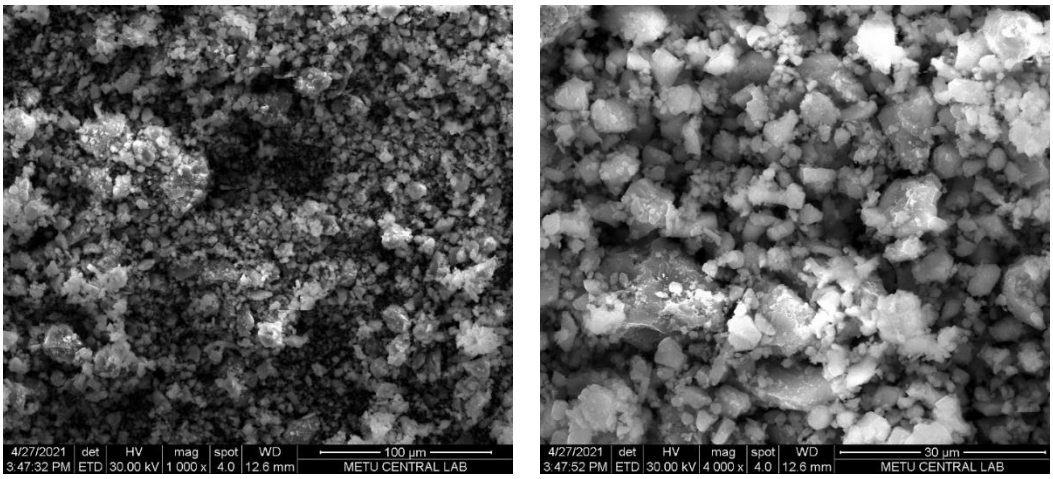

(a) (b)

Figure 4.5 SEM images of Mix C (a) 1000 X (b) 4000 X

Table 4.8 EDX quantitative analysis results of Mix C

Element (wt%)	(a)	(b)
O	35.70	37.53
Ca	29.86	30.87
Al	11.22	9.29
Si	6.91	6.85
S	7.36	8.83
Mg	2.73	2.87
Fe	0.86	0.93
C	5.37	2.82

4.3 Characterization of the Hydration Behavior of the CSA Cements

4.3.1 Heat Evolution

The measured cumulative heat profiles of the CSA cement pastes during the 72 hours and the calculated heat flow of the pastes are shown in Figure 4.6 and Figure 4.7 for 10 hours and 48 hours, respectively.

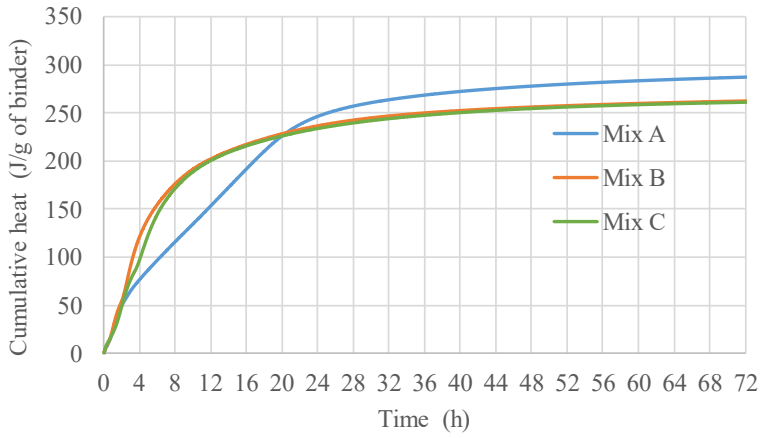

Figure 4.6 Cumulative heat of the CSA cements

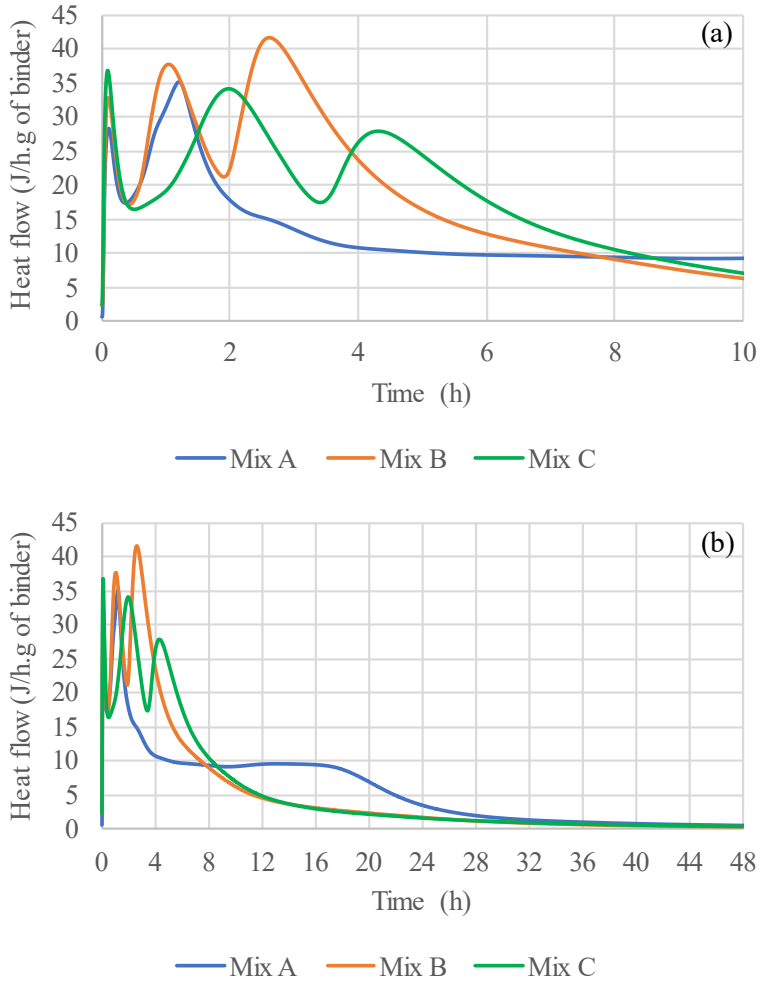

Figure 4.7 Heat flows of the CSA cements (a) for 10 hours (b) for 48 hours

As seen in Figure 4.6, Mix B and Mix C revealed a similar cumulative heat profile. Although Mix A showed a higher cumulative heat at the end of 3 days, it evolved a lower cumulative heat until the 20th hour of hydration. At the 20th hour, the cumulative heat value of all three mixes was approximately 226 J/g. The total heat evolution after 72 h of hydration for Mix A, Mix B, and Mix C is 287, 262, and 261 J/g, respectively.

As seen in Figure 4.7, the heat flow curves of the pastes have three distinct heat release peaks. All the mixes showed a very rapid heat release peak around the first five minutes of hydration. The first heat release peak is due to wetting and a dissolution of anhydrous phases such as ye'elimite and anhydrite (Winnefeld & Barlag, 2010; Bullerjahn et al., 2015). The second heat release peak occurred at about one hour of hydration for Mix A and B. Mix C showed similar heat flow curve as Mix B, but its hydration rate was slower than Mix B. The second peak was located at about two hours for Mix C. The second heat release peak is associated with nucleation and growth of hydrate phases, mostly probably ettringite. AH_3 is also formed in addition to ettringite (Winnefeld & Barlag, 2010; Chen & Juenger, 2012). Depending on the molar ratio of calcium sulfate to ye'elimite in the medium (if less than 2), monosulfate may also form as a product, and the third heat release peak is associated with the formation of AFm-type phases after sulfate depletion (Winnefeld & Barlag, 2010; Aranda & De la Torre, 2013). The molar ratio of calcium sulfate to ye'elimite was calculated from XRD quantitative analysis data and was found as 1.2, 1.7, and 3.4 for Mix A, Mix B, and Mix C, respectively. Since the calculated molar ratio of calcium sulfate to ye'elimite for Mix A and B was less than 2, the monosulfate formation, i.e., another peak, was expected. In contrast, the monosulfate formation was not expected for Mix C due to its molar ratio being greater than 2. It is thought that the third peak may also be related to the ongoing ettringite and AH_3 formation. The rate of heat of hydration of Mix A slowed down after the second heat release peak and showed a less intense and broad third peak at about 13 h. The third peak occurred at 2.6 h and 4.3 h for Mix B and Mix C, respectively, after which heat release gradually decreased up to 24 h. It has been reported that in the absence of a

source of calcium sulfate, ye'elimite hydration is slow (Winnefeld & Barlag, 2010; Juenger et al., 2011). Thus, compared to Mix B and C, the slower hydration kinetics of Mix A can be attributed to its relatively higher content of ye'elimite and lower content of anhydrite.

4.3.2 X-Ray Diffraction Analysis

The hydration progress of the CSA cements was qualitatively monitored by XRD analyses of the pastes from 1 hour to 360 days. Figure 4.8 shows the XRD patterns of Mix A pastes at different curing times in water. The figure also includes the XRD pattern of the unhydrated Mix A. The patterns given in Figure 4.8 indicate that the primary hydration product of Mix A is ettringite. Monosulfate is hardly visible in XRD analysis due to its low crystallinity (Winnefeld & Barlag, 2010). Also considering its overlap peak with the ettringite peak, it is difficult to infer the presence of monosulfate as a hydration product. After one hour of hydration, the intensity of ye'elimite and anhydrite peaks began to decrease, while the ettringite peaks started to be seen simultaneously. At the end of the third, sixth, and 24th hours, further reductions in the intensity of ye'elimite and anhydrite peaks and further increases in the intensity of ettringite peaks were observed. Ye'elimite appeared to be extensively hydrated after three days and was almost completely depleted after seven days of hydration. However, a minimal ye'elimite peak still existed on the 360th day of hydration. As a result of the reaction of ye'elimite with anhydrite, aluminum hydroxide is also formed together with ettringite. Due to its initial amorphous nature, AH_3 may not be directly identified by XRD; however, it may be crystallized as gibbsite later (Aranda & De la Torre, 2013). Traces of gibbsite were found from the seventh day. The rate of ettringite formation decreased from the seventh day of hydration. A slight increase was observed in the intensity of ettringite peaks up to the 180th day, and a decrease in the intensity of these peaks occurred on the 360th day of hydration. This decrease is thought to be related to the carbonation of ettringite, as $CaCO_3$ peaks were observed in the samples from 90th day. In

addition, no significant change was detected when the merwinite peaks were followed. Regarding fluorellestadite, when its two main diffraction peaks were followed, it was observed to have a slight reduction in the intensity of the peaks on the 360th day. However, this observation alone does not necessarily indicate that fluorellestadite has hydrated. Haha et al. (2019) stated that the hydration reaction of fluorellestadite might lead to strätlingite formation. Martin et al. (2017) also noted that they expect the hydration reactions of fluorellestadite to be similar to those of belite and to provide additional sulfate for the ettringite and/or monosulfate formation. Although a slight decrease in the main fluorellestadite peaks was observed, no new product formation was detected in the XRD results of Mix A at 360th day.

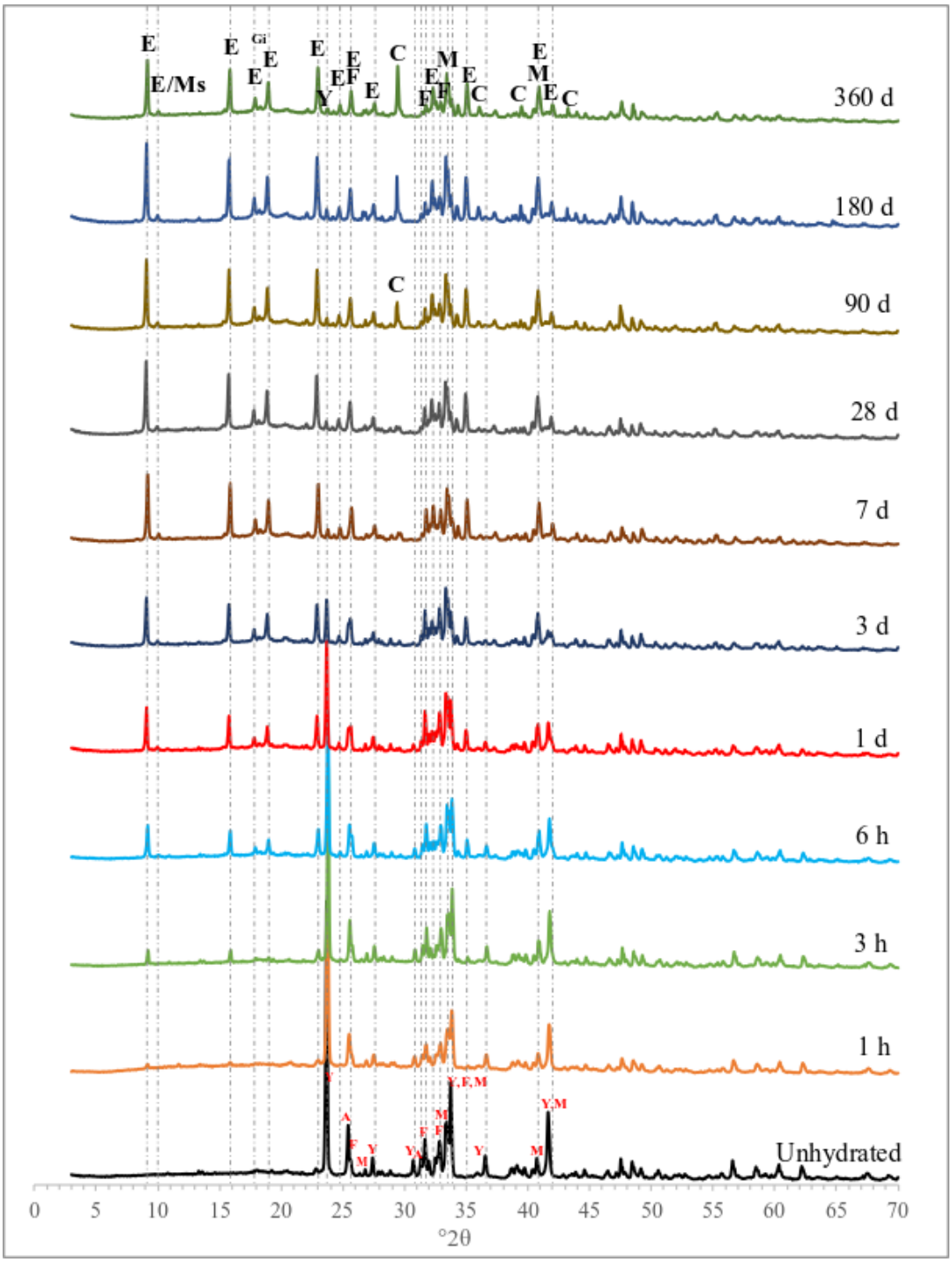

Figure 4.8 XRD patterns of Mix A at different curing times (Y: Ye'elimite and, A: Anhydrite, M: Merwinite, F: Fluorellestadite, E: Ettringite , Ms: Monosulfate, C: Calcium carbonate, Gi: Gibbsite)

Figure 4.9 shows the XRD patterns of Mix B pastes at different curing times in water. The figure also includes the XRD pattern of the unhydrated compounds of Mix B. The patterns shown in Figure 4.9 confirm that ettringite forms while consuming ye'elimite and anhydrite with time. Ettringite peaks, which started to be seen from the first hour of hydration, became clearly visible at the end of the first day, and the decline in the intensity of ye'elimite and anhydrite peaks continued. Considering the gypsum peaks observed in the XRD analysis performed at the 1st and 3rd hours of hydration, it can be said that gypsum is formed as an intermediate hydration product because of anhydrite conversion to gypsum. However, no gypsum peaks were observed at the 6th hour. Accordingly, it can be said that gypsum is consumed while ettringite is formed. The ye'elimite phase, highly hydrated at the end of the third day, seems to be almost completely consumed by the end of the seventh day. Traces of gibbsite were found from the seventh day. Since the seventh day of hydration, the rate of ettringite generation has decreased. There was a slight increase in the intensity of ettringite peaks until the 180th day of hydration, and a drop was observed in the intensity of these peaks on the 360th day. As with Mix A, $CaCO_3$ peaks were also observed for Mix B from day 90. Hence, the decrease in the ettringite peaks is thought to be related to the carbonation of ettringite. In addition, no significant change was detected when the merwinite peaks were followed. Regarding fluorellestadite, a similar behavior to Mix A was observed. There was a slight reduction in the intensity of two main diffraction peaks of fluorellestadite on the 360th day. However, a new hydration product formation was not detected in the XRD results of Mix B at 360th day.

Figure 4.10 shows the XRD patterns of Mix C pastes at different curing times in water. The figure also includes the XRD pattern of the unhydrated compounds of Mix C. Similar observations made for Mix B were also made for Mix C. Differently, a small anhydrite peak was still identified in Mix C after about one year of hydration.

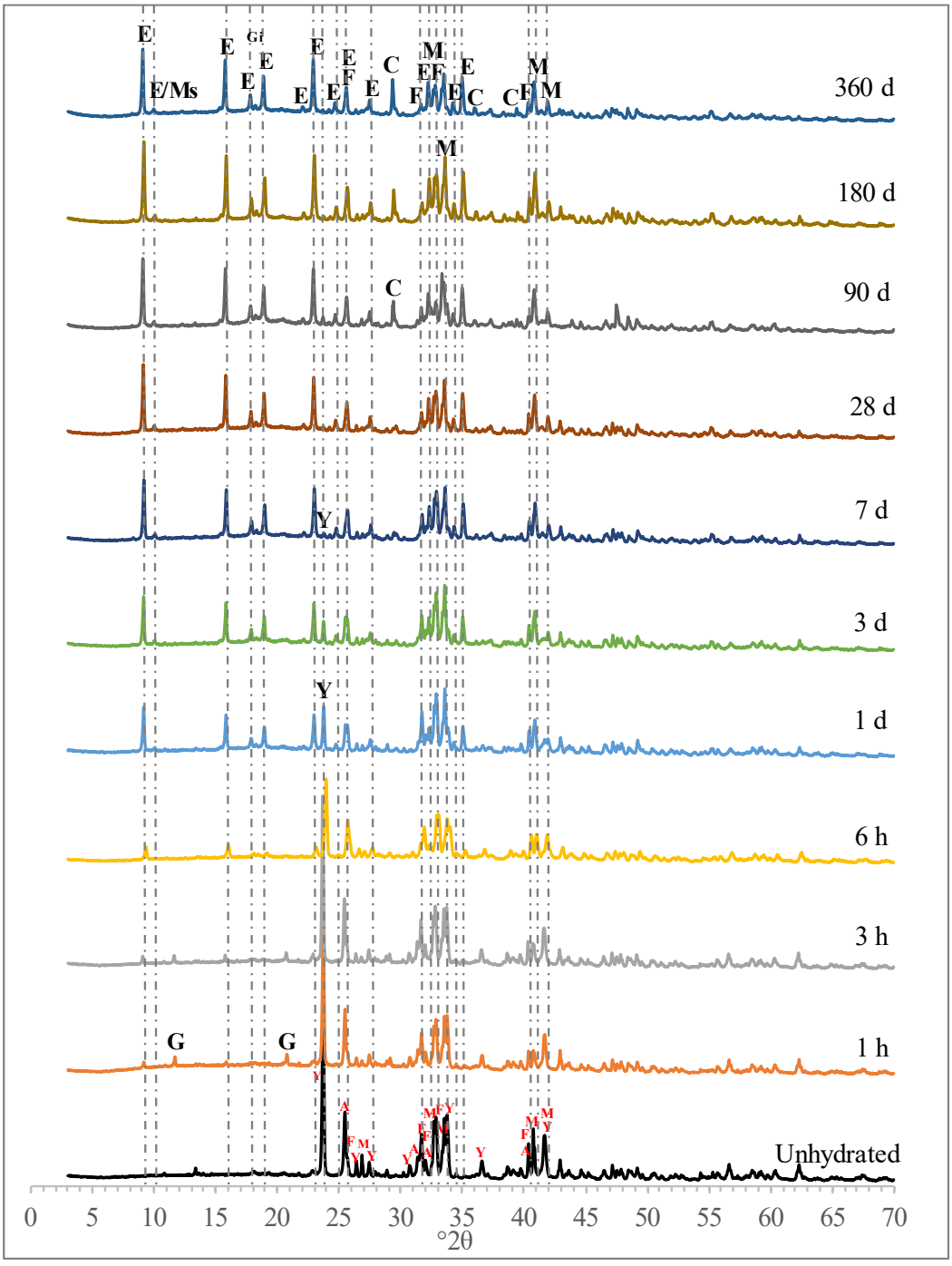

Figure 4.9 XRD patterns of Mix B at different curing times (Y: Ye'elimite and, A: Anhydrite, M: Merwinite, F: Fluorellestadite, E: Ettringite , Ms: Monosulfate, C:Calcium carbonate, G: Gypsum, Gi:Gibbsite)

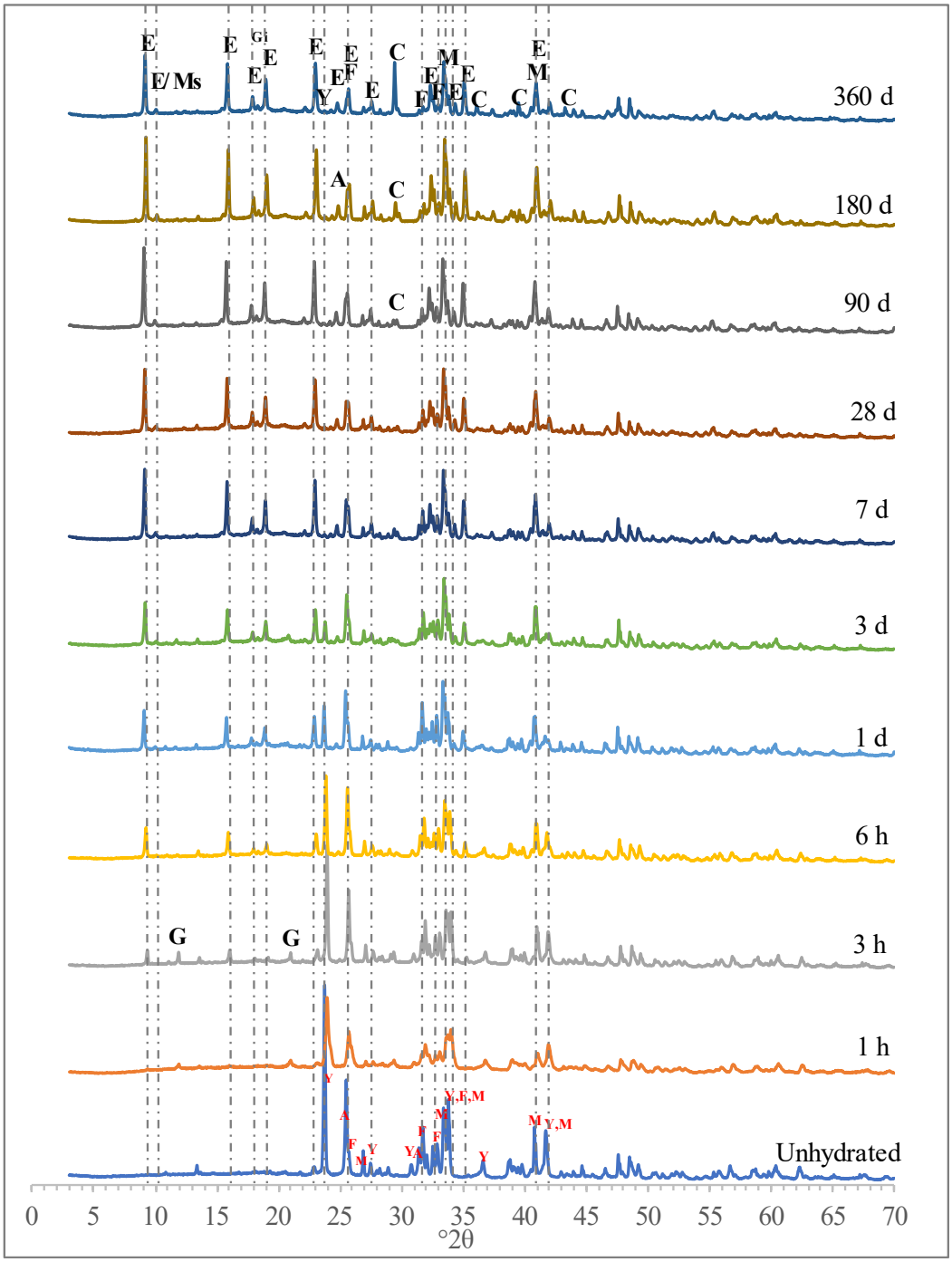

Figure 4.10 XRD patterns of Mix C at different curing times (Y: Ye'elimite and, A: Anhydrite, M: Merwinite, F: Fluorellestadite, E: Ettringite , Ms: Monosulfate, C: Calcium carbonate, G: Gypsum, Gi: Gibbsite)

4.3.3 TGA/DTA Analysis

The hydration progress of the CSA cements was also monitored with thermal analyses. The DTA and TGA curves of Mix A pastes cured in water for 7, 28, 90, 180, and 360 days are indicated in Figure 4.11. Figure 4.11-a shows that three endothermic peaks at around 100 °C, in the range of 200 °C to 300 °C, and 650 °C to 700 °C were found on all test days. In addition, a tiny endothermic peak was seen at around 115°C at 180 d and 360 d of hydration days. In cementitious systems the mass loss up to about 600 °C is generally due to the loss of water, and over 600 °C, mostly with the release of CO_2 (Scrivener et al., 2016).

The first endothermic peak at around 100 °C in the curves is associated with the decomposition of ettringite. During the hydration of ye'elimite, AH_3 is also formed in addition to ettringite, and monosulfate may also be formed depending on the amount of calcium sulfate in the medium. While it is difficult to detect the presence of AH_3 and monosulfate in XRD due to their amorphous structure, their presence can be detected through thermal analysis. Amorphous AH_3 loses its bound water at around 250-280 °C and monosulfate at around 170 °C (Winnefeld & Barlag, 2010). Consistent with this information, the endothermic peak between 200-300 °C can be associated with weight loss due to AH_3. A clear peak was not observed at around 170 °C. From the 7^{th} day of hydration, a peak associated with the decomposition of $CaCO_3$ was seen at around 700 °C. Although this peak is not very evident for the first 90 days, it is clearly visible on the 180^{th} and 360^{th} hydration days. At the same time, a very small peak around 115 °C was observed in the analyses performed on the 180^{th} and 360^{th} hydration days, which can be associated with weight loss of gypsum (Song et al., 2015). Furthermore, the ettringite peak slightly decreased on the 360^{th} day compared to the 180^{th} day. All of this has been associated with the carbonation of ettringite, which leads to the decomposition of ettringite into gypsum, calcium carbonate, and aluminum hydroxide, as seen in Equation 21.

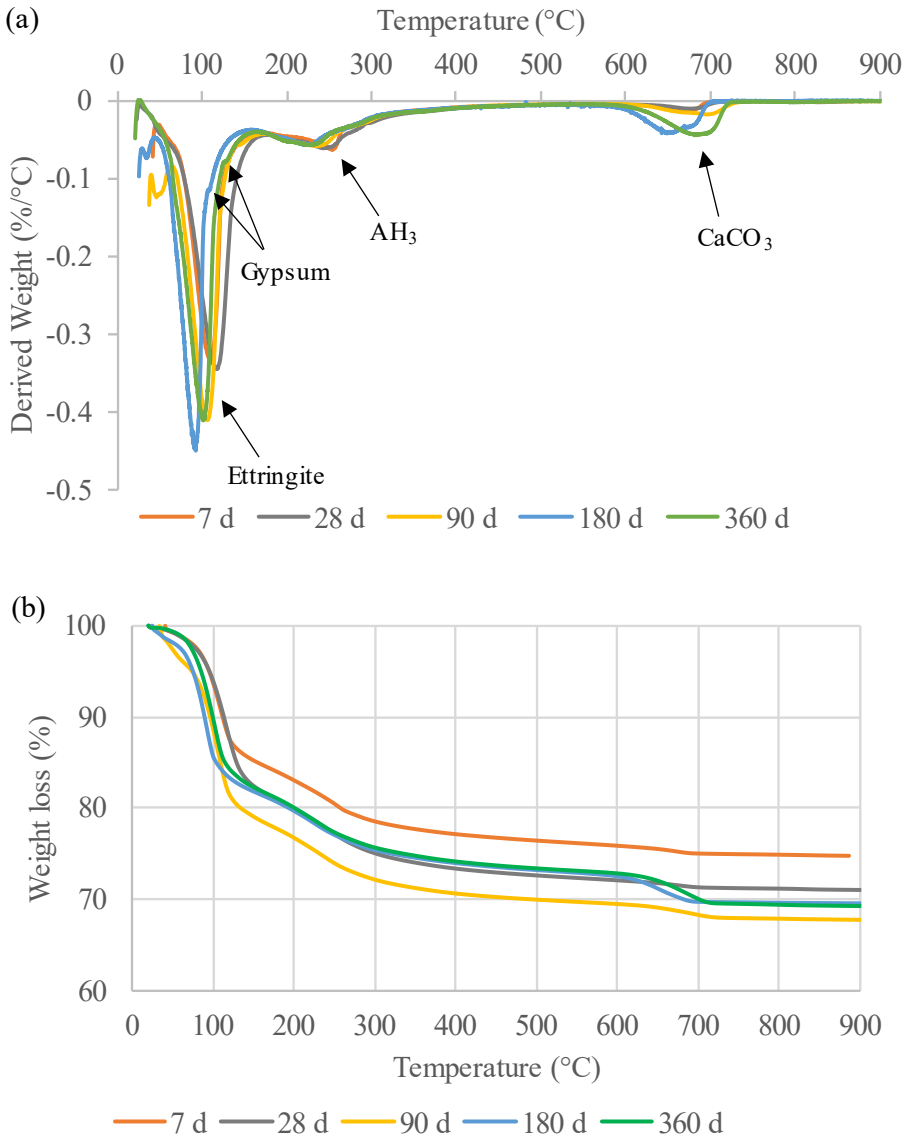

Figure 4.11 (a) DTA and (b) TGA results of Mix A pastes at different curing times

The DTA and TGA curves of Mix B and Mix C pastes cured in water for 7, 28, 90, 180, and 360 days are shown in Figure 4.12 and Figure 4.13, respectively. Similar observations made for Mix A were also made for Mix B and Mix C. It should be noted that 7th day results for Mix B and C were obtained from air-cured specimen and the presence of a small amount of peak can be associated with weight loss of gypsum.

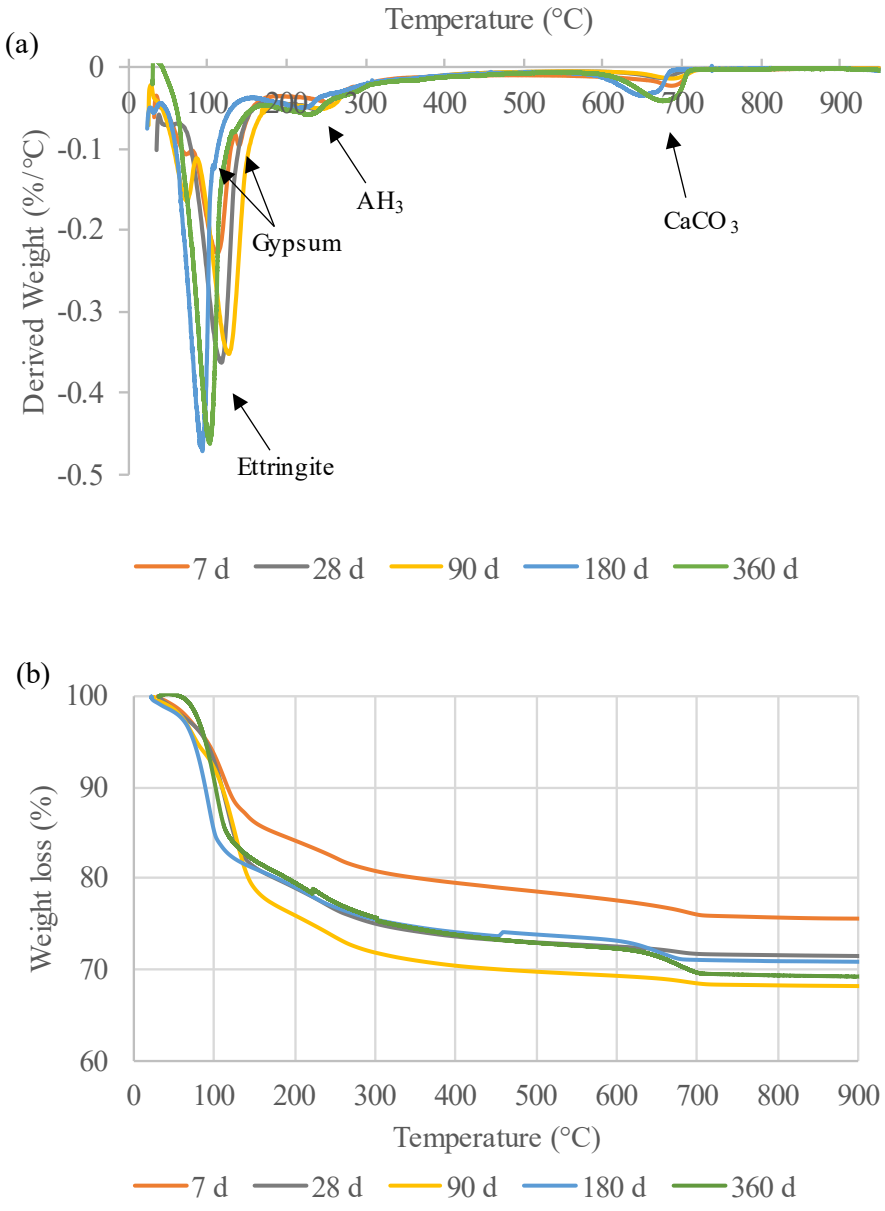

Figure 4.12 (a) DTA and (b) TGA results of Mix B pastes at different curing times

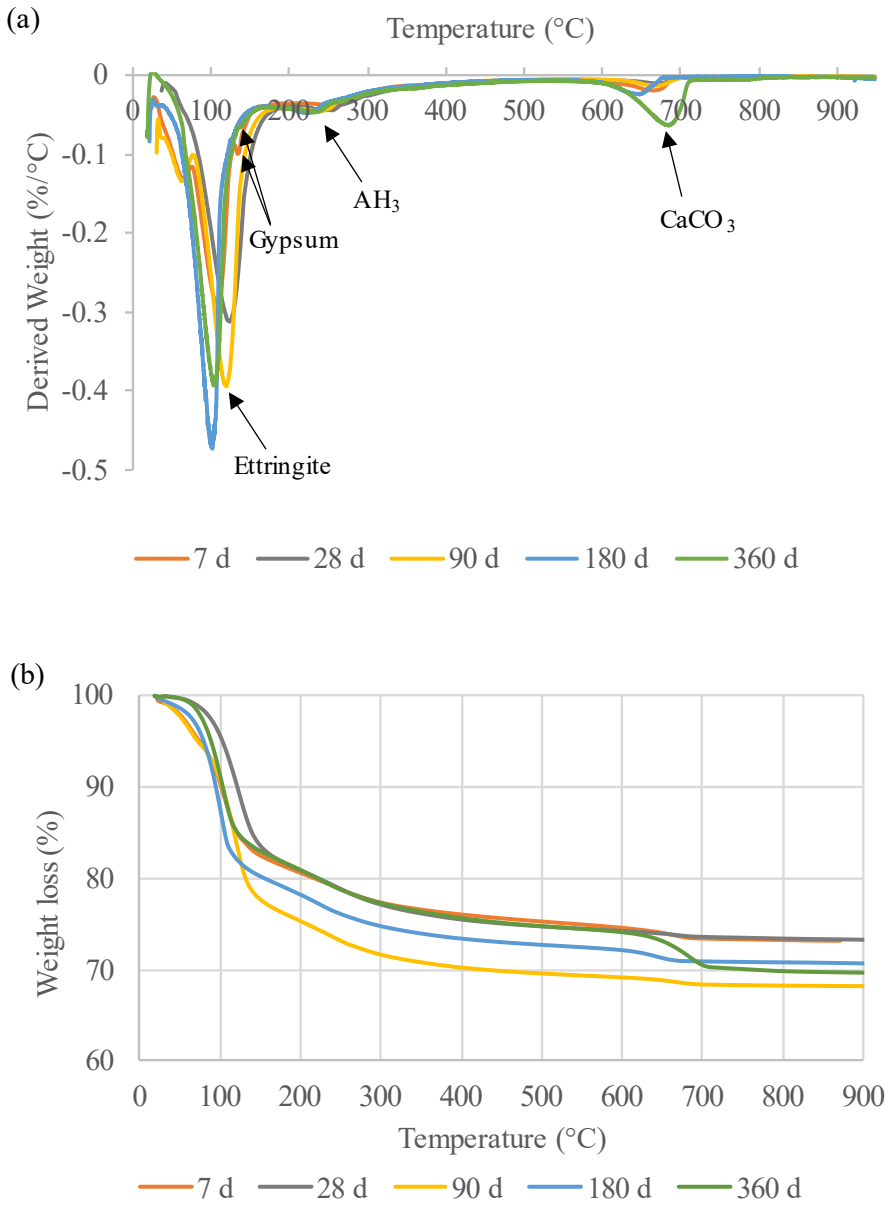

Figure 4.13 (a) DTA and (b) TGA results of Mix C pastes at different curing times

4.3.4 Carbonation Issue

As mentioned earlier, $CaCO_3$ peaks were observed in the XRD analyses performed from the 90th day of hydration in all three water-cured CSA cements. Moreover, especially on the 360th day, a decrease in the intensity of the ettringite peaks while

an increase in the intensity of $CaCO_3$ peaks signaled occurrence of carbonation during CSA hydration. Similar carbonation related observations have also been made with TGA/DTA analyses. Besides the $CaCO_3$ peak, a very tiny gypsum peak was also detected during thermal analyses on 180th and 360th day. It is believed that the reason why gypsum could not be detected in XRD analyses is because of its small amount. At the same time, the main $CaCO_3$ peak at about 29-30 °2θ and a gypsum peak overlap, making a clear distinction difficult. These phenomena have been associated with the carbonation of ettringite, which is accompanied by the formation of calcium carbonate, gypsum, and aluminum hydroxide, as shown in Equation 21 presented in Chapter 2.

Therefore, in addition to water-cured CSA cements, the air-cured pastes were analyzed by XRD and TGA/DTA on the 180th and 360th day of hydration in terms of carbonation behavior. Figure 4.14, Figure 4.15, and Figure 4.16 show the XRD patterns of air-cured paste samples for 180 and 360 days for Mix A, Mix B, and Mix C, respectively. As can be seen from the diffraction patterns in the figures, the gypsum peaks are clearly visible in the air-cured samples, unlike the water-cured samples. Comparing the hydration results of 180 and 360 days, we can see that the intensity of gypsum peaks slightly increases while the intensity of the ettringite peaks slightly decreases on the 360th day. Since the main peak of calcium carbonate coincides with a peak of gypsum, a precise observation about the calcium carbonate could not be made. However, it can be stated that carbonation of ettringite increases relatively from the 180th day to the 360th day. The results show more clearly that ettringite is carbonated with time in air-cured samples in a more noticeable amount when compared to water-cured samples. It should be noted that the samples analyzed were quite small, having a circular plate geometry with an average diameter of 30 mm, and a thickness of 5 mm.

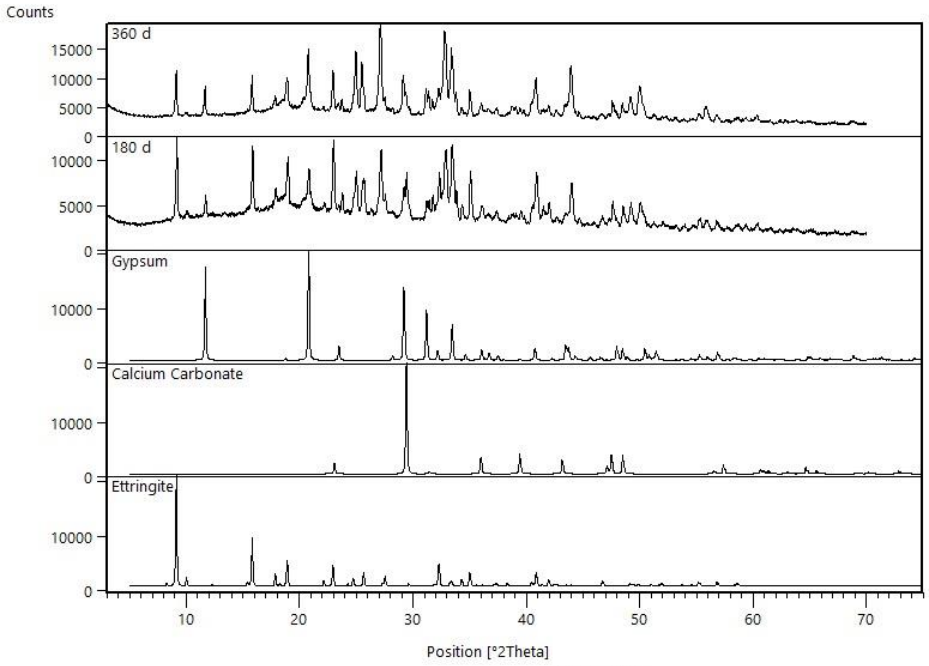

Figure 4.14 XRD patterns of air-cured Mix A pastes at 180 and 360 days of hydration

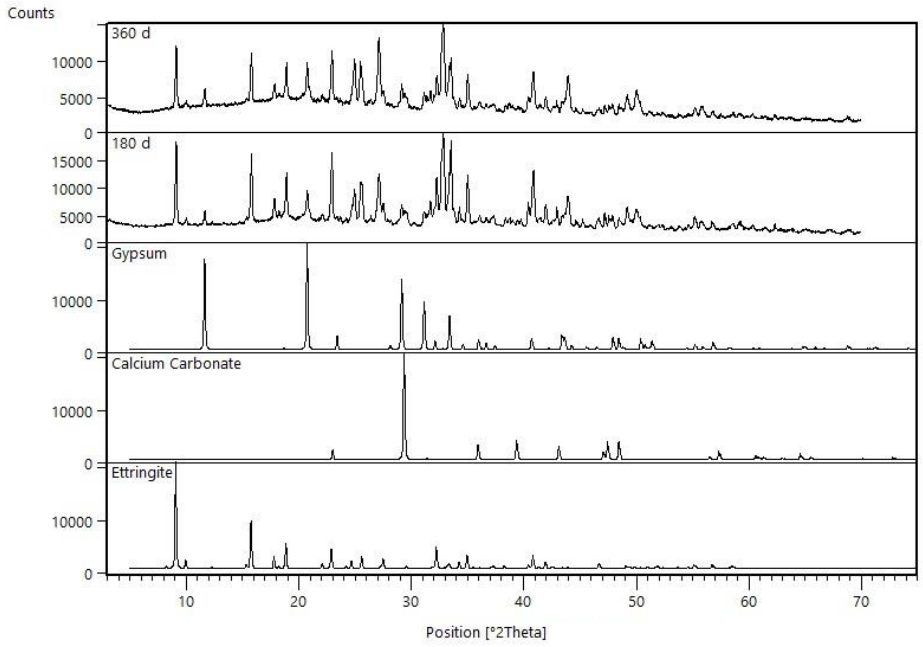

Figure 4.15 XRD patterns of air-cured Mix B pastes at 180 and 360 days of hydration

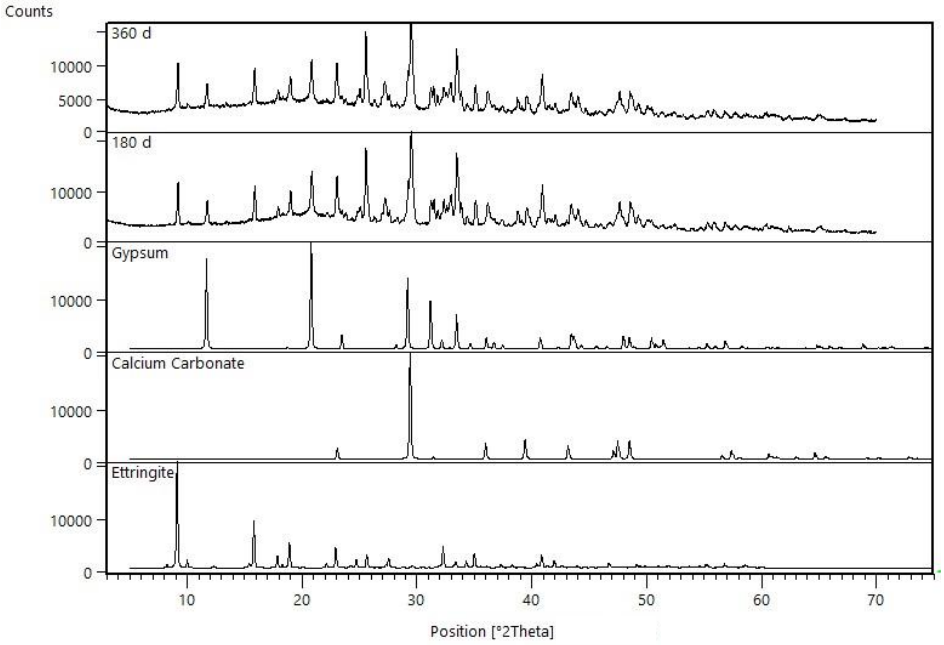

Figure 4.16 XRD patterns of air-cured Mix C pastes at 180 and 360 days of hydration

In addition to XRD analyses, TGA/DTA analyses were also performed for the air-cured pastes on the 180th and 360th day of hydration. Figure 4.17, Figure 4.18, and Figure 4.19 show the DTA and TGA curves of air-cured paste samples for 180 and 360 days for Mix A, Mix B, and Mix C, respectively. As seen in the three figures, there are four distinct endothermic peaks in the range of 90 °C to 100 °C, 100 °C to 115°C, 200 °C to 300 °C, and 650 °C to 700 °C, which can be associated with dehydration of ettringite, gypsum, aluminum hydroxide, and calcium carbonate, respectively. Therefore, the XRD results are the confirmed by thermal analyses results. In addition, the presence of aluminum hydroxide was revealed in thermal analyses, which could not be detected in XRD analyses due to its amorphous structure. In other words, the carbonation products of ettringite, calcium carbonate, gypsum, and aluminum hydroxide, were identified with thermal analyses for all three mixes, as shown in Equation 21. According to TGA data of the mixes, the weight losses above 600 °C were calculated as 6.4%, 5.3%, and 6.7% for Mix A, Mix B, and Mix C on the 180th day, respectively. On the other hand, the losses on the 360th day were found as 7.5%, 7.5%, and 7.9% for Mix A, Mix B, and Mix C, respectively.

Considering both the increase in weight loss at day 360 and the intensity of the phases in DTA curves, it can be concluded that the carbonation of ettringite increases relatively from day 180 to day 360. In parallel with the XRD analyses, the results of the thermal analyses also confirm that ettringite shows more noticeable carbonation over time in air-cured samples than in water-cured samples.

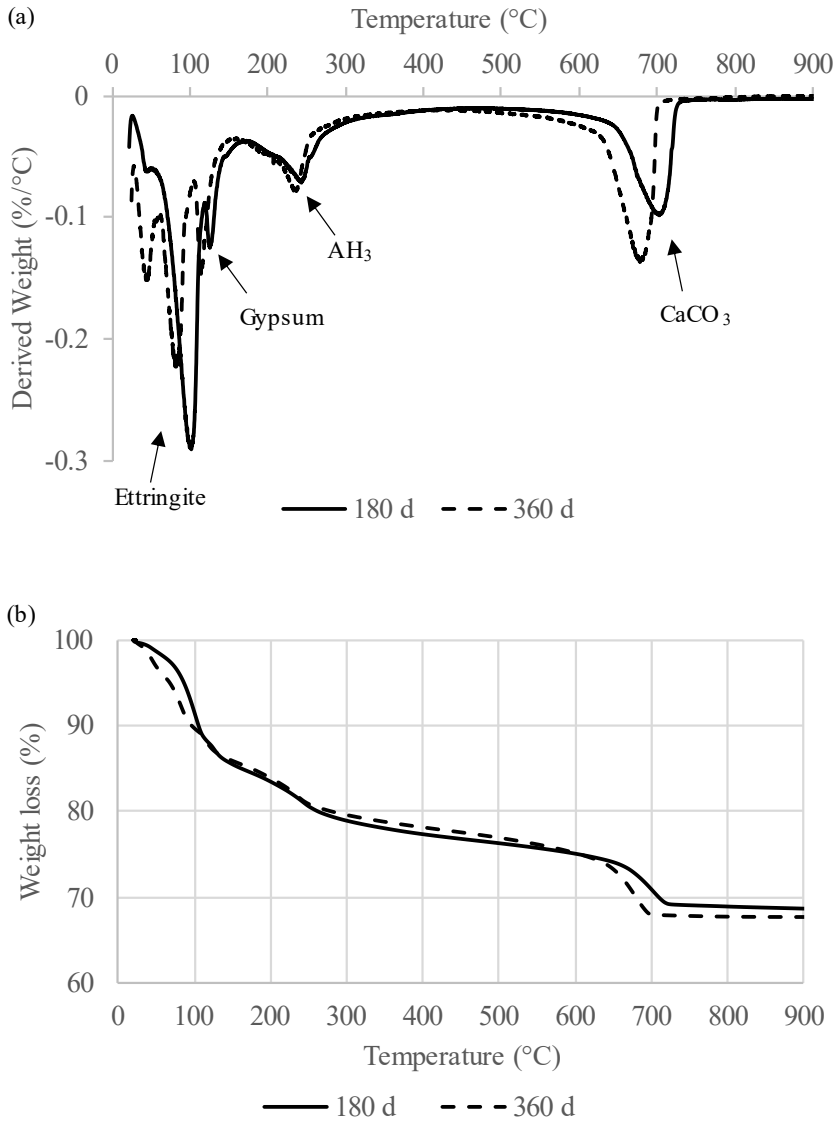

Figure 4.17 (a) DTA and (b) TGA results of Mix A pastes at 180 and 360 days of hydration

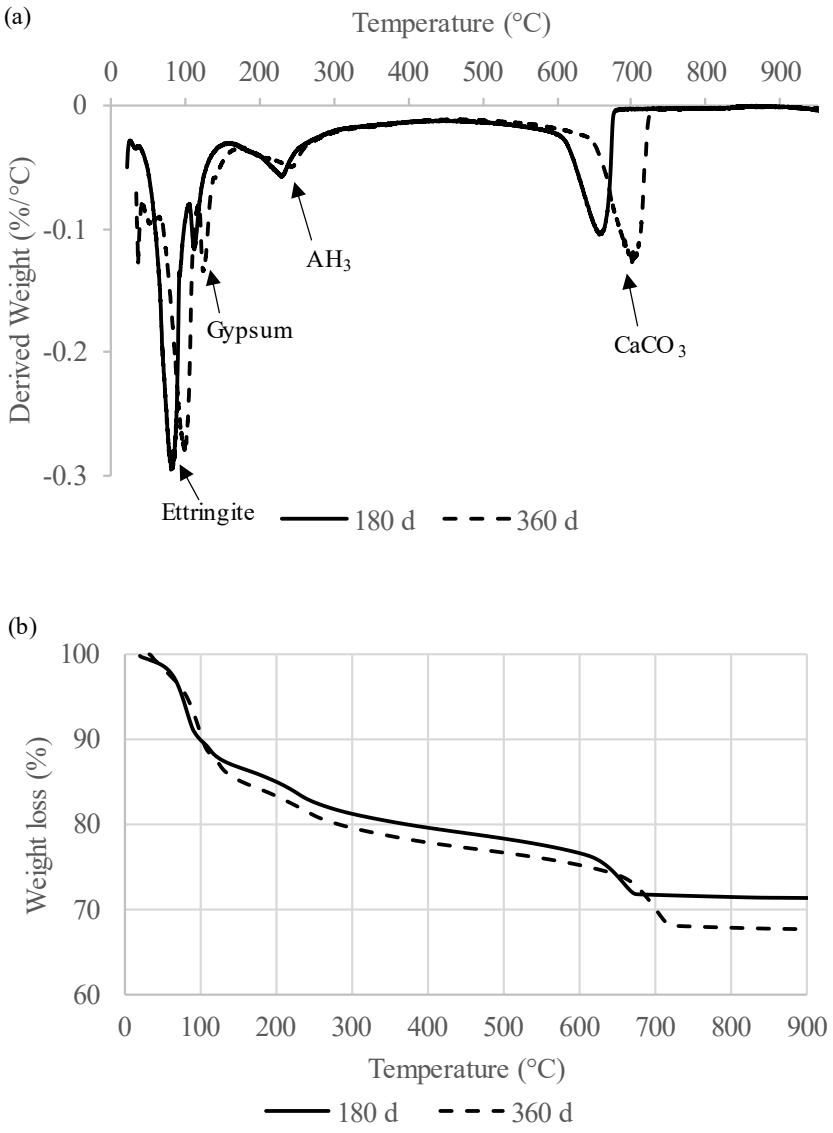

Figure 4.18 (a) DTA and (b) TGA results of Mix B pastes at 180 and 360 days of hydration

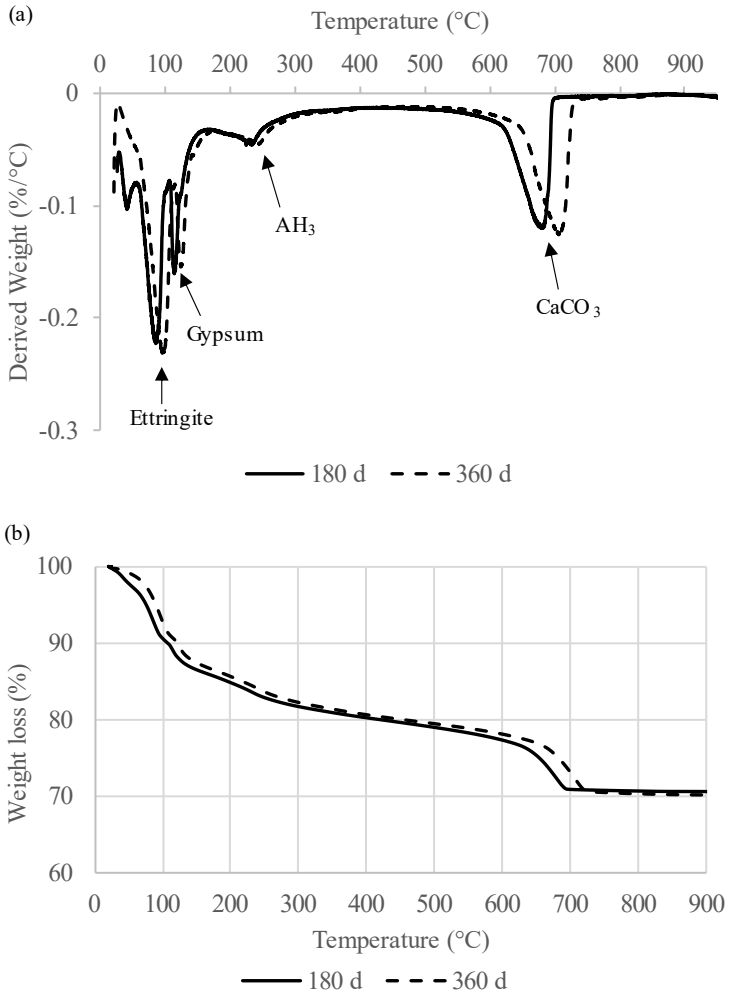

Figure 4.19 (a) DTA and (b) TGA results of Mix C pastes at 180 and 360 days of hydration

4.3.5 SEM Images of CSA Cement Pastes

SEM analyses were performed to examine the microstructure of the CSA cement pastes on the 28th, 90th, and 360th days. In Figure 4.20, Figure 4.21, and Figure 4.22, SEM images for hydrated Mix A, Mix B, and Mix C are shown, respectively, at 28 days, 90 days, and 360 days of curing. The EDX analysis results of Mix A, B, and C, taken from the center of the images, are listed in Table 4.9, Table 4.10, and Table 4.11, respectively. Ettringite, the main hydration product, was identified in all SEM analyses except on day 28 of hydration of Mix A and Mix B.

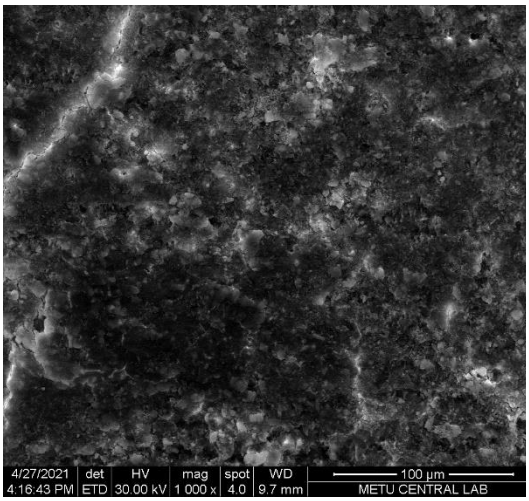

(a) 28 d

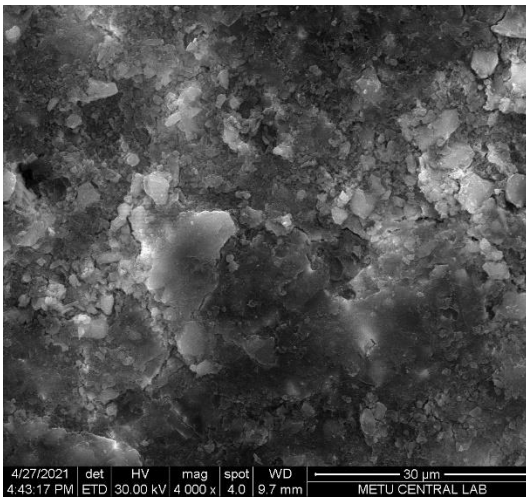

(b) 28 d

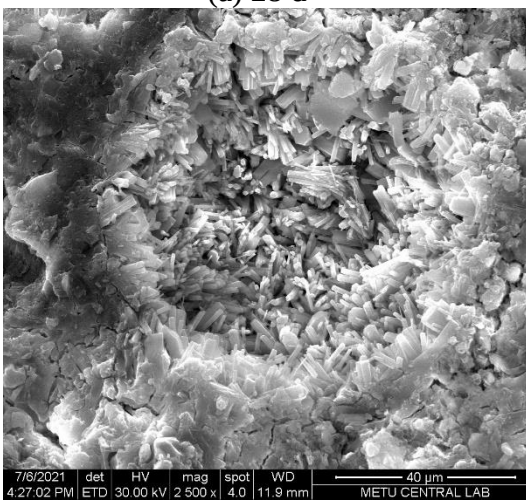

(c) 90 d

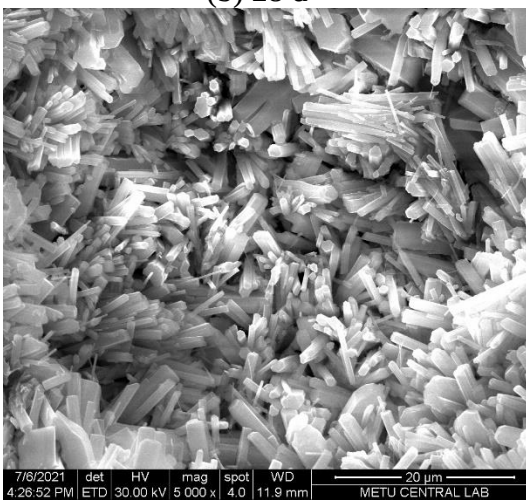

(d) 90 d

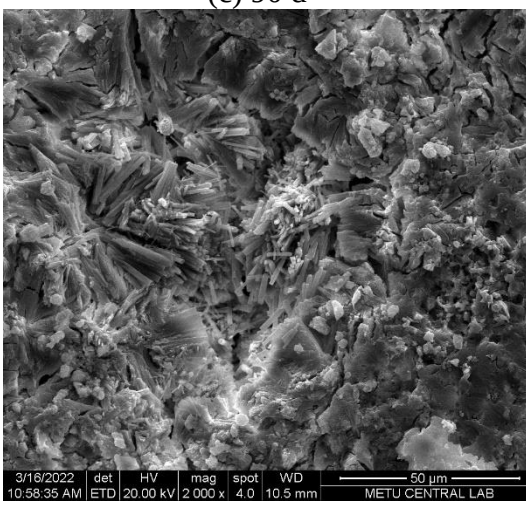

(e) 360 d

(f) 360 d

Figure 4.20 SEM images of Mix A pastes at (a,b) 28 d (c,d) 90 d (e,f) 360 d

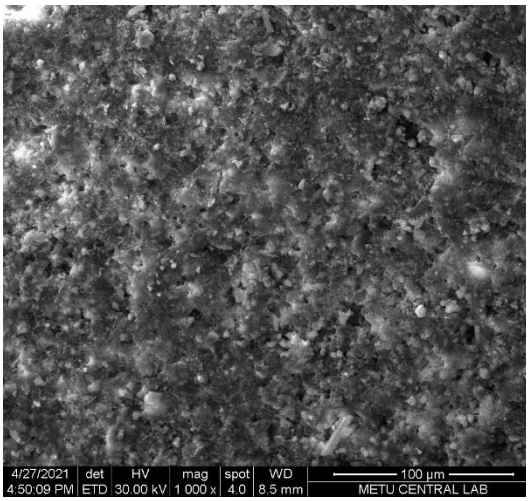

(a) 28 d

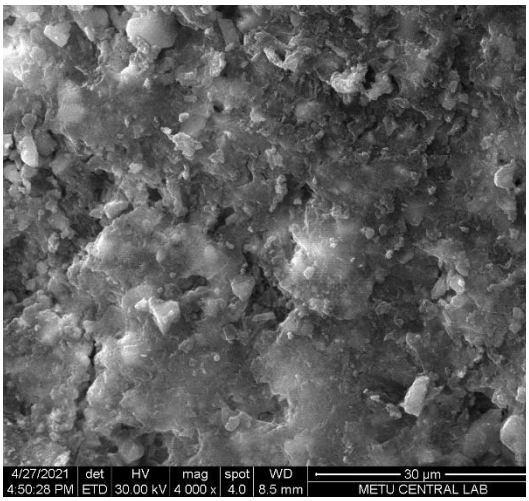

(b) 28 d

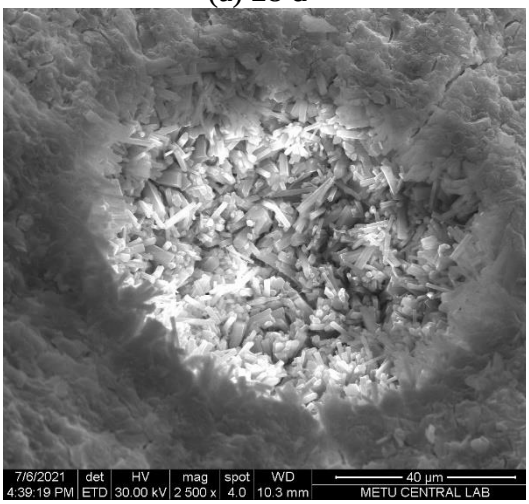

(c) 90 d

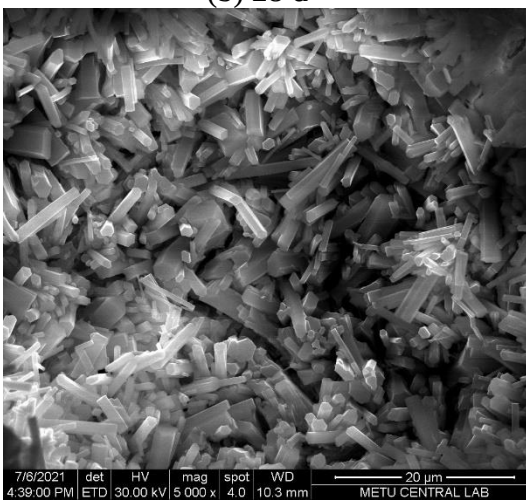

(d) 90 d

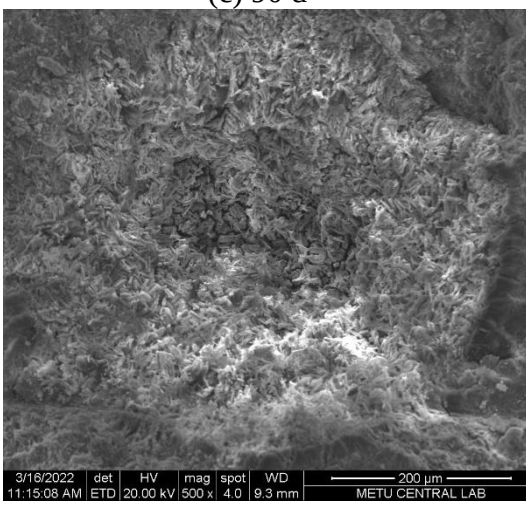

(e) 360 d

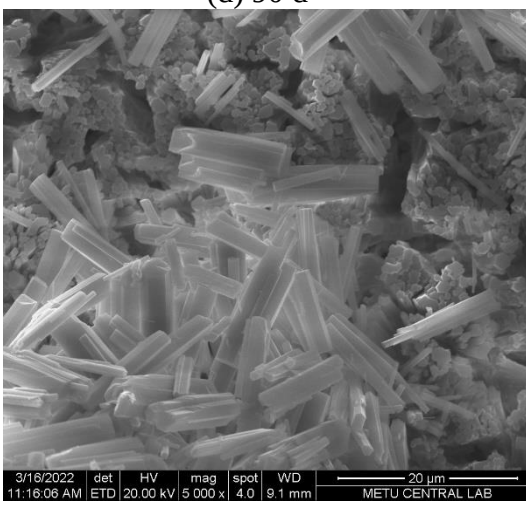

(f) 360 d

Figure 4.21 SEM images of Mix B pastes at (a, b) 28 d (c, d) 90 d (e, f) 360 d

Table 4.9 EDX quantitative analysis results of hydrated Mix A pastes

Element (wt%)	(a)	(b)	(d)	(e)
O	41.12	40.76	52.51	50.62
Ca	23.86	21.45	26.72	29.93
Al	13.83	16.65	9.24	6.83
Si	5.23	4.92	-	-
S	1.80	2.62	11.53	10.92
Mg	2.66	2.56	-	-
Fe	1.42	1.36	-	-
C	10.09	9.67	-	4.69

Table 4.10 EDX quantitative analysis results of hydrated Mix B pastes

Element (wt%)	(a)	(b)	(d)	(f)
O	39.05	51.56	48.22	59.43
Ca	31.40	16.89	31.57	23.77
Al	8.09	9.99	7.88	6.74
Si	4.27	4.05	0.58	-
S	4.46	4.91	11.77	10.07
Mg	1.46	3.41	-	-
Fe	1.34	0.86	-	-
C	9.92	8.32	-	-

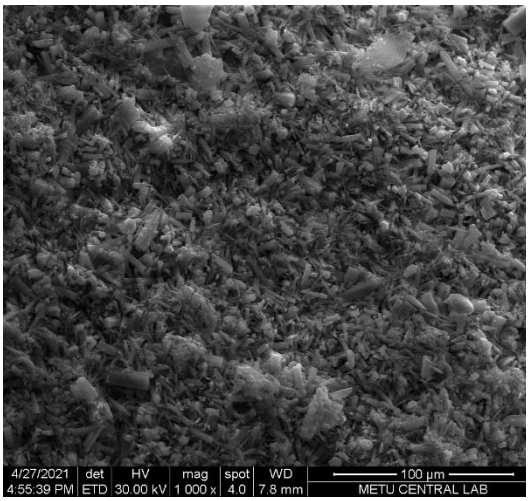

(a) 28 d

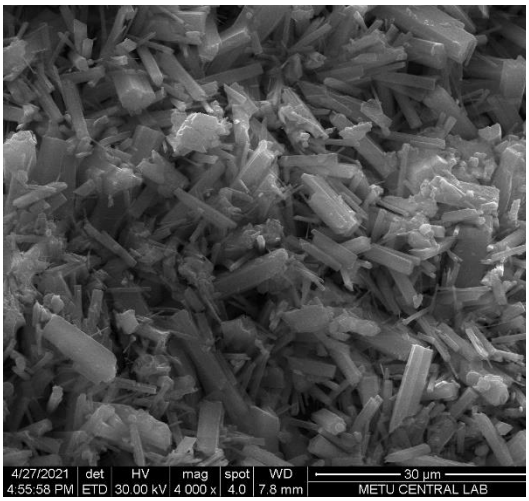

(b) 28 d

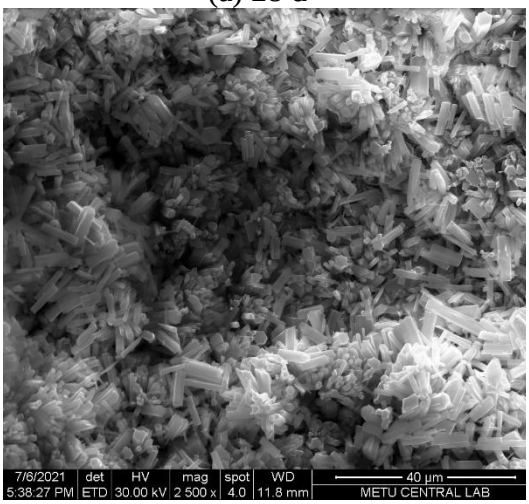

(c) 90 d

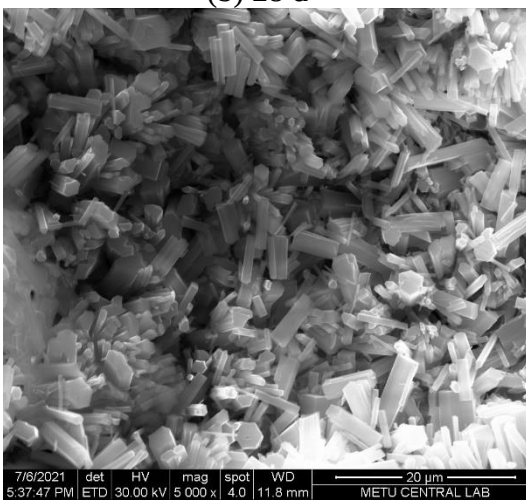

(d) 90 d

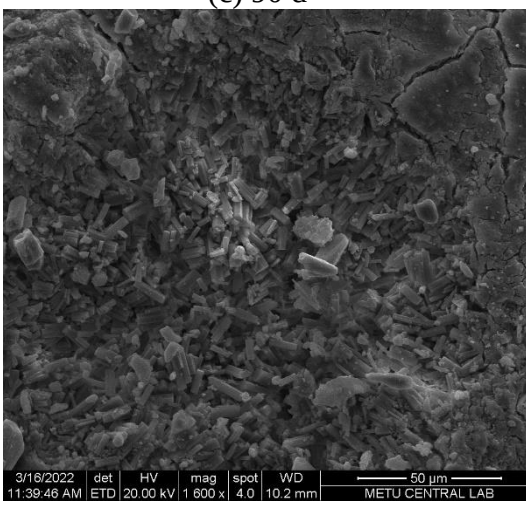

(e) 360 d

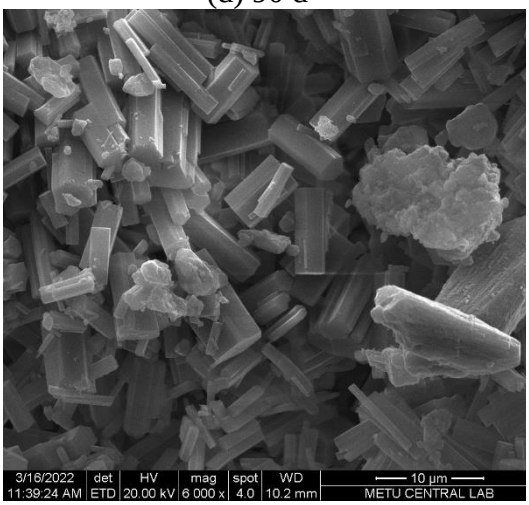

(f) 360 d

Figure 4.22 SEM images of Mix C pastes at (a,b) 28 d (c,d) 90 d (e,f) 360 d

Table 4.11 EDX quantitative analysis results of hydrated Mix C pastes

Element (wt%)	(a)	(b)	(d)
O	45.65	48.46	25.69
Ca	24.19	25.93	61.38
Al	6.32	6.58	2.60
Si	0.55	0.60	-
S	9.80	10.08	10.33
Mg	0.85	0.72	-
Fe	0.57	0.38	-
C	12.07	7.26	-

4.3.6 Compressive Strength Development

The compressive strength development of the water-cured CSA cement mortars from 3 hours to 180 days is shown in Figure 4.23.

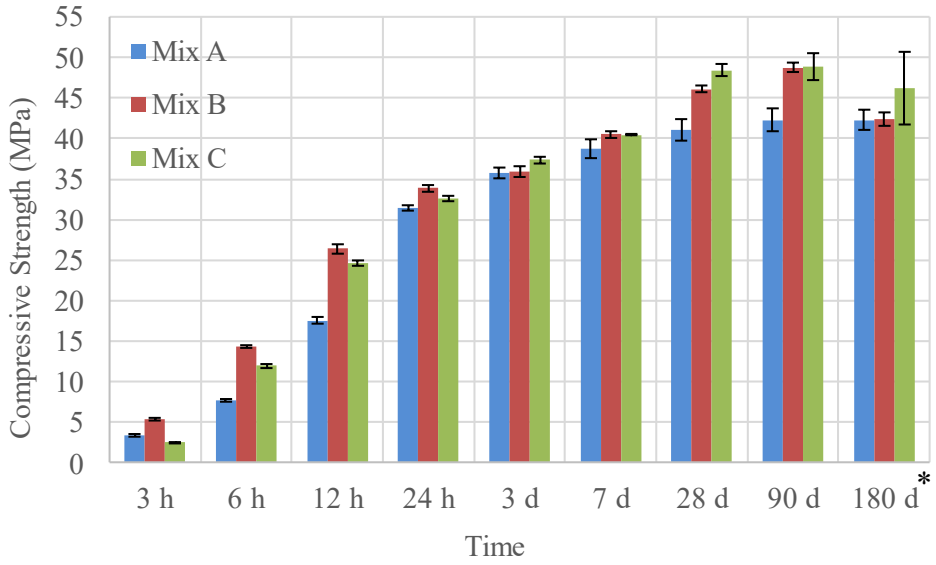

**180d results are average of two samples*

Figure 4.23 Compressive strength of the CSA cements

At 3 hours, the compressive strengths of the mortars were obtained as 3.3 MPa, 5.3 MPa, and 2.5 MPa for Mix A, Mix B, and Mix C, respectively. Within one day, the compressive strength of the mortars increased rapidly, and all mixes achieved a strength of over 30 MPa at 1st day. However, the rate of strength development was relatively slow in the following curing ages. On the 3rd curing day, the compressive strengths of the mixes reached over 35 MPa, and on the 7th day, they exceeded 38 MPa. For each curing age except 3 hours, Mix A showed lower strength than the other two mixes. As also seen in the heat flow curves of mixes, the slower hydration kinetics of Mix A is thought to be related to the fact that Mix A contains less anhydrite despite the higher ye'elimite content. Mix B and Mix C at seven days reached the same compressive strength level. Although Mix C has slightly higher strength at 28 days, Mix B and Mix C achieved the same compressive strength level, 48.8 MPa, at 90 days. It is seen that there is no considerable difference between the 28- and 90-day compressive strength results of the mixes. Especially for Mix C, the strength remained almost stable after 28 days. Mix A achieved approximately 77% of its 28-day compressive strength by one day, while the corresponding values for Mix B and Mix C are about 73% and 67%. When the compressive strength results of the 180th day were examined, no change was observed in the compressive strength of Mix A from the 90th day. On the other hand, the compressive strengths of Mix B and Mix C decreased by 13% and 5 % compared to the compressive strengths on the 90th day, respectively. Hargis et al. (2017) stated that carbonation of ettringite causes solid volume reduction, leading to strength losses, especially in CSA-based products with higher w/c. Similarly, the decrease in strength in mixes may be due to the carbonation of ettringite. However, it should be noted that two samples were tested on day 180. More samples need to be tested for definitive conclusions.

CHAPTER 5

ENVIRONMENTAL ASSESSMENT of CSA CEMENTS

5.1 General

A life cycle assessment (LCA) is a tool used to estimate and assess the environmental impacts of a product or service throughout its life cycle, from resource extraction to production, delivery, and after consumer use to final waste or recycling into a new product. Environmental impacts include factors that affect the environment, such as depletion of natural resources, climate change, toxic emissions, destruction of the ozone layer, eutrophication, acidification, etc. LCA consists of four main stages: goal and scope definition, inventory analysis, impact assessment, and interpretation. (Rebitzer et al., 2004; Salas et al., 2016).

This study considered energy consumption and CO_2 emission of CSA cements as environmental performance indicators. However, a comprehensive LCA study could not be conducted due to the unavailability of data on the whole system. Instead, the mixes' environmental performance has been determined statistically using a life cycle perspective. Based on the data published in the literature on the energy consumption and CO_2 emission of each material used for the produced CSA cements, the mixes' energy consumption and CO_2 emission values were estimated statistically using the Monte Carlo simulation method. The energy consumption and CO_2 emission values obtained were compared with the environmental analysis results of PC.

5.2 Monte Carlo Simulation Technique

Monte Carlo simulation is a type of simulation in which results are calculated based on repeated random sampling and statistical analysis (Raychaudhuri, 2008). In

Monte Carlo simulation, the probability distribution of the possibility of a particular situation occurring is determined by taking into account the uncertainty in the independent variables using their probability distribution functions (Pereira et al., 2014). This simulation technique can be viewed as a systematic way of performing a what-if analysis since this method is based on random experiments where the exact outcome is unknown beforehand (Raychaudhuri, 2008).

Mathematical models are often used to define interactions in a system with mathematical expressions. While the relationship between input and output values in deterministic models is expressed in Figure 5.1-a, in Monte Carlo simulation, inputs and outputs are defined with a probability distribution, as seen in Figure 5.1-b. In a deterministic model, there is no randomness. Monte Carlo analysis, on the other hand, uses random input from a given dataset to determine possible outputs (Platon & Constantinescu, 2014).

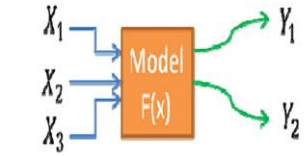

(a)

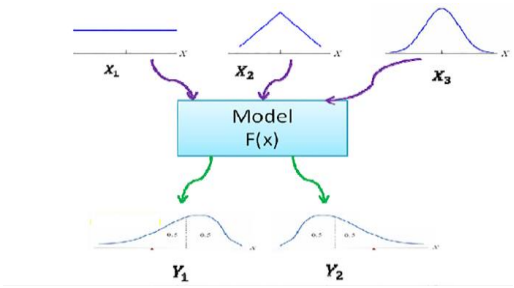

(b)

Figure 5.1 (a) Deterministic model (b) Monte Carlo model (Platon & Constantinescu, 2014)

The Monte Carlo simulation model has a number of benefits, such as the ability to simulate correlations between many dependent variables, the use of straightforward algebra, computer-based distribution function calculation with available several commercial software, relatively easy processing of the simple to complex linear and nonlinear models, allowing for quick and easy model changes and tests, being able to run the model simultaneously with multiple independent variables, generating a probability distribution function for the output variable, and helping to interpret the results for a particular action (Pereira et al., 2014).

In this chapter of the thesis, the energy consumption and CO_2 emission of CSA cements are estimated using the Monte Carlo simulation technique, as outlined below. As seen below, each material used in the production of CSA cements refers to an independent variable. Each independent variable is affected by many parameters, such as production technology and raw material composition used. These parameters lead to different output values, which increases the number of combinations and causes the process to have a random structure. Therefore, it is important to use the Monte Carlo simulation model, where randomness is considered, in determining the environmental performance of the CSA cements production.

5.3 Environmental Assessment Methodology

The methodology applied in assessing the environmental impact of CSA cements produced in this thesis follows the steps given below:

5.3.1 Mathematical Model

The simulation model of this study aims to determine the values for energy consumption and CO_2 emissions of the produced CSA cement with a confidence interval of 90%. The values for energy consumption were calculated using Equation 22, and the values for CO_2 emission were calculated using Equation 23.

$$\mathrm{EC} = (\sum_{i=1}^{n}(EC_{i,p} \times a_{i,w} \times q_{i,w}) + \sum_{j=1}^{n}(EC_{j,p} \times q_{j,nm}))/(1 - LOI) + EC_k \quad (22)$$

$$\mathrm{CE} = (\sum_{i=1}^{n}(CE_{i,p} \times a_{i,w} \times q_{i,w}) + \sum_{j=1}^{n}(CE_{j,p} \times q_{j,nm}))/(1 - LOI) + CE_f \quad (23)$$

where EC is the energy consumption; CE is the CO_2 emission; a and q are the allocation amount and the used amount of the wastes/by-products or natural materials; and the subscripts *p*, *w*, and *nm* are used for the process, the waste/by-product, and the natural material, respectively. The functional unit of this study is 1 t of clinker. Hence, the terms regarding mix-ingredient are corrected by the LOI of the raw meal. Moreover, EC_k is the energy consumption of the kiln, and CE_f is the CO_2 emissions related to the fuel.

5.3.2 Probability Distribution of the Independent Variable

The independent variables are the most critical parameters affecting the CSA cement's outputs. Here, the independent variables are glass, ceramic, secondary steelmaking, salt slag recovery, gypsum and limestone processes, kiln heat demand, and fuel-related emission. Some of the following sections are represented by the following designations: g, c, s, ssr, gy, l, k, and f, respectively, and their probability distributions in terms of probability density functions were defined based on the data published in the literature to obtain information about the behavior of independent variables. While determining the probability distributions of the independent variables, a commercial software @RISK 8.1 was used.

5.3.3 Dependent Variables

Here, energy consumption (EC) and CO_2 emissions (CE) were determined as the dependent variables. They are considered as a good indicator in determining the environmental performance of cements.

5.3.4 Monte Carlo Simulations and Results

Monte Carlo simulation analyses were performed in @RISK 8.1 software using 1000 iterations. In Monte Carlo simulation, energy consumption and CO_2 emission values were calculated by Equations 22 and 23, respectively, by taking into account the probability distributions of the independent variables. After all simulations were run, the results were summarized to show the environmental performance of cements.

5.4 Environmental Analysis Results of CSA Cements

5.4.1 Energy Consumptions of CSA Cements

First, the energy consumption data for each input in CSA cement production, along with kiln heat demand data, were compiled from the literature. In preparing the data taken from the literature, different units were encountered, all of which were converted to MJ/t of product units. The data for each input, i.e., the independent variable, can vary depending on parameters such as the technology used in the production process and the raw meal components. Using the data compiled for each input, the probability distributions of the inputs were determined using the software @ RISK 8.1. The inputs, their minimum and maximum values, and probability distributions used in the Monte Carlo simulation model to calculate the energy consumption of produced CSA cement are listed in Table 5.1. In attempting to determine the heat demand of the kiln, the theoretical heat required for CSA cement production were first considered. A data set was formed from the theoretical heats calculated for CSA mixes in different scenarios in the literature (e.g., different raw materials, different mix ratios). However, when determining the total heat demand of the kiln process, the heat loss in the kiln should also be considered. Here, the total heat loss was calculated based on the ratio between the theoretical heat required for PC and the actual heat consumed in the kiln. The required theoretical heat for an ordinary PC clinker with 67% C_3S is 1760 MJ/t clinker (Haha et al., 2019). In

determining the total energy consumption in the kiln at PC production, the data set of EVÇED (2020) was considered, which contains the data of 52 cement plants in Türkiye in 2019. A relationship between them was found as "$EC_{th\text{-}PC} \times Normal\ (1.94, 0.14) = EC_k$." A similar relationship was assumed for CSA cement production. Therefore, "$EC_{th} \times Normal\ (1.94, 0.14)$" was written instead of "EC_k" in the Equation 22.

Table 5.1 Inputs used for energy consumption calculation

Input	Min	Max	Probability distribution and related parameters**
$EC_{g,p}$ (MJ/t glass)	4200	10000	Normal distribution μ:6977.5; σ:1401.3
$EC_{c,p}$ (MJ/t ceramic)	3310	7090	Triangular distribution a:2938.2; b:7090; c:7090
$EC_{s,p}$ (MJ/t steel)	4000	11950	Triangular distribution a:2483.7; b:11950; c:11950
$EC_{ssr,p}$ (MJ/t salt slag rec.)	1900	3845	Triangular distribution a:1900; b:2890; c:3845
$EC_{gy,p}$ (MJ/t gypsum)	200	500	Triangular distribution a:200; b:350; c:500
$EC_{l,p\text{-}mining}$ (MJ/t limestone)	10.3	109.8	Exponential distribution λ:42.1
$EC_{l,p\text{-}grinding}$ (MJ/t limestone)	24	360	Exponential distribution λ:123.7
EC_{th}* (MJ/t CSA clinker)	1099	1339	Triangular distribution a:1075.3; b:1244; c:1357.8

Glass:(Sinton, 2004; OECD/IEA, 2007; Rue et al., 2007; Schmitz et al., 2011; WSP & DNV.GL, 2015; BEIS, 2017; Testa et al., 2017; P. Hu et al., 2018; Papadogeorgos & Schure, 2019)
Ceramic: (European Comission, 2007; Monfort et al., 2008; Ecofys, 2009a; Osama & Soliman, 2016)
Steelmaking: (Price et al., 2001; C. Hu et al., 2006; Hasanbeigi et al., 2011; Kirschen et al., 2011; Yellishetty et al., 2011; Pardo et al., 2012; Burchart-Korol, 2013; He et al., 2017)
Salt slag recovery: (Cusano et al., 2017; FISSAC, 2017; Befesa, 2020)
Gypsum:(Ecofys, 2009c; Hossain et al., 2017; Fořt & Černý, 2018)
Limestone:(Tokyay, 2016; Kittipongvises, 2017; Hagemann et al., 2019; Bendouma et al., 2020)
*Theoretical heat: (Hanein et al., 2018a; Gálvez-Martos et al., 2020)
** μ: mean, σ: standard deviation, a: minimum value, b: mode, c: maximum value, λ: rate parameter

5.4.2 Allocation for Energy Consumption

According to the ISO standards, allocation is "the partitioning of the input and/or output flows of a process in the product system being studied" (Marinković et al., 2013). The allocation of environmental impacts has an important place in the LCA methodology. In most LCA studies, waste from a manufacturing process is not considered to have an environmental impact because it is unintentionally generated. However, if a waste is considered as a by-product, some of the environmental impact caused by the process should be allocated to that waste. Allocation can be made by either mass or by economic value. It does not seem possible to agree on a single correct method based on the studies conducted on allocation processes. The allocation method choice is considered one of the most controversial issues on LCA. The ISO standard for LCA states that for allocation procedures that are deemed applicable, a sensitivity analysis should be performed to show the impact of the procedure on the results (Chen et al., 2010; Van Den Heede & De Belie, 2012).

Glass waste, ceramic waste, LFS, and Serox were used as waste/by-product in the production of CSA cements. The allocation amount for Serox, obtained from the salt slag recycling, was set at 60%. This means that 60% of the energy consumption from the salt slag recycling is attributed to SEROX (FISSAC, 2017). The allocation amount for other wastes/by-products used was set at 10%. In other words, 10% of the energy consumed in the production of glass, ceramic or secondary steel is attributed to the corresponding waste/by-product. Its suitability was tested by sensitivity analyses, which are described in the following section.

5.4.2.1 Sensitivity Analyses for Allocation of Energy Consumption

Monte Carlo simulation analyses were performed with allocation amounts of 1%, 5%, 10%, and 20% for glass waste, ceramic waste, and LFS, respectively. As a result of the analyses, the percentage changes in the mean values of the distributions of energy consumption obtained for the allocation amounts of 1%, 5%, and 20% were

calculated according to the mean values in the case of the 10% allocation amount with 90% confidence. The percentage changes are presented in Table 5.2, Table 5.3, and Table 5.4 for Mix A, Mix B, and Mix C, respectively.

Table 5.2 Sensitivity analysis for mean energy consumption of Mix A

Allocation amount	Change in mean energy consumption when allocation amount of waste/by-product is changed from 10% (%)		
	Glass waste	Ceramic waste	LFS
1%	-0.3	-1.4	-4.2
5%	-0.2	-0.8	-2.4
10%	***0.0***	***0.0***	***0.0***
20%	0.3	1.5	4.7

Table 5.3 Sensitivity analysis for mean energy consumption of Mix B

Allocation amount	Change in mean energy consumption when allocation amount of waste/by-product is changed from 10% (%)		
	Glass waste	Ceramic waste	LFS
1%	-0.7	-0.8	-5.9
5%	-0.4	-0.4	-3.3
10%	***0.0***	***0.0***	***0.0***
20%	0.8	0.9	6.5

Table 5.4 Sensitivity analysis for mean energy consumption of Mix C

Allocation amount	Change in mean energy consumption when allocation amount of waste/by-product is changed from 10% (%)		
	Glass waste	Ceramic waste	LFS
1%	-0.3	-0.3	-9.5
5%	-0.2	-0.2	-5.3
10%	***0.0***	***0.0***	***0.0***
20%	0.4	0.3	10.5

As seen in Table 5.2, Table 5.3, and Table 5.4, the different allocation amounts for glass waste and ceramic waste do not have a major impact on the energy consumption results. This is due to the low percentage of glass waste and ceramic waste used in the CSA cement. The different allocation amounts for LFS had a relatively larger impact due to the higher usage proportion in the CSA cement. The change percentages according to the 10% allocation amount were around maximum ±5%, ±6%, and ±10% for Mix A, Mix B, and Mix C respectively. Considering these percentages, it can be said that when the allocation amount is changed from 10% to either 1, 5, or 20%, its effect on the energy consumption is quite low (the highest is 10% for mix C); therefore, this assumption seems viable.

5.4.3 Monte Carlo Simulation Results for Energy Consumption

While determining the energy consumption amounts using Monte Carlo simulation model, the probability distribution functions in Table 5.1 were considered in all mixes. For each mix, the probability distributions found were multiplied by the raw meal mixing ratios. Since the allocation ratio was set at 10%, a coefficient of 0.1 was added to the inputs for glass, ceramics, and LFS in the energy consumption function considered in the Monte Carlo simulation. Since the allocation rate determined for Serox was 60%, a coefficient of 0.6 was also added to the Serox input (see Equation 22). The energy consumption of each mix is formulated according to Equation 22 and the EC formula for Mix A is given below as an example:

$$
\begin{aligned}
EC_{Mix\ A} = (&Normal(6977.5,1401.3) \times 0.1 \times 0.01 \\
&+ Triang(2938.2,7090,7090) \times 0.1 \times 0.07 \\
&+ Triang(2483.7,11950,11950) \times 0.1 \times 0.14 \\
&+ Triang(1900,2890,3845) \times 0.6 \times 0.23 \\
&+ Triang(200,350,500) \times 0.27 + (Exp(42.1) \\
&+ Exp(123.7)) \times 0.28)/(1 - 0.20) \\
&+ Triang(1075.3,1244,1357.8) \times Normal\ (1.94,0.14)
\end{aligned}
$$

Energy consumption for Mix A, Mix B, and Mix C were determined by 1000 iterations of Monte Carlo simulation, and the probability distribution of energy consumptions of the mixes were obtained. The probability distribution of energy consumption based on the Monte Carlo simulation for Mix A is given in Figure 5.2. As seen in Figure 5.2, the limit values found for the 90% confidence interval are 2888 MJ to 3648 MJ per ton of clinker. In other words, with 90% confidence, the energy consumption for Mix A is less than 3648 MJ and more than 2888 MJ per ton of clinker. The mean value of the distribution is about 3270 MJ. The minimum energy consumption can go as low as 2538 MJ, and the maximum energy consumption can go as high as 3966 MJ per ton of clinker with very low probabilities.

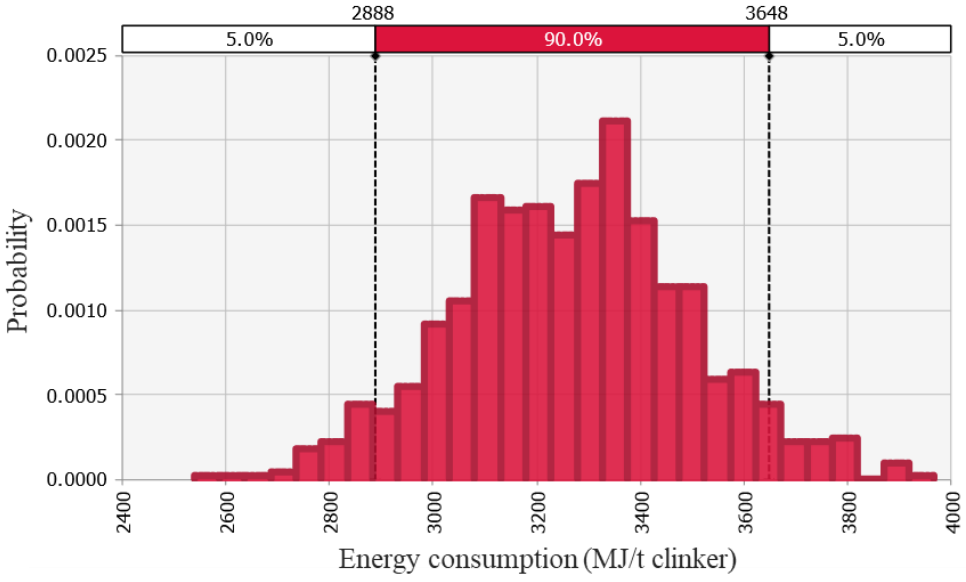

Figure 5.2 Probability distribution of energy consumption of Mix A

The probability distribution of energy consumption based on the Monte Carlo simulation for Mix B is shown in Figure 5.3. As seen in Figure 5.3, the limit values found for the 90% confidence interval are 2798 to 3540 MJ per ton of clinker. It means that with 90% confidence, the energy consumption for Mix B is less than 3540 MJ per ton of clinker. The mean value of the distribution is about 3181 MJ.

The minimum energy consumption can decrease to 2510 MJ, and the maximum energy consumption can be up to 3821 MJ per ton of clinker with very low probabilities.

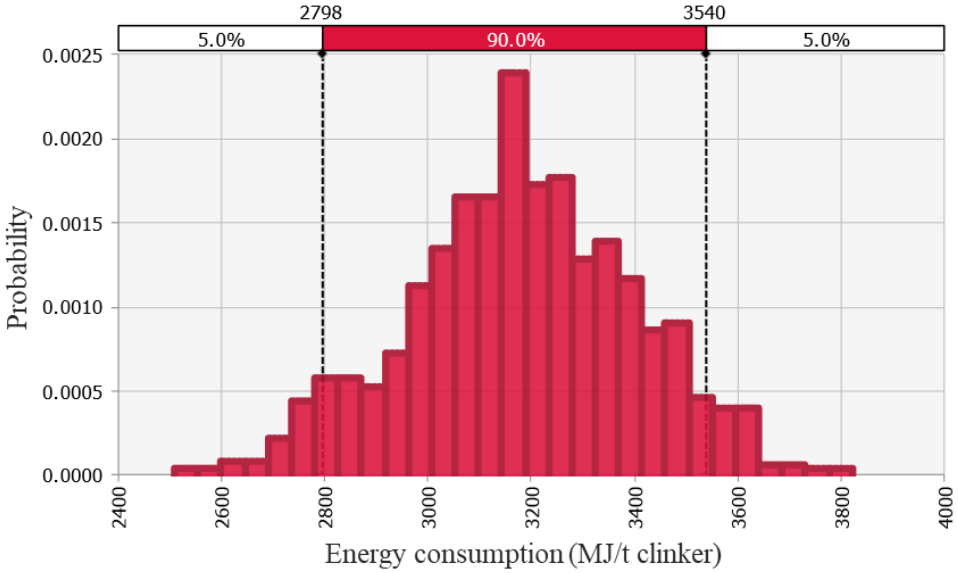

Figure 5.3 Probability distribution of energy consumption of Mix B

The probability distribution of energy consumption based on the Monte Carlo simulation for Mix C is shown in Figure 5.4. As seen in Figure 5.4, the limit values found for the 90% confidence interval are 2853 to 3631 MJ per ton of clinker, i.e., with 90% confidence, the energy consumption for Mix C is below 3631 MJ and above than 2853 MJ per ton of clinker. The mean value of the distribution is about 3243 MJ per ton of clinker. The minimum energy consumption can go as low as 2392 MJ, and the maximum energy consumption can go as high as 3997 MJ per ton of clinker with very low probabilities.

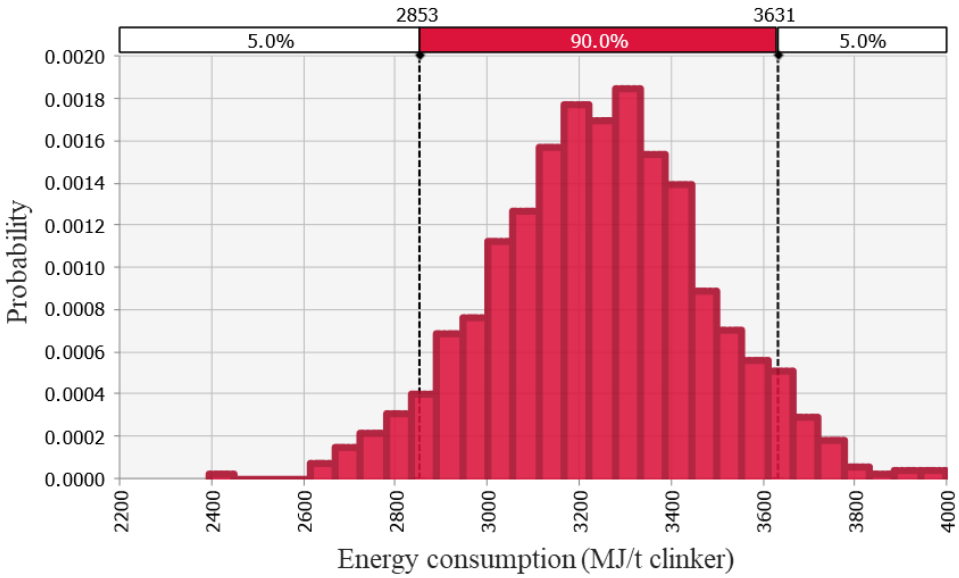

Figure 5.4 Probability distribution of energy consumption of Mix C

5.4.4 CO_2 Emissions of CSA Cements

While determining the CO_2 emission amounts of CSA cements, the same steps were followed with the energy consumption calculation. First, the CO_2 emission data for each input in CSA cement production, along with fuel-related emission data, were compiled from the literature. In preparing the data taken from the literature, different units were encountered, all of which were converted to kg CO_2/t of product units. The data for each input, i.e., the independent variable, can vary depending on parameters such as the technology used in the production process and the raw meal components. Using the data compiled for each input, the probability distributions of the inputs were determined using the software @ RISK 8.1. The inputs, their minimum and maximum values, and probability distributions used in the Monte Carlo simulation model to determine the amount of the CO_2 emissions due to produced CSA cements are given in Table 5.5.

Table 5.5 Inputs used for CO_2 emission calculation

Input	Min	Max	Probability distribution and related parameters**
$CE_{g,p}$ (kg CO_2/t glass)	450	1192	Triangular distribution a:450, b:450, c:967.8
$CE_{c,p}$ (kg CO_2/t ceramic)	263	806	Exponential distribution λ:114
$CE_{s,p}$ (kg CO_2/t steel)	240	1080	Triangular distribution a:240, b:240, c:1013.3
CE_{ssr} (kg CO_2/t salt slag rec.)	171	346.1	Triangular distribution a:171, b:260.1 c:346.1
$CE_{gy,p}$ (kg CO_2/t gypsum)	50	140.2	Triangular distribution a:50, b:120, c:140.2
$CE_{l,p\text{-}calcining}$ (kg CO_2/t PC clinker)	510	553	Normal distribution μ:527, σ:18.9
$CE_{l,p\text{-}grinding}$ (kg CO_2/t limestone	4.7	50.9	Exponential distribution λ:18.2
CE_f (kg CO_2/ton PC clinker)	271	542	Loglogistic distribution β:59.5, α:3.4

Glass:(Enviros Consulting Ltd, 2003; OECD/IEA, 2007; Ecofys, 2009b; Schmitz et al., 2011; WSP & DNV.GL, 2015; Testa et al., 2017; P. Hu et al., 2018; Papadogeorgos & Schure, 2019)
Ceramic: (Monfort et al., 2008; Ecofys, 2009a; González et al., 2011; Mezquita et al., 2014; Tikul, 2014)
Steelmaking: (Sandberg et al., 2001; C. Hu et al., 2006; K. Wang et al., 2007; Kirschen et al., 2009, 2011; European Commission, 2010; Pardo et al., 2012; Burchart-Korol, 2013; Hasanbeigi et al., 2016; Nidheesh & Kumar, 2019)
Salt slag recovery: (Cusano et al., 2017; FISSAC, 2017; Befesa, 2020)
Gypsum:(Hossain et al., 2017; Fořt & Černý, 2018; Hanein et al., 2018b; Gálvez-Martos et al., 2020)
Limestone:(Marceau et al., 2007; Habert et al., 2010; Ali et al., 2011; C. Li et al., 2014; Xu et al., 2015; Feiz et al., 2015; García-Gusano et al., 2015; Hossain et al., 2017; Kittipongvises, 2017; Hanein et al., 2018b; Gálvez-Martos et al., 2020)
Fuel:(EVÇED, 2020)
** a: minimum value, b: mode, c: maximum value, μ: mean, σ: standard deviation, λ: rate parameter, β: scale parameter, α: shape parameter

While calculating the fuel-related emission distribution of CSA cements, fuel emission data of the PC production were used with a slight reduction. According to Ukrainczyk et al. (2013), the fuel-related emissions from CSA cement are 20% less than that of PC. Since the fuel-related emission data from PC production were used to calculate the fuel-related emission of CSA cements, a coefficient of 0.80 was added to the "CE_f" distribution function in the Monte Carlo analysis. CO_2 emissions

from salt slag recovery were calculated based on estimated emissions from fuel combustion (90 kg CO_2/1 GJ) (Ukrainczyk et al., 2013)

5.4.5 Allocation for CO_2 Emissions

General information on allocation is given in section 5.4.2. In the production of CSA cements, glass waste, ceramic waste, LFS, and Serox were used as waste/by product. The allocation rate for Serox obtained from salt slag recycling was determined as 60% (FISSAC, 2017). The allocation rate for other waste used was set at 10%. Its suitability was tested again by sensitivity analyses.

5.4.5.1 Sensitivity Analyses for Allocation of CO_2 Emissions

Monte Carlo simulation analyses were performed for 1%, 5%, 10%, and 20% allocation amounts for glass waste, ceramic waste, and LFS. As a result of the analyses, the percentage changes of the mean values of the distributions of CO_2 emission obtained for the allocation amount of 1%, 5%, and 20% are calculated according to the mean values in case the allocation amount is 10%. The percentage changes are presented in Table 5.6, Table 5.7, and Table 5.8 for Mix A, Mix B, and Mix C, respectively.

Table 5.6 Sensitivity analysis for mean CO_2 emission of Mix A

Allocation amount	Change in mean CO_2 emission when allocation amount of waste/by-product is changed from 10% (%)		
	Glass waste	Ceramic waste	LFS
1%	-0.1	-0.5	-1.4
5%	-0.1	-0.3	-0.8
10%	***0.0***	***0.0***	***0.0***
20%	0.1	0.6	1.6

Table 5.7 Sensitivity analysis for mean CO_2 emission of Mix B

Allocation amount	Change in mean CO_2 emission when allocation amount of waste/by-product is changed from 10% (%)		
	Glass waste	Ceramic waste	LFS
1%	-0.4	-0.3	-1.9
5%	-0.2	-0.2	-1.1
10%	***0.0***	***0.0***	***0.0***
20%	0.4	0.3	2.2

Table 5.8 Sensitivity analysis for mean CO_2 emission of Mix C

Allocation amount	Change in mean CO_2 emission when allocation amount of waste/by-product is changed from 10% (%)		
	Glass waste	Ceramic waste	LFS
1%	-0.2	-0.1	-4.0
5%	-0.1	-0.1	-2.2
10%	***0.0***	***0.0***	***0.0***
20%	0.3	0.1	4.4

As can be seen from Table 5.6, Table 5.7, and Table 5.8, the percentages of change according to the 10% allocation amount were around maximum ±2%, ±2%, and ±4% for Mix A, Mix B, and Mix C, respectively. Considering these percentages, it can be said that when the allocation amount is changed from 10% to either 1, 5, or 20%, its effect on the CO_2 emission is very low; hence, this assumption seems viable.

5.4.6 Monte Carlo Simulation Results for CO_2 emission

While determining CO_2 emission levels using the Monte Carlo simulation model, the probability distribution functions in Table 5.5 were considered in all mixes. For each mix, these probability distributions found were multiplied by the raw meal mixing ratios. Since the allocation amount was set at 10%, a coefficient of 0.1 was added to the inputs for glass, ceramics, and LFS in the CO_2 emission function considered in the Monte Carlo simulation. Since the allocation rate determined for Serox was 60%,

a coefficient of 0.6 was also added to the Serox input (see Equation 23). The CO_2 emission amount of each mix is formulated according to Equation 23 and the CE formula for Mix A is given below as an example:

$$CE_{Mix\,A} = (Triang(450, 450, 967.8) \times 0.1 \times 0.01 + Exp(114) \times 0.1 \times 0.07 + Triang(240,240,1013.2) \times 0.1 \times 0.14 + Triang(171, 260.1, 346.1) \times 0.6 \times 0.23 + Triang(50,120, 140.2) \times 0.27 + (Normal(527, 18.9) + Exp(18.2)) \times 0.28))/(1 - 0.20) + Loglogistic(59.5, 3.4) \times 0.80$$

CO_2 emissions for Mix A, Mix B, and Mix C were determined by 1000 iterations of Monte Carlo simulation, and the probability distribution of CO_2 emissions of the mixes were obtained. Figure 5.5 shows the probability distribution of CO_2 emission based on Monte Carlo simulation for Mix A. According to Figure 5.5, the limit values found for the 90% confidence interval are 503.5 to 607.5 kg CO_2 per ton of clinker. The mean value of the distribution is about 555 kg CO_2 per ton of clinker.

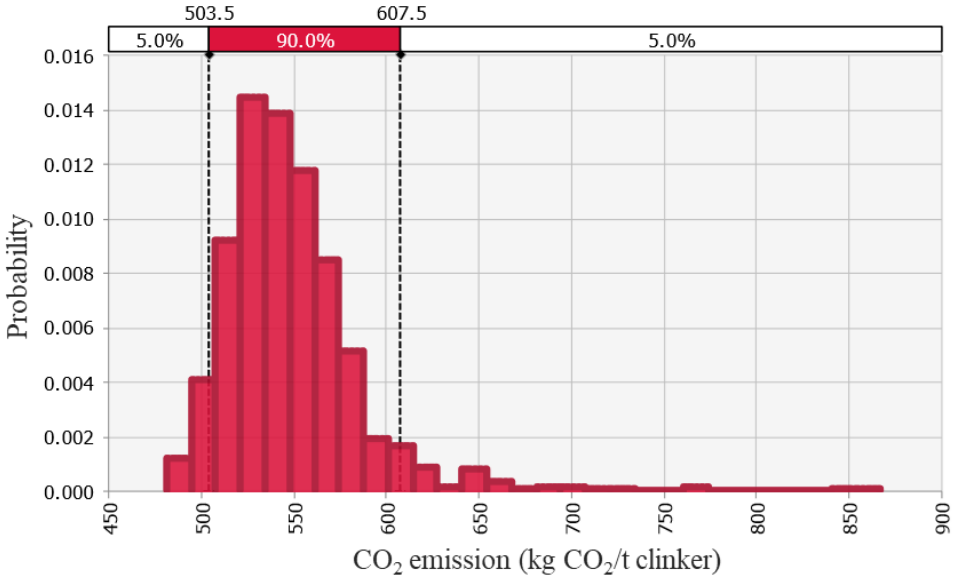

Figure 5.5 Probability distribution of CO_2 emission of Mix A

Figure 5.6 shows the probability distribution of CO_2 emission based on the Monte Carlo simulation for Mix B. According to Figure 5.6, the limits for the 90% confidence interval are 501 to 607 kg of CO_2 per ton of clinker, i.e., with 90% confidence, the CO_2 emission is above 501 kg and below 607 kg per ton of clinker. The mean value of the distribution is about 546 kg CO_2 per ton of clinker.

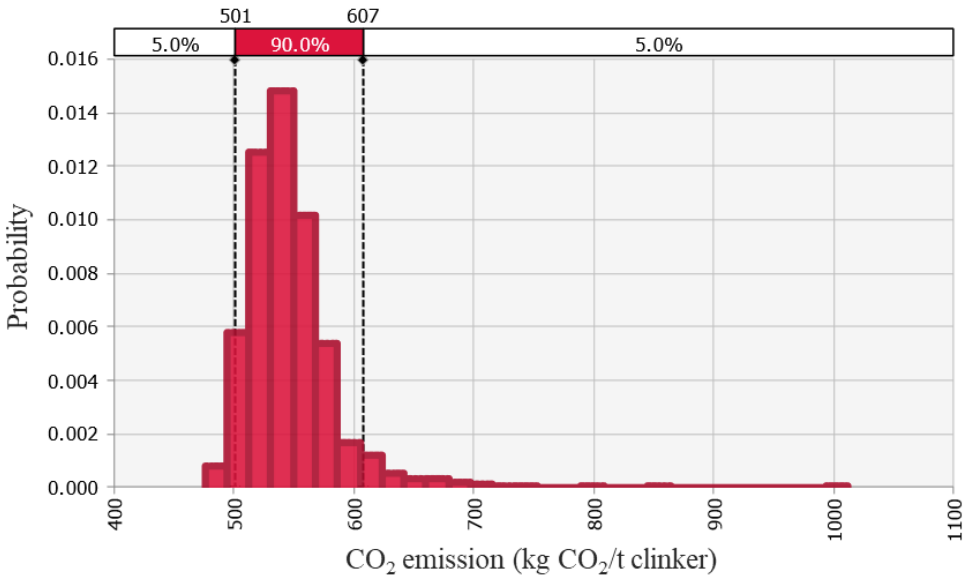

Figure 5.6 Probability distribution of CO_2 emission of Mix B

Figure 5.7 shows the probability distribution of CO_2 emission based on Monte Carlo simulation for Mix C. According to Figure 5.7, the limits for the 90% confidence interval are 393.4 to 496 kg of CO_2 per ton of clinker, i.e., with 90% confidence, the CO_2 emission is above 393.4 kg and below 496 kg per ton of clinker. The mean value of the distribution is about 436 kg CO_2 per ton of clinker.

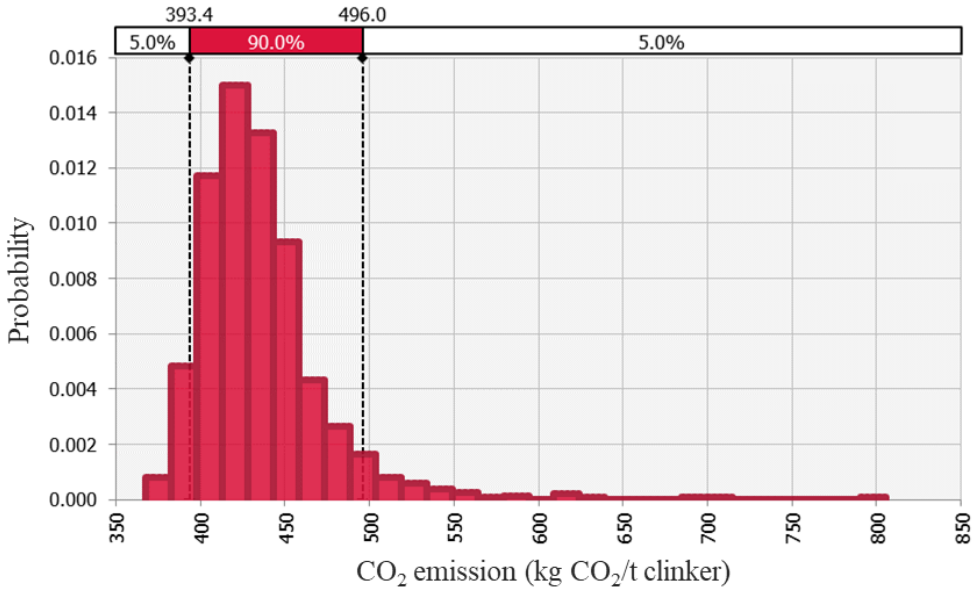

Figure 5.7 Probability distribution of CO_2 emission of Mix C

5.5 Environmental Analysis Results of Portland Cement (PC)

In order to compare the abovementioned CSA results, environmental analysis of Portland cement was also performed as follows.

5.5.1 Descriptive Statistics of PC

The values for energy consumption and CO_2 emissions in the production of PC clinker were compiled from reported statistics and published studies in the literature. The minimum and maximum value of the obtained data and the probability distributions of the energy and CO_2 emission used in the Monte Carlo simulation model are presented in Table 5.9. According to the obtained data, thermal energy consumption, power consumption up to and including clinker production, and direct CO_2 emissions excluding on-site power generation are in the range of 2900 to 5568 MJ, 47 to 88 kWh, and 612 to 1097 kg CO_2 for 1 ton of PC clinker production, respectively.

Table 5.9 Energy consumption and CO_2 emission values of PC

	Min	Max	Probability distribution and related parameters**
Thermal energy consumption (MJ/t clinker)	2900	5568	Loglogistic distribution β:1151.2, α:6.3
Power consumption (kWh/t clinker)	47	88	Normal distribution μ:66.0, σ:9.6
CO_2 emissions (kg CO_2/t clinker)	612	1067	Logistic distribution μ:840.2, s:36.9

References: (Habert et al., 2010; Ali et al., 2011; C. Li et al., 2014; Feiz et al., 2015; García-Gusano et al., 2015; Xu et al., 2015; Hossain et al., 2017; WBCSD, 2019; EVÇED, 2020)
** β: scale parameter, α: shape parameter, μ: mean, σ: standard deviation, s: scale parameter

5.5.2 Monte Carlo Simulation Results of PC

Monte Carlo analyses were performed using the distribution functions in Table 5.9, and the probability distributions of the energy consumption (sum of thermal and electric energy) and CO_2 emission values for PC were obtained.

Figure 5.8 shows the probability distribution of the energy consumption of 1 ton of PC clinker. Accordingly, the 90% confidence interval limits are 3286 to 4409 MJ per ton of PC clinker. The results show that the mean value of the distribution is 3772 MJ. The minimum energy consumption can go as low as 2927 MJ, but the maximum energy consumption could go as high as 6423 MJ per ton of clinker with very low probabilities.

Figure 5.9 shows the probability distribution of the CO_2 emissions due to the production of 1 ton of PC clinker. As seen from Figure 5.9, the 90% confidence interval limits are 731 to 948 kg per ton of clinker. In other words, with 90% confidence, the CO_2 emission of the PC clinker production is less than 948 kg and greater than 731 kg per ton of clinker. The mean value of the distribution is 840 kg CO_2.

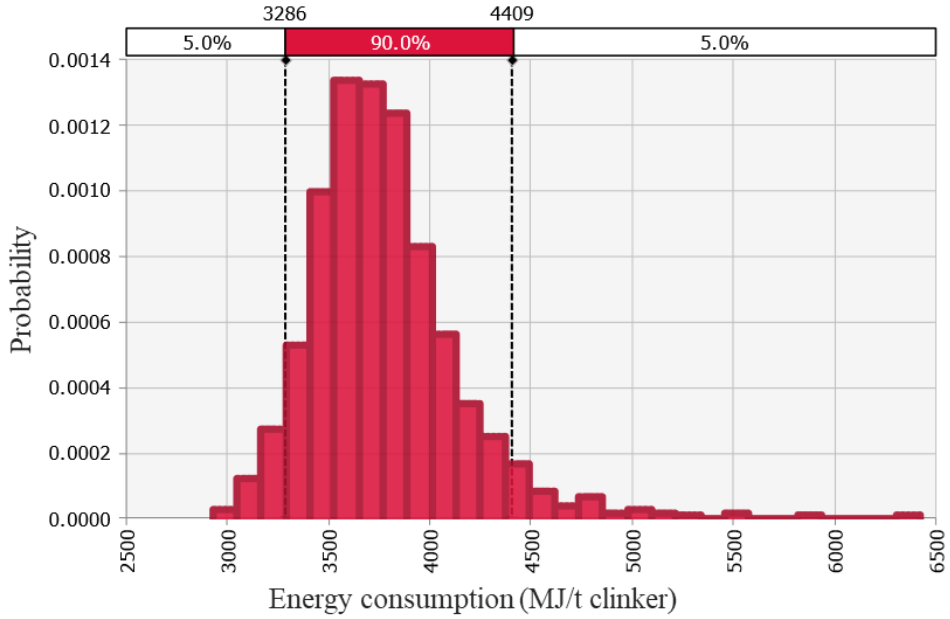

Figure 5.8 Probability distribution of total energy consumption of PC (MJ/t clinker)

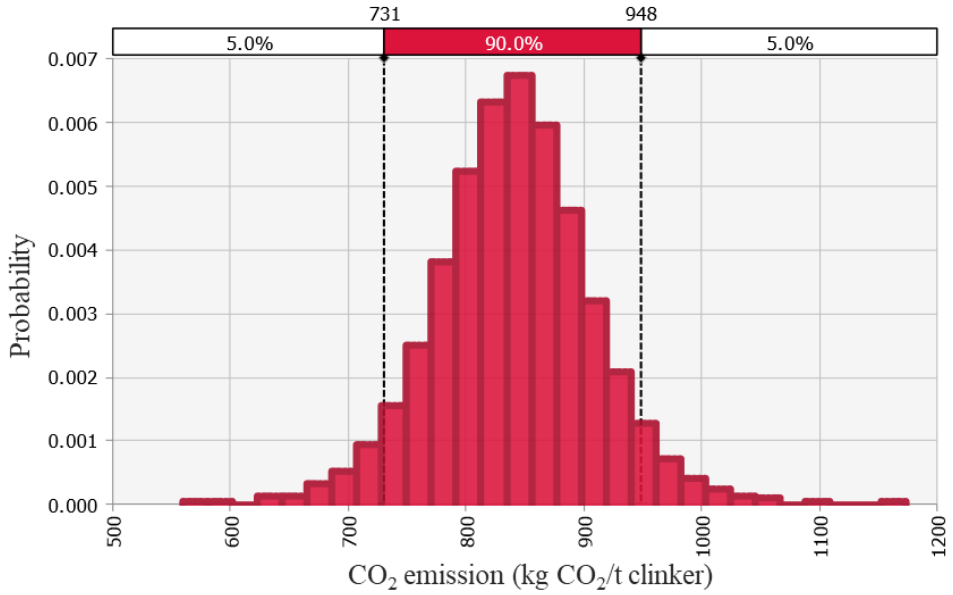

Figure 5.9 Probability distribution of CO_2 emissions of PC (kg CO_2/t clinker)

5.6 Comparison of the Environmental Impacts of CSA Cements and PC

The 90% confidence intervals of the calculated energy consumptions for the produced CSA cements and PC are shown in Figure 5.10.

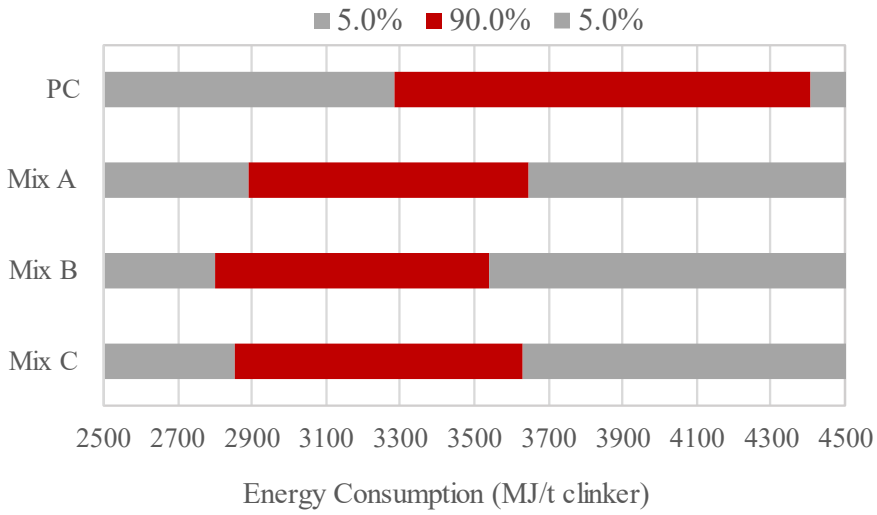

Figure 5.10 Energy consumption values of PC and CSA cements

From Figure 5.10, it can be seen how the energy consumption ranges of CSA cements have shifted to the left compared to PC. As expected, the production of CSA cement consumes less energy than PC. Comparing CSA cements and PC with the lower limit of the 90% confidence interval, the energy consumption of Mix A, B, and C is lower than that of PC by about 12%, 15%, and 13%, respectively. Based on the mean values, this reduction is almost 13%, 16%, and 14%, respectively. A comparison with the upper limit shows that the energy consumption is lower than that of PC by about 17%, 20%, and 18%, respectively. Comparing CSA cements among each other, the energy demand of Mix B is slightly less compared to the others. This can be attributed to the relatively lower content of Serox and LFS in Mix B.

Similarly, CO_2 emission values of produced CSA cements and PC were compared, and the results for the 90% confidence interval are presented in Figure 5.11. It is very clearly seen that CSA cements cause much lower CO_2 emissions compared to PC.

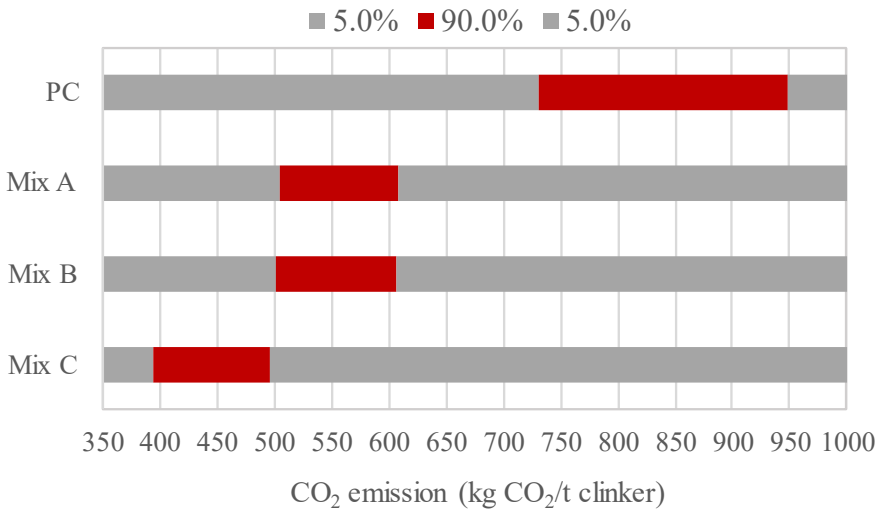

Figure 5.11 CO_2 emissions of PC and CSA cements

Comparing the CO_2 emissions of CSA cements with that of PC, the reduction at the lower limits is about 31% for Mix A and B and 46% for Mix C; on the mean, this reduction is about 35% for Mix A and B and 48% for Mix C; and at the upper limits, the decrease is about 36% for Mix A and B and 48% for Mix C. When the CSA cements are compared among each other, it is seen that the emission values of Mix A and Mix B are quite close to each other, while Mix C causes about 20% less CO_2 than the other two mixes due to its lower limestone content. Note that the amount of limestone used in Mix C is 12%, whereas Mix A and Mix B is 28% and 29%, respectively.

The results of the statistical analysis show that the environmental impact of CSA cements is lower than that of PC, when both the energy consumption and CO_2 emissions of cements are considered. The highest energy consumption occurs during burning, and a large part of the CO_2 emissions is due to calcination and fuel, as in the production of PC.

Aranda & De la Torre (2013) stated that 1 ton of PC clinker production causes a maximum of 0.98 t of CO_2 emissions, and the CO_2 emission caused by 1 ton of CSA clinker production can be 0.25 to 0.35 t less compared to PC, depending on its composition. Accordingly, 1 t of CSA clinker emits 0.63 to 0.73 t CO_2. Similarly, Hanein et al. (2018) calculated that CO_2 emissions for different CSA production scenarios decrease by 25-35% compared to PC, in the range of 588 to 644 kg CO2 per ton of clinker. Considering the mean emission values of the produced CSA mixes, it is found that CO_2 emissions have decreased to 436-555 kg thanks to the use of waste/by-product and less limestone, which represents a decrease of 35-48% compared to the mean PC emission; therefore, it can be said that a more environmentally friendly production is possible using the industrial symbiosis approach.

CHAPTER 6

CONCLUSIONS AND RECOMMENDATIONS

6.1 Conclusions

In this study, CSA cements with three different mix formulations were synthesized using an industrial symbiosis approach. Industrial symbiosis is a network in which independent companies work together in mutually beneficial cooperation. The industrial symbiosis network in this study includes the ceramic industry, the secondary steel industry, the secondary aluminum (non-ferrous metals) industry, the glass industry, and the cement industry. The wastes/by-products from the first four industries listed, i.e., ceramic wastes, LFS, Serox, and glass wastes, together with limestone and gypsum, became the raw material for CSA cements.

First, environmentally friendly CSA cements were synthesized on a laboratory scale using natural and waste materials. Second, the chemical, physical, and mineralogical properties of the CSA cements were investigated. Then, the hydration behavior and long-term performance of CSA cements were evaluated by various test methods. Finally, the environmental performance of CSA cements was assessed with a "life cycle perspective." The CSA cement's energy consumption and CO_2 emission were estimated using a Monte Carlo simulation.

According to the test results, the following conclusions can be drawn:

- Serox, LFS, ceramic waste, and glass waste can be used in the raw mix to produce CSA cement. It was possible to produce environmentally friendly CSA cement by combining these waste materials, whose total content varied between 42% and 52%, with limestone and gypsum and burning them at 1250 °C for 90 minutes.

- The mineralogical composition of all three CSA cements includes ye'elimite, anhydrite, merwinite, fluorellestadite, belite, and perovskite. Mix A, whose Al_2O_3 is the highest, has the highest ye'elimite content. On the other hand, Mix C, whose SO_3 is the highest, has the highest anhydrite content. In contrast to the literature, higher amounts of merwinite and fluorellestadite phases were detected in all cements. CaO and SiO_2, two important oxides required for the formation of belite, played a role in forming the merwinite and fluorellestadite phases. In addition, the formation of fluorellestadite in the produced CSA cements was associated with the fluorine (F) and chlorine (C) contents in the raw materials used for their production.
- The total heat evolution after 72 h of hydration for Mix A, Mix B, and Mix C was 287, 262, and 261 J/g, respectively, and the heat flow curves of the CSA cement pastes showed three distinct heat release peaks. The rate of the heat of hydration of Mix A slowed down after the second heat release peak. The reason why the hydration kinetics of Mix A was slower compared to Mix B and Mix C can be attributed to the relatively higher content of ye'elimite and lower content of anhydrite.
- The main hydration products of the produced CSA cements are ettringite and aluminum hydroxide. The presence of ettringite was also detected by SEM analyses. It was in the form of well-crystallized needles.
- Within a day, the compressive strength of the CSA cement mortars increased rapidly, and all mixes reached a strength of over 30 MPa after one day of curing. However, at subsequent curing times, the development of strength was relatively slow. Mix A reached about 77% of its 28-day compressive strength by one day, while the corresponding values for Mix B and Mix C were about 73% and 67%, respectively. There is no considerable difference between the 28- and 90-day compressive strength results of the mixes. When the compressive strength results of the 180^{th} day was examined, no change was observed for Mix A compared to the 90^{th} day, while the compressive strength of Mix B and Mix C decreased by 13% and 5%, respectively.

Although it is thought that the decrease in strength may be due to the carbonation of ettringite, more samples need to be tested for definitive conclusions.

- XRD and thermal analyses showed that ettringite, the main hydration product of the produced CSA cements, was carbonated over time and decomposed into gypsum, calcium carbonate, and aluminum hydroxide. Compared to the water-cured samples, the air-cured samples revealed more clearly that ettringite was carbonated over time. It should be noted that the samples analyzed were quite small, having a circular plate geometry with an average diameter of 30 mm, and a thickness of 5 mm.

The main conclusions regarding the environmental assessment of the CSA cements are as follows:

- Despite conservative assumptions, the results of the Monte Carlo simulation revealed that the environmental performance of the produced CSA cements is better than the PC in terms of energy consumption and CO_2 emissions. However, just as with PC, the highest energy consumption occurs during burning, and most of the CO_2 emissions come from calcination and fuel combustion.
- Compared to PC, the energy consumption of CSA cements was lower by 12% to 15%, 13% to 16%, and 17% to 20%, considering the lower limit, mean, and upper limit of the distribution of the energy consumptions, respectively. Comparing CSA cements among each other, the energy demand of Mix B is slightly less compared to the others. This can be attributed to the relatively lower content of Serox and LFS in Mix B.
- Compared to PC, the CO_2 emission consumption of CSA cements was lower by 31% to 46%, 35% to 48%, and 36% to 48%, considering the lower limit, mean, and upper limit of the distribution of CO_2 emissions, respectively. Comparing CSA cements among each other, the CO_2 emission values of Mix

A and Mix B are quite close to each other, while Mix C causes about 20% less CO_2 than the other two mixes due to its lower limestone content.

6.2 Recommendations

- In this study, the hydration behavior and the compressive strength of the CSA cements produced using different wastes were studied. However, for a comprehensive usage of such cements, their durability related properties need to be well understood. Among the many durability-related properties, carbonation of CSA cements is an issue that needs further investigation. It seems that CSA cements undergo carbonation when cured even under water. Therefore, the consequences of carbonation and their implications on the mechanical and durability properties of the hardened product can also be studied.
- It seems that using wastes in the production of CSA cements may cause the formation of F, Cl, Mg, etc. bearing compounds like the Fluorellestadite and Merwinite observed in this study. The hydration behavior as well as the mechanical and durability properties of such compounds can be studied.

REFERENCES

Adolfsson, D., Menad, N., Viggh, E., & Björkman, B. (2007). Steelmaking slags as raw material for sulphoaluminate belite cement. *Advances in Cement Research*, *19*(4), 147–156. https://doi.org/10.1680/adcr.2007.19.4.147

Ali, M. B., Saidur, R., & Hossain, M. S. (2011). A review on emission analysis in cement industries. *Renewable and Sustainable Energy Reviews*, *15*(5), 2252–2261. https://doi.org/10.1016/j.rser.2011.02.014

Alkaya, E., Böğürcü, M., & Ulutaş, F. (2014). Industrial Symbiosis in Iskenderun Bay: A journey from Pilot Applications to a National Program in Turkey. *Technology Development Foundation of Turkey*, 1–8.

Álvarez-Pinazo, G., Cuesta, A., García-Maté, M., Santacruz, I., Losilla, E. R., La Torre, A. G. D., León-Reina, L., & Aranda, M. A. G. (2012). Rietveld quantitative phase analysis of Yeelimite-containing cements. *Cement and Concrete Research*, *42*(7), 960–971. https://doi.org/10.1016/j.cemconres.2012.03.018

Andac, O., & Glasser, F. P. (1994). Polymorphism of calcium sulphoaluminate (Ca4Al6O16 · SO3) and its solid solutions. *Advances in Cement Research*, *6*(22), 57–60. https://doi.org/10.1680/adcr.1994.6.22.57

Aranda, M. A. G., & De la Torre, A. G. (2013). Sulfoaluminate cement. In *Eco-Efficient Concrete*. Woodhead Publishing. https://doi.org/10.1533/9780857098993.4.488

Arjunan, P., Silsbee, M. R., & Roy, D. M. (1999). Sulfoaluminate-belite cement from low-calcium fly ash and sulfur-rich and other industrial by-products. *Cement and Concrete Research*, *29*(8), 1305–1311. https://doi.org/10.1016/S0008-8846(99)00072-1

ASTM C219 - 20a. (2020). Standard Terminology Relating to Hydraulic and Other Inorganic Cements. In *American Society for Testing and Materials*. https://doi.org/10.1520/C0219-20A.2

Avdontceva, M. S., Zolotarev, A. A., Krivovichev, S. V., Krzhizhanovskaya, M. G., Sokol, E. V., Kokh, S. N., Bocharov, V. N., Rassomakhin, M. A., & Zolotarev, A. A. (2021). Fluorellestadite from burned coal dumps: crystal structure refinement, vibrational spectroscopy data and thermal behavior. *Mineralogy and Petrology*, *115*, 271–281. https://doi.org/10.1007/s00710-021-00740-4

Awoyera, P. O., Dawson, A. R., Thom, N. H., & Akinmusuru, J. O. (2017). Suitability of mortars produced using laterite and ceramic wastes: Mechanical and microscale analysis. *Construction and Building Materials*, *148*, 195–203. https://doi.org/10.1016/j.conbuildmat.2017.05.031

Ayres, R. U. (1989). Industrial Metabolism. In *Industrial Metabolism, The Environment, and Application of Materials-Balance Principles for Selected Chemicals* (pp. 1–15). IIASA, Laxenburg, Austria.

Befesa. (2019). *2019 Sustainabilty Report*. https://www.befesa.com/sustainability/reports-policies-certifications/

Befesa. (2020). *Sustainability Reports: ESG Progress Update 2020*. https://www.befesa.com/sustainability/reports-policies-certifications/

BEIS. (2017). *Glass Sector-Industrial Decarbonisation and Energy Efficiency Roadmap Action Plan* (Issue October).

Bendouma, S., Serradj, T., & Vapur, H. (2020). A case study of the life cycle impact of limestone quarrying on the environment. *International Journal of Global Warming*, *22*(4).

Beretka, J., Marroccoli, M., Sherman, N., & Valenti, G. L. (1996). The influence of C4A3$\bar{S}$ content and w/s ratio on the performance of calcium sulfoaluminate-based cements. *Cement and Concrete Research*, *26*(11), 1673–1681.

https://doi.org/10.1016/S0008-8846(96)00164-0

Berger, S., Cau Dit Coumes, C., Le Bescop, P., & Damidot, D. (2011). Stabilization of ZnCl2-containing wastes using calcium sulfoaluminate cement: Cement hydration, strength development and volume stability. *Journal of Hazardous Materials*, *194*, 256–267. https://doi.org/10.1016/j.jhazmat.2011.07.095

Bernardo, G., Telesca, A., & Valenti, G. L. (2006). A porosimetric study of calcium sulfoaluminate cement pastes cured at early ages. *Cement and Concrete Research*, *36*(6), 1042–1047. https://doi.org/10.1016/j.cemconres.2006.02.014

Bescher, E., & Kim, J. (2019). Belitic Calcium Sulfoaluminate Cement: History, Chemistry, Performance, and Use in the United States. *Conference: 1st International Conference on Innovation in Low Carbon Cement and Concrete Technology*, *July*, 2–5.

Bescher, E. P., Kim, J., Ramseyer, C., & Vallens, J. K. (2018). Low Carbon Footprint Pavement: History of Use, Performance And New Opportunities For Belitic Calcium Sulfoaluminate. *Proceedings of the 13th International Symposium on Concrete Roads*.

Bizzozero, J., Gosselin, C., & Scrivener, K. L. (2014). Expansion mechanisms in calcium aluminate and sulfoaluminate systems with calcium sulfate. *Cement and Concrete Research*, *56*, 190–202. https://doi.org/10.1016/j.cemconres.2013.11.011

Borštnar, M., Daneu, N., & Dolenec, S. (2020). Phase development and hydration kinetics of belite-calcium sulfoaluminate cements at different curing temperatures. *Ceramics International*, *46*(18), 29421–29428. https://doi.org/10.1016/j.ceramint.2020.05.029

Bullerjahn, F. (2018). *Characterisation and hydration of ye'elimite containing cements*. [Doctoral dissertation, École Polytechnique Fédérale de Lausanne].

Bullerjahn, F., Schmitt, D., & Ben Haha, M. (2014). Effect of raw mix design and of clinkering process on the formation and mineralogical composition of (ternesite) belite calcium sulphoaluminate ferrite clinker. *Cement and Concrete Research*, *59*, 87–95. https://doi.org/10.1016/j.cemconres.2014.02.004

Bullerjahn, F., Zajac, M., & Ben Haha, M. (2015). CSA raw mix design: effect on clinker formation and reactivity. *Materials and Structures/Materiaux et Constructions*, *48*(12), 3895–3911. https://doi.org/10.1617/s11527-014-0451-z

Burchart-Korol, D. (2013). Life cycle assessment of steel production in Poland: A case study. *Journal of Cleaner Production*, *54*, 235–243. https://doi.org/10.1016/j.jclepro.2013.04.031

Burris, L. E., & Kurtis, K. E. (2018). Influence of set retarding admixtures on calcium sulfoaluminate cement hydration and property development. *Cement and Concrete Research*, *104*(November 2017), 105–113. https://doi.org/10.1016/j.cemconres.2017.11.005

Canbek, O., & Erdoğan, S. T. (2020). Influence of production parameters on calcium sulfoaluminate cements. *Construction and Building Materials*, *239*(117866). https://doi.org/10.1016/j.conbuildmat.2019.117866

Canbek, O., Shakouri, S., & Erdoğan, S. T. (2020). Laboratory production of calcium sulfoaluminate cements with high industrial waste content. *Cement and Concrete Composites*, *106*(103475). https://doi.org/10.1016/j.cemconcomp.2019.103475

Cau Dit Coumes, C., Courtois, S., Peysson, S., Ambroise, J., & Pera, J. (2009). Calcium sulfoaluminate cement blended with OPC: A potential binder to encapsulate low-level radioactive slurries of complex chemistry. *Cement and Concrete Research*, *39*(9), 740–747. https://doi.org/10.1016/j.cemconres.2009.05.016

Chang, J., Zhang, Y., Shang, X., Zhao, J., & Yu, X. (2017). Effects of amorphous AH3 phase on mechanical properties and hydration process of C4A3S̄-CS̄H2-

CH-H2O system. *Construction and Building Materials*, *133*, 314–322. https://doi.org/10.1016/j.conbuildmat.2016.11.111

Chang, W., Li, H., Wei, M., Zhu, Z., Zhang, J., & Pei, M. (2009). Effects of polycarboxylic acid based superplasticiser on properties of sulphoaluminate cement. *Materials Research Innovations*, *13*(1), 7–10. https://doi.org/10.1179/143307509X402101

Chen, C., Habert, G., Bouzidi, Y., Jullien, A., & Ventura, A. (2010). LCA allocation procedure used as an incitative method for waste recycling: An application to mineral additions in concrete. *Resources, Conservation and Recycling*, *54*(12), 1231–1240. https://doi.org/10.1016/j.resconrec.2010.04.001

Chen, I. A. (2009). *Synthesis of Portland Cement and Calcium Sulfoaluminate-Belite Cement for Sustainable Development and Performance*. [Doctoral dissertation, The University of Texas at Austin].

Chen, I. A., & Juenger, M. C. G. (2011). Synthesis and hydration of calcium sulfoaluminate-belite cements with varied phase compositions. *Journal of Materials Science*, *46*(8), 2568–2577. https://doi.org/10.1007/s10853-010-5109-9

Chen, I. A., & Juenger, M. C. G. (2012). Incorporation of coal combustion residuals into calcium sulfoaluminate-belite cement clinkers. *Cement and Concrete Composites*, *34*(8), 893–902. https://doi.org/10.1016/j.cemconcomp.2012.04.006

Chertow, M. R. (2000). Industrial ecology : Literature and taxonomy. *Annual Review of Energy and Environment*, *25*(1), pp 313-337. https://www.annualreviews.org/doi/pdf/10.1146/annurev.energy.25.1.313

Connelly, L., & Koshland, C. P. (2001). Exergy and industrial ecology—Part 1: An exergy-based definition of consumption and a thermodynamic interpretation of ecosystem evolution. *Exergy, an International Journal*, *1*(3), 146–165. https://doi.org/10.1016/s1164-0235(01)00021-8

CRW. (2020). *Ceramic World Review* (Vol. 138).

Cusano, G., Rodrigo Gonzalo, M., Farrell, F., Remus, R., Roudier, S., & Delgado Sancho, L. (2017). *Best Available Techniques (BAT) Reference Document for the Non-Ferrous Metals Industries*. https://doi.org/10.2760/8224

da Costa, E. B., Rodríguez, E. D., Bernal, S. A., Provis, J. L., Gobbo, L. A., & Kirchheim, A. P. (2016). Production and hydration of calcium sulfoaluminate-belite cements derived from aluminium anodising sludge. *Construction and Building Materials*, *122*, 373–383. https://doi.org/10.1016/j.conbuildmat.2016.06.022

Dolenec, S., Šter, K., Borštnar, M., Nagode, K., Ipavec, A., & Žibret, L. (2020). Effect of the cooling regime on the mineralogy and reactivity of belite-sulfoaluminate clinkers. *Minerals*, *10*(10), 1–16. https://doi.org/10.3390/min10100910

Dolgen, D., & Alpaslan, M. N. (2020). Eco-Industrial Parks: Experiences from Turkey. *Global Journal of Ecology*, *5*, 030–032. https://doi.org/10.17352/gje.000016

Dong, K., Xie, F., Wang, W., Chang, Y., Chen, C., & Gu, X. (2020). Calcination of calcium sulphoaluminate cement using pyrite-rich cyanide tailings. *Crystals*, *10*(11), 1–13. https://doi.org/10.3390/cryst10110971

Ecofys. (2009a). Methodology for the free allocation of emission allowances in the EU ETS post 2012. *Sector report for the ceramics industry*.

Ecofys. (2009b). Methodology for the free allocation of emission allowances in the EU ETS post 2012. *Sector report for the glass industry*.

Ecofys. (2009c). Methodology for the free allocation of emission allowances in the EU ETS post 2012. *Sector report for the gypsum industry*.

Ehrenfeld, J. R., & Chertow, M. R. (2002). Industrial symbiosis: the legacy of Kalundborg. In R. U. Ayres & L. W. Ayres (Eds.), *A Handbook of Industrial*

Ecology (pp. 334–348). Edward Elgar Publishing Limited. https://doi.org/10.1162/108819803322564406

Elçi, H. (2016). Utilisation of crushed floor and wall tile wastes as aggregate in concrete production. *Journal of Cleaner Production*, *112*, 742–752. https://doi.org/10.1016/j.jclepro.2015.07.003

Enviros Consulting Ltd. (2003). *Glass Recycling- Life Cycle Carbon Dioxide Emissions* (Issue November). http://www.gpi.org/recycling/glass-recycling-facts

EOTA. (2017a). European Assesment Document EAD 150001-00-0301. *Calcium Sulphoaluminate Based Cement*.

EOTA. (2017b). European Assesment Document EAD 150004-00-0301. *Rapid Hardening Sulfate Resistant Calcium Sulphoaluminate Based Cement.*

EPA. (2002). Environmental Protection Agency. *European Waste Catalogue and Hazardous Waste List - Valid from 1 January 2002.*

Erdoğan, T. Y. (2016). *Beton* (6.Basım). ODTÜ Geliştirme Vakfı Yayıncılık ve İletişim A.Ş.

Erkman, S. (2001). Industrial ecology: A new perspective on the future of the industrial system. *Swiss Medical Weekly*, *131*(37–38), 531–538. https://doi.org/2001/37/smw-09845

European Comission. (2007). Reference Document on Best Available Techniques in the Ceramic Manufacturing Industry. In *European Commission* (Issue August).

European Commission. (2010). *Final Report of the SET-Plan workshop on Technology Innovations for Energy Efficiency and Greenhouse Gas (GHG) emissions reduction in the Iron and Steel Industries in the EU27 up to 2030* (Issue 2).

EVÇED. (2020). T.C. Enerji ve Tabii Kaynaklar Bakanlığı. *2019 Yılı Çimento Sektörü Kıyaslama Raporu*.

Feiz, R., Ammenberg, J., Baas, L., Eklund, M., Helgstrand, A., & Marshall, R. (2015). Improving the CO2 performance of cement, part I: Utilizing life-cycle assessment and key performance indicators to assess development within the cement industry. *Journal of Cleaner Production*, *98*, 272–281. https://doi.org/10.1016/j.jclepro.2014.01.083

FISSAC. (2017). *Lifecycle assessment of new processes , materials and products*.

FISSAC. (2020). http://fissacproject.eu/en/

Flatt, R. J., Roussel, N., & Cheeseman, C. R. (2012). Concrete: An eco material that needs to be improved. *Journal of the European Ceramic Society*, *32*(11), 2787–2798. https://doi.org/10.1016/j.jeurceramsoc.2011.11.012

Font, A., Soriano, L., Monzó, J., Moraes, J. C. B., Borrachero, M. V., & Payá, J. (2020). Salt slag recycled by-products in high insulation alternative environmentally friendly cellular concrete manufacturing. *Construction and Building Materials*, *231*, 117114. https://doi.org/10.1016/j.conbuildmat.2019.117114

Fořt, J., & Černý, R. (2018). Carbon footprint analysis of calcined gypsum production in the Czech Republic. *Journal of Cleaner Production*, *177*, 795–802. https://doi.org/10.1016/j.jclepro.2018.01.002

Fraccascia, L., Albino, V., & Garavelli, C. A. (2017). Technical efficiency measures of industrial symbiosis networks using enterprise input-output analysis. *International Journal of Production Economics*, *183*(August 2015), 273–286. https://doi.org/10.1016/j.ijpe.2016.11.003

Frosch, R. A., & Gallopoulos, N. E. (1989). Strategies for Manufacturing. *Scientific American*, *September*, 144–153.

Fukuda, N. (1961). On the Constitution of Sulfo-Aluminous Clinker. *Bulletin of the Chemical Society of Japan*, *34*(1), 138–139. https://doi.org/10.1246/bcsj.34.138

Galan, I., Beltagui, H., García-Maté, M., Glasser, F. P., & Imbabi, M. S. (2016). Impact of drying on pore structures in ettringite-rich cements. *Cement and Concrete Research*, *84*, 85–94. https://doi.org/10.1016/j.cemconres.2016.03.003

Galan, I., Glasser, F. P., Elhoweris, A., Tully, S., & Murdoch, A. (2014). Novel Process for Calcium Sulfoaluminate Cement Production. *34 Th Cement and Concrete Science Conference*, *September*, 1–4. https://doi.org/10.13140/RG.2.1.3322.3284

Gálvez-Martos, J. L., Valente, A., Martínez-Fernández, M., & Dufour, J. (2020). Eco-efficiency assessment of calcium sulfoaluminate clinker production. *Journal of Industrial Ecology*, *24*(3), 695–706. https://doi.org/10.1111/jiec.12967

Gao, D., Zhang, Z., Meng, Y., Tang, J., & Yang, L. (2021). Effect of flue gas desulfurization gypsum on the properties of calcium sulfoaluminate cement blended with ground granulated blast furnace slag. *Materials*, *14*(2), 1–17. https://doi.org/10.3390/ma14020382

García-Gusano, D., Herrera, I., Garraín, D., Lechón, Y., & Cabal, H. (2015). Life cycle assessment of the Spanish cement industry: Implementation of environmental-friendly solutions. *Clean Technologies and Environmental Policy*, *17*(1), 59–73. https://doi.org/10.1007/s10098-014-0757-0

García-Maté, M. (2014). *Processing and characterisation of calcium sulphoaluminate (CSA) eco-cements with tailored performances.* [Doctoral dissertation, Universidad de Málaga].

García-Maté, M., De La Torre, A. G., León-Reina, L., Losilla, E. R., Aranda, M. A. G., & Santacruz, I. (2015). Effect of calcium sulfate source on the hydration of calcium sulfoaluminate eco-cement. *Cement and Concrete Composites*, *55*, 53–61. https://doi.org/10.1016/j.cemconcomp.2014.08.003

García-Maté, M., Londono-Zuluaga, D., De La Torre, A. G., Losilla, E. R., Cabeza, A., Aranda, M. A. G., & Santacruz, I. (2016). Tailored setting times with high compressive strengths in bassanite calcium sulfoaluminate eco-cements. *Cement and Concrete Composites*, *72*, 39–47. https://doi.org/10.1016/j.cemconcomp.2016.05.021

García-Maté, M., Santacruz, I., De La Torre, Á. G., León-Reina, L., & Aranda, M. A. G. (2012). Rheological and hydration characterization of calcium sulfoaluminate cement pastes. *Cement and Concrete Composites*, *34*(5), 684–691. https://doi.org/10.1016/j.cemconcomp.2012.01.008

Garner, A., & Keoleian, G. A. (1995). Industrial ecology: An introduction. *National Pollution Prevention Center for Higher Education*, *November*, 1–32. https://doi.org/10.4337/9781847202956.00009

Gartner, E. (2004). Industrially interesting approaches to "low-CO2" cements. *Cement and Concrete Research*, *34*(9), 1489–1498. https://doi.org/10.1016/j.cemconres.2004.01.021

Gastaldi, D., Canonico, F., Capelli, L., Bianchi, M., Pace, M., Telesca, A., & Valenti, G. (2011). Hydraulic Behaviour of Calcium Sulfoaluminate Cement alone and in Mixture with Portland Cement. *13th International Congress on the Chemistry of Cement.*, *January*, 1–7.

GB/T 20472-2016. (2006). *Sulphoaluminate cement*.

Gil, A., & Korili, S. A. (2016). Management and valorization of aluminum saline slags: Current status and future trends. *Chemical Engineering Journal*, *289*, 74–84. https://doi.org/10.1016/j.cej.2015.12.069

Glasser, F. P., & Zhang, L. (2001). High-performance cement matrices based on calcium sulfoaluminate-belite compositions. *Cement and Concrete Research*, *31*(12), 1881–1886. https://doi.org/10.1016/S0008-8846(01)00649-4

González, I., Galán, E., Miras, A., & Vázquez, M. A. (2011). CO2 emissions derived from raw materials used in brick factories. Applications to Andalusia (Southern Spain). *Applied Clay Science*, *52*(3), 193–198. https://doi.org/10.1016/j.clay.2011.01.003

Gursel, A. P., Masanet, E., Horvath, A., & Stadel, A. (2014). Life-cycle inventory analysis of concrete production: A critical review. *Cement and Concrete Composites*, *51*, 38–48. https://doi.org/10.1016/j.cemconcomp.2014.03.005

Habert, G., Billard, C., Rossi, P., Chen, C., & Roussel, N. (2010). Cement production technology improvement compared to factor 4 objectives. *Cement and Concrete Research*, *40*(5), 820–826. https://doi.org/10.1016/j.cemconres.2009.09.031

Hagemann, S. E., Gastaldini, A. L. G., Cocco, M., Jahn, S. L., & Terra, L. M. (2019). Synergic effects of the substitution of Portland cement for water treatment plant sludge ash and ground limestone: Technical and economic evaluation. *Journal of Cleaner Production*, *214*, 916–926. https://doi.org/10.1016/j.jclepro.2018.12.324

Haha, M. Ben, Winnefeld, F., & Pisch, A. (2019). Advances in understanding ye'elimite-rich cements. *Cement and Concrete Research*, *123*(February). https://doi.org/10.1016/j.cemconres.2019.105778

Hanein, T., Galvez-Martos, J. L., & Bannerman, M. N. (2018a). Carbon footprint of calcium sulfoaluminate clinker production. *Journal of Cleaner Production*, *172*(November), 2278–2287. https://doi.org/10.1016/j.jclepro.2017.11.183

Hanein, T., Galvez-Martos, J. L., & Bannerman, M. N. (2018b). Carbon footprint of calcium sulfoaluminate clinker production. *Journal of Cleaner Production*, *172*, 2278–2287. https://doi.org/10.1016/j.jclepro.2017.11.183

Hargis, C. W., Lothenbach, B., Müller, C. J., & Winnefeld, F. (2017). Carbonation of calcium sulfoaluminate mortars. *Cement and Concrete Composites*, *80*, 123–134. https://doi.org/10.1016/j.cemconcomp.2017.03.003

Hargis, C. W., Telesca, A., & Monteiro, P. J. M. (2014). Calcium sulfoaluminate (Ye'elimite) hydration in the presence of gypsum, calcite, and vaterite. *Cement and Concrete Research*, *65*, 15–20. https://doi.org/10.1016/j.cemconres.2014.07.004

Hasanbeigi, A., Arens, M., Cardenas, J. C. R., Price, L., & Triolo, R. (2016). Comparison of carbon dioxide emissions intensity of steel production in China, Germany, Mexico, and the United States. *Resources, Conservation and Recycling*, *113*, 127–139. https://doi.org/10.1016/j.resconrec.2016.06.008

Hasanbeigi, A., Price, L., Aden, N., Chunxia, Z., Xiuping, L., & Fangqin, S. (2011). A Comparison of Iron and Steel Production Energy Intensity in China and the U.S. In *Berkeley National Laboratory*. http://eetd.lbl.gov/sites/all/files/publications/lbl-5746e-steel-ei-comparisonjune-2012.pdf

He, H., Guan, H., Zhu, X., & Lee, H. (2017). Assessment on the energy flow and carbon emissions of integrated steelmaking plants. *Energy Reports*, *3*, 29–36. https://doi.org/10.1016/j.egyr.2017.01.001

Hossain, M. U., Poon, C. S., Lo, I. M. C., & Cheng, J. C. P. (2017). Comparative LCA on using waste materials in the cement industry: A Hong Kong case study. *Resources, Conservation and Recycling*, *120*, 199–208. https://doi.org/10.1016/j.resconrec.2016.12.012

Hu, C., Chen, L., Zhang, C., Qi, Y., & Yin, R. (2006). Emission Mitigation of CO2 in Steel Industry: Current Status and Future Scenarios. *Journal of Iron and Steel Research International*, *13*(6), 38–42. https://doi.org/10.1016/S1006-706X(06)60107-6

Hu, P., Li, Y., Zhang, X., Guo, Z., & Zhang, P. (2018). CO2 emission from container glass in China, and emission reduction strategy analysis. *Carbon Management*, *9*(3), 303–310. https://doi.org/10.1080/17583004.2018.1457929

Huang, Y., Pei, Y., Qian, J., Gao, X., Liang, J., Duan, G., Zhao, P., Lu, L., & Cheng, X. (2020). Bauxite free iron rich calcium sulfoaluminate cement: Preparation, hydration and properties. *Construction and Building Materials*, *249*, 118774. https://doi.org/10.1016/j.conbuildmat.2020.118774

Huang, Y., Qian, J., Liu, C., Liu, N., Shen, Y., Ma, Y., Sun, H., & Fan, Y. (2017). Influence of phosphorus impurities on the performances of calcium sulfoaluminate cement. *Construction and Building Materials*, *149*, 37–44. https://doi.org/10.1016/j.conbuildmat.2017.05.028

Huntzinger, D. N., & Eatmon, T. D. (2009). A life-cycle assessment of Portland cement manufacturing: comparing the traditional process with alternative technologies. *Journal of Cleaner Production*, *17*(7), 668–675. https://doi.org/10.1016/j.jclepro.2008.04.007

Iacobescu, R. I., Pontikes, Y., Koumpouri, D., & Angelopoulos, G. N. (2013). Synthesis, characterization and properties of calcium ferroaluminate belite cements produced with electric arc furnace steel slag as raw material. *Cement and Concrete Composites*, *44*, 1–8. https://doi.org/10.1016/j.cemconcomp.2013.08.002

Ioannou, S., Paine, K., & Quillin, K. (2010). Strength and Durability of Calcium Sulfoaluminate Based Concretes. *IC-NOCMAT 2010 International Conference on Non-Conventional Materials and Technologies: Ecological Materials and Technologies for Sustainable Building*, *February*.

Isteri, V., Ohenoja, K., Hanein, T., Kinoshita, H., Illikainen, M., Tanskanen, P., & Fabritius, T. (2021). The Effect of Fluoride and Iron Content on the Clinkering of Alite-Ye'elimite-Ferrite (AYF) Cement Systems. *Frontiers in Built Environment*, *7*(July), 1–12. https://doi.org/10.3389/fbuil.2021.698830

Isteri, V., Ohenoja, K., Hanein, T., Kinoshita, H., Tanskanen, P., Illikainen, M., & Fabritius, T. (2020). Production and properties of ferrite-rich CSAB cement from metallurgical industry residues. *Science of the Total Environment*, *712*(136208). https://doi.org/10.1016/j.scitotenv.2019.136208

Jacobsen, N. B. (2006). Industrial symbiosis in Kalundborg, Denmark. A Quantitative Assessment of Economic and Environmental Aspects. *Journal of Industrial Ecology*, *10*(1–2), 239–255.

Jen, G., Stompinis, N., & Jones, R. (2017). Chloride ingress in a belite-calcium sulfoaluminate cement matrix. *Cement and Concrete Research*, *98*, 130–135. https://doi.org/10.1016/j.cemconres.2017.02.013

Jeong, Y., Hargis, C. W., Chun, S. C., & Moon, J. (2018). The effect of water and gypsum content on strätlingite formation in calcium sulfoaluminate-belite cement pastes. *Construction and Building Materials*, *166*, 712–722. https://doi.org/10.1016/j.conbuildmat.2018.01.153

Johansson, A. (2002). Industrial ecology and industrial metabolism:use and misuse of metaphors. In R. U. Ayres & L. W. Ayres (Eds.), *A Handbook of Industrial Ecology* (pp. 70–75). Edward Elgar Publishing Limited. https://doi.org/10.1162/108819803322564406

Juenger, M. C. G., Winnefeld, F., Provis, J. L., & Ideker, J. H. (2011). Advances in alternative cementitious binders. *Cement and Concrete Research*, *41*(12), 1232–1243. https://doi.org/10.1016/j.cemconres.2010.11.012

Katsioti, M., Tsakiridis, P. E., Agatzini-Leonardou, S., & Oustadakis, P. (2005). Examination of the jarosite-alunite precipitate addition in the raw meal for the production of Portland and sulfoaluminate-based cement clinkers. *International Journal of Mineral Processing*, *76*(4), 217–224. https://doi.org/10.1016/j.minpro.2005.01.007

Kirschen, M., Badr, K., & Pfeifer, H. (2011). Influence of direct reduced iron on the energy balance of the electric arc furnace in steel industry. *Energy*, *36*(10),

6146–6155. https://doi.org/10.1016/j.energy.2011.07.050

Kirschen, M., Risonarta, V., & Pfeifer, H. (2009). Energy efficiency and the influence of gas burners to the energy related carbon dioxide emissions of electric arc furnaces in steel industry. *Energy*, *34*(9), 1065–1072. https://doi.org/10.1016/j.energy.2009.04.015

Kittipongvises, S. (2017). Assessment of environmental impacts of limestone quarrying operations in Thailand. *Environmental and Climate Technologies*, *20*(1), 67–83. https://doi.org/10.1515/rtuect-2017-0011

Klein, A. (1964). Calcium aluminosulfate and expansive cement containing same (Patent No. 3,155,526). In *United States Patent Office* (3,155,526).

Kriskova, L., Pontikes, Y., Cizer, Ö., Malfliet, A., Dijkmans, J., Sels, B., Van Balen, K., & Blanpain, B. (2014). Hydraulic behavior of mechanically and chemically activated synthetic merwinite. *Journal of the American Ceramic Society*, *97*(12), 3973–3981. https://doi.org/10.1111/jace.13221

Lan, W., & Glasser, F. P. (1996). Hydration of calcium sulphoaluminate cements. *Advances in Cement Research*, *8*(31), 127–134. https://doi.org/10.1680/adcr.1996.8.31.127

Li, C., Nie, Z., Cui, S., Gong, X., Wang, Z., & Meng, X. (2014). The life cycle inventory study of cement manufacture in China. *Journal of Cleaner Production*, *72*, 204–211. https://doi.org/10.1016/j.jclepro.2014.02.048

Li, G., Zhang, J., Song, Z., Shi, C., & Zhang, A. (2018). Improvement of workability and early strength of calcium sulphoaluminate cement at various temperature by chemical admixtures. *Construction and Building Materials*, *160*, 427–439. https://doi.org/10.1016/j.conbuildmat.2017.11.076

Liu, G., & Müller, D. B. (2012). Addressing sustainability in the aluminum industry: A critical review of life cycle assessments. *Journal of Cleaner Production*, *35*, 108–117. https://doi.org/10.1016/j.jclepro.2012.05.030

Lowe, E. A., Moran, S. R., & Holmes, D. B. (1996). Fieldbook for the Development of Eco-Industrial Parks. *Indigo Development*, 1–344. http://infohouse.p2ric.org/ref/10/09932.pdf

Lura, P., Winnefeld, F., & Klemm, S. (2010). Simultaneous measurements of heat of hydration and chemical shrinkage on hardening cement pastes. *Journal of Thermal Analysis and Calorimetry*, *101*(3), 925–932. https://doi.org/10.1007/s10973-009-0586-2

Ma, B., Li, X., Mao, Y., & Shen, X. (2013). Synthesis and characterization of high belite sulfoaluminate cement through rich alumina fly ash and desulfurization gypsum. *Ceramics - Silikaty*, *57*(1), 7–13.

Ma, B., Ma, M., Shen, X., Li, X., & Wu, X. (2014). Compatibility between a polycarboxylate superplasticizer and the belite-rich sulfoaluminate cement: Setting time and the hydration properties. *Construction and Building Materials*, *51*, 47–54. https://doi.org/10.1016/J.CONBUILDMAT.2013.10.028

Majling, J., Sahu, S., Vlna, M., & Roy, D. M. (1993). Relationship between raw mixture and mineralogical composition of sulphoaluminate belite clinkers in the system CaOSiO2Al2O3Fe2O3 SO3. *Cement and Concrete Research*, *23*(6), 1351–1356. https://doi.org/10.1016/0008-8846(93)90072-H

Mancio, M., Kirchheim, A. P., & Masuero, A. B. (2011). Use of high-calcium Ladle slag as a partial limestone substitute for clinker manufacturing with reduced CO2 emissions. *XIII ICCC – International Congress on the Chemistry of Cement, 3-8 July*.

Marceau, M. L., Nisbet, M. A., & Vangeem, M. G. (2007). *Life Cycle Inventory of Portland Cement Concrete*. Portland Cement Association.

Marinković, S. B., Malešev, M., & Ignjatović, I. (2013). Life cycle assessment (LCA) of concrete made using recycled concrete or natural aggregates. *Eco-Efficient Construction and Building Materials: Life Cycle Assessment (LCA), Eco-Labelling and Case Studies*, 239–266.

https://doi.org/10.1533/9780857097729.2.239

Marroccoli, M., Montagnaro, F., Pace, M. L., Telesca, A., & Valenti, G. L. (2009). Use of Fluidized Bed Combustion Ash and Other Industrial Wastes as Raw Materials for the Manufacture of Calcium Sulphoaluminate Cements. *Proceedings of the 20th International Conference on Fluidized Bed Combustion*. https://doi.org/10.1007/978-3-642-02682-9

Marroccoli, M., Montagnaro, F., Pace, M. L., Telesca, A., & Valenti, G. L. (2010). Synthesis of calcium sulfoaluminate cements from blends of coal combustion ashes with flue gas desulfurization gypsum. *Processes and Technologies for a Sustainable Energy*. https://doi.org/10.4405/ptse2010.P1.8

Martín-Sedeño, M. C., Cuberos, A. J. M., De la Torre, Á. G., Álvarez-Pinazo, G., Ordónez, L. M., Gateshki, M., & Aranda, M. A. G. (2010). Aluminum-rich belite sulfoaluminate cements: Clinkering and early age hydration. *Cement and Concrete Research*, *40*(3), 359–369. https://doi.org/10.1016/j.cemconres.2009.11.003

Martin, L. H. J., Winnefeld, F., Tschopp, E., Müller, C. J., & Lothenbach, B. (2017). Influence of fly ash on the hydration of calcium sulfoaluminate cement. *Cement and Concrete Research*, *95*, 152–163. https://doi.org/10.1016/j.cemconres.2017.02.030

Martin, M., Svensson, N., & Eklund, M. (2015). Who gets the benefits? An approach for assessing the environmental performance of industrial symbiosis. *Journal of Cleaner Production*, *98*, 263–271. https://doi.org/10.1016/j.jclepro.2013.06.024

Meena, R. V., Jain, J. K., Chouhan, H. S., & Beniwal, A. S. (2022). Use of waste ceramics to produce sustainable concrete: A review. *Cleaner Materials*, *4*(January), 100085. https://doi.org/10.1016/j.clema.2022.100085

Mehta, P. K. (1973). Mechanism of expansion associated with ettringite formation. *Cement and Concrete Research, 3*(1), 1–6. https://doi.org/10.1016/0008-8846(73)90056-2

Mehta, P. K. (2002). Greening of the Concrete Industry for Sustainable Development. *Concrete International, 24(7),* 23-28.

Mehta, P. K., & Monteiro, P. J. M. (2006). *Concrete: microstructure, properties, and materials* (3rd ed.). McGraw-Hill Education.

Mezquita, A., Boix, J., Monfort, E., & Mallol, G. (2014). Energy saving in ceramic tile kilns: Cooling gas heat recovery. *Applied Thermal Engineering*, *65*(1–2), 102–110. https://doi.org/10.1016/j.applthermaleng.2014.01.002

Mirata, M. (2004). Experiences from early stages of a national industrial symbiosis programme in the UK: Determinants and coordination challenges. *Journal of Cleaner Production*, *12*(8–10), 967–983. https://doi.org/10.1016/j.jclepro.2004.02.031

Mirata, M., & Emtairah, T. (2005). Industrial symbiosis networks and the contribution to environmental innovation: The case of the Landskrona industrial symbiosis programme. *Journal of Cleaner Production*, *13*(10–11), 993–1002. https://doi.org/10.1016/j.jclepro.2004.12.010

Monfort, E., Mezquita, A., Granel, R., Vaquer, E., Miralles, A., & Zaera, V. (2008). Analysis of the energy consumption and production of ceramic tile. *Qualicer 10*.

Morales, E. M., Diemer, A., Cervantes, G., & Carrillo-González, G. (2019). "By-product synergy" changes in the industrial symbiosis dynamics at the Altamira-Tampico industrial corridor: 20 Years of industrial ecology in Mexico. *Resources, Conservation and Recycling*, *140*, 235–245. https://doi.org/10.1016/j.resconrec.2018.09.026

Murri, A. N., Rickard, W. D. A., Bignozzi, M. C., & van Riessen, A. (2013). High temperature behaviour of ambient cured alkali-activated materials based on ladle slag. *Cement and Concrete Research*, *43*, 51–61. https://doi.org/10.1016/j.cemconres.2012.09.011

Neves, A., Godina, R., Azevedo, S. G., Pimentel, C., & Matias, J. C. O. (2019). The Potential of Industrial Symbiosis: Case Analysis and Main Drivers and Barriers to Its Implementation. *Sustainability (Switzerland)*, *11*(24), 1–68. https://doi.org/10.3390/su11247095

Nguyen, H., Adesanya, E., Ohenoja, K., Kriskova, L., Pontikes, Y., Kinnunen, P., & Illikainen, M. (2019). Byproduct-based ettringite binder – A synergy between ladle slag and gypsum. *Construction and Building Materials*, *197*, 143–151. https://doi.org/10.1016/j.conbuildmat.2018.11.165

Nidheesh, P. V., & Kumar, M. S. (2019). An overview of environmental sustainability in cement and steel production. *Journal of Cleaner Production*, *231*, 856–871. https://doi.org/10.1016/j.jclepro.2019.05.251

Odler, I. (2000). *Special Inorganic Cements*. E & FN Spon, London and New York.

OECD/IEA. (2007). *Tracking Industrial Energy Efficiency and CO2 emissions*. International Energy Agency.

Osama, A., & Soliman, F. (2016). *Industrial Energy Efficiency Benchmarking Report of the Ceramics Sector*.

Pace, M. L., Telesca, A., Marroccoli, M., & Valenti, G. L. (2011). Use of industrial byproducts as alumina sources for the synthesis of calcium sulfoaluminate cements. *Environmental Science and Technology*, *45*(14), 6124–6128. https://doi.org/10.1021/es2005144

Padilla-Encinas, P., Palomo, A., Blanco-Varela, M. T., & Fernández-Jiménez, A. (2020). Calcium sulfoaluminate clinker hydration at different alkali concentrations. *Cement and Concrete Research*, *138*(September).

https://doi.org/10.1016/j.cemconres.2020.106251

Padilla, I., Romero, M., López-Andrés, S., & López-Delgado, A. (2022). Sustainable Management of Salt Slag. *Sustainability*, 1–13.

Pajares, I., De la Torre, Á. G., Martínez-Ramírez, S., Puertas, F., Blanco-Varela, M.-T., & Aranda, M. A. G. (2002). Quantitative analysis of mineralized white Portland clinkers: The structure of Fluorellestadite. *Powder Diffraction*, *17*(4), 281–286. https://doi.org/10.1154/1.1505045

Papadogeorgos, I., & Schure, K. M. (2019). *Decarbonisation Options for the Dutch Container and Tableware Glass Industry*. PBL Netherlands Environmental Assessment Agency.

Pardo, N., Moya, J. A., & Vatopoulos, K. (2012). *Prospective Scenarios on Energy Efficiency and CO2 Emissions in the EU Iron & Steel Industry*. https://doi.org/10.2790/64264

Park, S. B., Lee, B. C., & Kim, J. H. (2004). Studies on mechanical properties of concrete containing waste glass aggregate. *Cement and Concrete Research*, *34*, 2181–2189. https://doi.org/10.1016/j.cemconres.2004.02.006

Paul, G., Boccaleri, E., Marchese, L., Buzzi, L., Canonico, F., & Gastaldi, D. (2021). Low temperature sulfoaluminate clinkers: The role of sulfates and silicates on the different hydration behavior. *Construction and Building Materials*, *268*, 121111. https://doi.org/10.1016/j.conbuildmat.2020.121111

Pelletier-Chaignat, L., Winnefeld, F., Lothenbach, B., Saout, G. Le, Müller, C. J., & Famy, C. (2011). Influence of the calcium sulphate source on the hydration mechanism of Portland cement-calcium sulphoaluminate clinker-calcium sulphate binders. *Cement and Concrete Composites*, *33*(5), 551–561. https://doi.org/10.1016/j.cemconcomp.2011.03.005

Pelletier, L., Winnefeld, F., & Lothenbach, B. (2010). The ternary system Portland cement-calcium sulphoaluminate clinker-anhydrite: Hydration mechanism and

mortar properties. *Cement and Concrete Composites*, *32*(7), 497–507. https://doi.org/10.1016/j.cemconcomp.2010.03.010

Péra, J., & Ambroise, J. (2004). New applications of calcium sulfoaluminate cement. *Cement and Concrete Research*, *34*(4), 671–676. https://doi.org/10.1016/j.cemconres.2003.10.019

Pereira, E. J. da S., Pinho, J. T., Galhardo, M. A. B., & Macêdo, W. N. (2014). Methodology of risk analysis by Monte Carlo Method applied to power generation with renewable energy. *Renewable Energy*, *69*, 347–355. https://doi.org/10.1016/j.renene.2014.03.054

Petríková, K., Borseková, K., & Blam, I. (2016). Industrial symbiosis in European policy: overview of recent progress. *Acta Universitatis Lodziensis. Folia Oeconomica*, *2*(320). https://doi.org/10.18778/0208-6018.320.07

Platon, V., & Constantinescu, A. (2014). Monte Carlo Method in Risk Analysis for Investment Projects. *Procedia Economics and Finance*, *15*(14), 393–400. https://doi.org/10.1016/s2212-5671(14)00463-8

Pöllman, H. (2002). Composition of cement phases. In J. Bensted & P. Barnes (Eds.), *Structure and Performance of Cements* (2nd ed., pp. 25–56). Spon Press.

Poyraz, M., & Yılmaz, Z. (2018). Seramik karo sektöründe sürdürülebilirlik ve geri dönüşüm. *Sanat & Tasarım Dergisi*, 256–270.

Price, L., Phylipsen, D., & Worrell, E. (2001). *Energy Use and Carbon Dioxide Emissions in the Steel Sector in Key Developing Countries* (Issue April).

Qian, G., Li, A., Xu, G., & Li, H. (1997). Hydrothermal products of the C3MS2-C12A7-MgO System. *Cement and Concrete Research*, *27*(12), 1791–1797.

Quillin, K. (2001). Performance of belite-sulfoaluminate cements. *Cement and Concrete Research*, *31*(9), 1341–1349. https://doi.org/10.1016/S0008-8846(01)00543-9

Raychaudhuri, S. (2008). Introduction to monte carlo simulation. *Proceedings of the 2008 Winter Simulation Conference, IEEE,* 91–100.

Rebitzer, G., Ekvall, T., Frischknecht, R., Hunkeler, D., Norris, G., Rydberg, T., Schmidt, W. P., Suh, S., Weidema, B. P., & Pennington, D. W. (2004). Life cycle assessment Part 1: Framework, goal and scope definition, inventory analysis, and applications. *Environment International*, *30*(5), 701–720. https://doi.org/10.1016/j.envint.2003.11.005

Renner, G. T. (1947). Geography of Industrial Localization. *Economic Geography*, *23*(3), 167. https://doi.org/10.2307/141510

Rouse, R. C., & Dunn, P. J. (1982). A contribution to the crystal chemistry of ellestadite and the silicate sulfate apatites. *American Mineralogist*, *67*, 90–96.

Rue, D. M., Servaites, J., & Wolf, W. (2007). *Industrial Glass Bandwidth Analysis Final Report* (Issue August).

Safiuddin, M., Jumaat, M. Z., Salam, M. A., Islam, M. S., & Hashim, R. (2010). Utilization of solid wastes in construction materials. *International Journal of Physical Sciences*, *5*(13), 1952–1963.

Salas, D. A., Ramirez, A. D., Rodríguez, C. R., Petroche, D. M., Boero, A. J., & Duque-Rivera, J. (2016). Environmental impacts, life cycle assessment and potential improvement measures for cement production: A literature review. *Journal of Cleaner Production*, *113*, 114–122. https://doi.org/10.1016/j.jclepro.2015.11.078

Sánchez de Rojas, M. I., Frías, M., Rodríguez, O., Ferreira, S. R., & Olmeda, J. (2009). Waste clay materials as pozzolanic additions. *1st Spanish National Conference on Advances in Materials Recycling and Eco – Energy*, *12-13 November2009*.

Sandberg, H., Lagneborg, R., Lindblad, B., Axelsson, H., & Bentell, L. (2001). CO2 emissions of the Swedish steel industry. *Scandinavian Journal of Metallurgy*,

30(6), 420–425. https://doi.org/10.1034/j.1600-0692.2001.300611.x

Schmitz, A., Kamiński, J., Maria Scalet, B., & Soria, A. (2011). Energy consumption and CO2 emissions of the European glass industry. *Energy Policy*, *39*, 142–155. https://doi.org/10.1016/j.enpol.2010.09.022

Schwarz, E. J., & Steininger, K. W. (1997). Implementing nature's lesson: The industrial recycling network enhancing regional development. *Journal of Cleaner Production*, *5*(1–2), 47–56. https://doi.org/10.1016/s0959-6526(97)00009-7

Scrivener, K., Snellings, R., & Lothenbach, B. (Eds. . (2016). *A Practical Guide to Microstructural Anaysis of Cementitious Materials*. CRC Press Taylor & Francis Group.

Senff, L., Castela, A., Hajjaji, W., Hotza, D., & Labrincha, J. A. (2011). Formulations of sulfobelite cement through design of experiments. *Construction and Building Materials*, *25*(8), 3410–3416. https://doi.org/10.1016/j.conbuildmat.2011.03.032

Şenlier, N., & Albayrak, A. N. (2011). Opportunities for Sustainable Industrial Development in Turkey: Eco-Industrial Parks. *Gazi University Journal of Science*, *24*(3), 637–646.

Serjun, V. Z., Mladenovič, A., Mirtič, B., Meden, A., Ščančar, J., & Milačič, R. (2015). Recycling of ladle slag in cement composites: Environmental impacts. *Waste Management*, *43*, 376–385. https://doi.org/10.1016/j.wasman.2015.05.006

Shao, Y., Lefort, T., Moras, S., & Rodriguez, D. (2000). Studies on concrete containing ground waste glass. *Cement and Concrete Research*, *30*, 91–100. https://doi.org/10.1109/ISFEE.2014.7050543

Sharp, J. H., Lawrence, C. D., & Yang, R. (1999). Calcium sulfoaluminate cements—low-energy cements, special cements or what? *Advances in Cement*

Research, *11*(1), 3–13. https://doi.org/10.1680/adcr.1999.11.1.3

Sherman, N., Beretka, J., Santoro, L., & Valenti, G. L. (1995). Long-term behaviour of hydraulic binders based on calcium sulfoaluminate and calcium sulfosilicate. *Cement and Concrete Research*, *25*(1), 113–126. https://doi.org/10.1016/0008-8846(94)00119-J

Shi, C., & Hu, S. (2003). Cementitious properties of ladle slag fines under autoclave curing conditions. *Cement and Concrete Research*, *33*, 1851–1856. https://doi.org/10.1016/S0008-8846(03)00211-4

Shi, C., Jiménez, A. F., & Palomo, A. (2011). New cements for the 21st century: The pursuit of an alternative to Portland cement. *Cement and Concrete Research*, *41*(7), 750–763. https://doi.org/10.1016/J.CEMCONRES.2011.03.016

Sinton, C. W. (2004). Glass and Energy. *Encyclopedia of Energy*, *3*, 1–10.

Skaf, M., Ortega-López, V., Fuente-Alonso, J. A., Santamaría, A., & Manso, J. M. (2016). Ladle furnace slag in asphalt mixes. *Construction and Building Materials*, *122*, 488–495. https://doi.org/10.1016/j.conbuildmat.2016.06.085

Snellings, R. (2016). X-ray powder diffraction applied to cement. In K. Scrivener, R. Snellings, & B. Lothenbach (Eds.), *A practical guide to microstructural analysis of cementitious materials* (pp. 108–176). CRC Press.

Song, F., Yu, Z., Yang, F., Lu, Y., & Liu, Y. (2015). Microstructure of amorphous aluminum hydroxide in belite-calcium sulfoaluminate cement. *Cement and Concrete Research*, *71*, 1–6. https://doi.org/10.1016/j.cemconres.2015.01.013

Taylor, H. F. W. (1997). *Cement chemistry* (2nd ed.). Thomas Telford Publishing.

Telesca, A., Marroccoli, M., Pace, M. L., Tomasulo, M., Valenti, G. L., & Monteiro, P. J. M. (2014). A hydration study of various calcium sulfoaluminate cements. *Cement and Concrete Composites*, *53*, 224–232. https://doi.org/10.1016/j.cemconcomp.2014.07.002

Telesca, A., Marroccoli, M., Pace, M. L., Tomasulo, M., Valenti, G. L., & Naik, T. R. (2013). Expansive and non-expansive calcium sulfoaluminate-based cements. *Third International Conference on Sustainable Construction Materials and Technologies*, *3*(1).

Telesca, A., Matschei, T., & Marroccoli, M. (2020). Study of eco-friendly belite-calcium sulfoaluminate cements obtained from special wastes. *Applied Sciences*, *10*(23), 1–14. https://doi.org/10.3390/app10238650

Telesca, A., Winnefeld, F., & Marroccoli, M. (2019). Synthesis and characterisation of calcium sulfoaluminate cements produced by different chemical gypsums. *Advances in Cement Research*, *31*(3), 113–123. https://doi.org/10.1680/jadcr.18.00122

Testa, M., Malandrino, O., Sessa, M. R., Supino, S., & Sica, D. (2017). Long-term sustainability from the perspective of cullet recycling in the container glass industry: Evidence from Italy. *Sustainability*, *9*(10). https://doi.org/10.3390/su9101752

Thomas, R. J., Maguire, M., Sorensen, A. D., & Quezada, I. (2018). Calcium Sulfoaluminate Cement: Benefits and Applications. *Concrete International*, *40*(4), 65–69.

Tikul, N. (2014). Assessing environmental impact of small and medium ceramic tile manufacturing enterprises in Thailand. *Journal of Manufacturing Systems*, *33*(1), 1–6. https://doi.org/10.1016/j.jmsy.2013.12.002

Tokyay, M. (2016). *Cement and concrete mineral admixtures*. CRC Press.

Tolaymat, T., & Huang, X. L. (2015). Secondary Aluminum Processing Waste: Salt Cake Characterization and Reactivity. In *National Risk Management Research Laboratory, Office of Research and Development, US Environmental Protection Agency, USEPA, Washington*.

Trauchessec, R., Mechling, J. M., Lecomte, A., Roux, A., & Le Rolland, B. (2014). Impact of anhydrite proportion in a calcium sulfoaluminate cement and Portland cement blend. *Advances in Cement Research*, *26*(6), 325–333. https://doi.org/10.1680/adcr.13.00051

Trauchessec, R., Mechling, J. M., Lecomte, A., Roux, A., & Le Rolland, B. (2015). Hydration of ordinary Portland cement and calcium sulfoaluminate cement blends. *Cement and Concrete Composites*, *56*, 106–114. https://doi.org/10.1016/j.cemconcomp.2014.11.005

Tsakiridis, P. E. (2012). Aluminium salt slag characterization and utilization - A review. *Journal of Hazardous Materials*, *217–218*, 1–10. https://doi.org/10.1016/j.jhazmat.2012.03.052

Tsubota, M., & Kitagawa, J. (2017). A necessary criterion for obtaining accurate lattice parameters by Rietveld method. *Scientific Reports*, *7*(15831). https://doi.org/10.1038/s41598-017-15766-y

Ukrainczyk, N., Franković Mihelj, N., & Šipušić, J. (2013). Calcium sulfoaluminate eco-cement from industrial waste. *Chemical and Biochemical Engineering Quarterly*, *27*(1), 83–93.

Van Den Heede, P., & De Belie, N. (2012). Environmental impact and life cycle assessment (LCA) of traditional and “green” concretes: Literature review and theoretical calculations. *Cement and Concrete Composites*, *34*(4), 431–442. https://doi.org/10.1016/j.cemconcomp.2012.01.004

Verguts, V., Dessein, J., Dewulf, A., Lauwers, L., Werkman, R., & Termeer, C. J. A. M. (2016). Industrial symbiosis as sustainable development strategy: Adding a change perspective. *International Journal of Sustainable Development*, *19*(1), 15–35. https://doi.org/10.1504/IJSD.2016.073650

Vilaplana, A. S., Ferreira, V. J., López-Sabirón, A. M., Aranda-Usón, A., Lausín-González, C., Berganza-Conde, C., & Ferreira, G. (2015). Utilization of Ladle Furnace slag from a steelwork for laboratory scale production of Portland

cement. *Construction and Building Materials*, *94*, 837–843. https://doi.org/10.1016/j.conbuildmat.2015.07.075

Vlček, J., Švrčinová, R., Burda, J., Topinková, M., Klárová, M., Ovčačíková, H., Jančar, D., & Velička, M. (2016). Hydraulic properties of ladle slags. *Metalurgija*, *55*(3), 399–402.

Wang, K., Wang, C., Lu, X., & Chen, J. (2007). Scenario analysis on CO2 emissions reduction potential in China's iron and steel industry. *Energy Policy*, *35*(4), 2320–2335. https://doi.org/10.1016/j.enpol.2006.08.007

Wang, Q., Yan, P., & Feng, J. (2011). A discussion on improving hydration activity of steel slag by altering its mineral compositions. *Journal of Hazardous Materials*, *186*(2–3), 1070–1075. https://doi.org/10.1016/j.jhazmat.2010.11.109

WBCSD. (2019). *Global Cement Database on CO2 and Energy Information – Getting the Numbers Right (GNR)*. https://gccassociation.org/sustainability-innovation/gnr-gcca-in-numbers/

Winnefeld, F., & Barlag, S. (2009). Influence of calcium sulfate and calcium hydroxide on the hydration of calcium sulfoaluminate clinker. *ZKG International*, *62*(12), 42–53.

Winnefeld, F., & Barlag, S. (2010). Calorimetric and thermogravimetric study on the influence of calcium sulfate on the hydration of ye'elimite. *Journal of Thermal Analysis and Calorimetry*, *101*(3), 949–957. https://doi.org/10.1007/s10973-009-0582-6

Winnefeld, F., & Lothenbach, B. (2010). Hydration of calcium sulfoaluminate cements - Experimental findings and thermodynamic modelling. *Cement and Concrete Research*, *40*(8), 1239–1247. https://doi.org/10.1016/j.cemconres.2009.08.014

WSP, P. B., & DNV.GL. (2015). *Industrial Decarbonisation & Energy Efficiency Roadmaps to 2050-Glass* (Issue March).

Wu, S., Wang, W., Ren, C., Yao, X., Yao, Y., Zhang, Q., & Li, Z. (2019). Calcination of calcium sulphoaluminate cement using flue gas desulfurization gypsum as whole calcium oxide source. *Construction and Building Materials*, *228*, 116676. https://doi.org/10.1016/j.conbuildmat.2019.116676

Xu, D., Cui, Y., Li, H., Yang, K., Xu, W., & Chen, Y. (2015). On the future of Chinese cement industry. *Cement and Concrete Research*, *78*, 2–13. https://doi.org/10.1016/j.cemconres.2015.06.012

Yellishetty, M., Mudd, G. M., Ranjith, P. G., & Tharumarajah, A. (2011). Environmental life-cycle comparisons of steel production and recycling: Sustainability issues, problems and prospects. *Environmental Science and Policy*, *14*(6), 650–663. https://doi.org/10.1016/j.envsci.2011.04.008

Yoldi, M., Fuentes-Ordoñez, E. G., Korili, S. A., & Gil, A. (2019). Efficient recovery of aluminum from saline slag wastes. *Minerals Engineering*, *140*(105884). https://doi.org/10.1016/j.mineng.2019.105884

Zajac, M., Skocek, J., Bullerjahn, F., & Ben Haha, M. (2016). Effect of retarders on the early hydration of calcium-sulpho-aluminate (CSA) type cements. *Cement and Concrete Research*, *84*, 62–75. https://doi.org/10.1016/j.cemconres.2016.02.014

Zhang. L (2000). *Microstructure and Performance of Calcium Sulfoaluminate Cements* (Issue June). [Doctoral dissertation, University of Aberdeen].

Zhang, L., & Glasser, F. P. (2002). Hydration of calcium sulfoaluminate cement at less than 24 h. *Advances in Cement Research*, *14*(4), 141–155. https://doi.org/10.1680/adcr.2002.14.4.141

Zhang, L., & Glasser, F. P. (2005). Investigation of the microstructure and carbonation of C$\bar{S}$A-based concretes removed from service. *Cement and*

Concrete Research, *35*(12), 2252–2260. https://doi.org/10.1016/j.cemconres.2004.08.007

Zhang, L., Su, M., & Wang, Y. (1999). Development of the use of sulfo- and ferroaluminate cements in China. *Advances in Cement Research*, *11*(1), 15–21. https://doi.org/10.1680/adcr.1999.11.1.15

Zhang, Su, M., & Wang, Y. (1999). Development of the use of sulfo- and ferroaluminate cements in China. *Advances in Cement Research*, *11*(1), 15–21. https://doi.org/10.1680/adcr.1999.11.1.15

Zhang, Y., Zheng, H., Chen, B., Su, M., & Liu, G. (2015). A review of industrial symbiosis research: theory and methodology. *Frontiers of Earth Science*, *9*(1), 91–104. https://doi.org/10.1007/s11707-014-0445-8

Zhou, Q., Milestone, N. B., & Hayes, M. (2006). An alternative to Portland Cement for waste encapsulation-The calcium sulfoaluminate cement system. *Journal of Hazardous Materials*, *136*(1 SPEC. ISS.), 120–129. https://doi.org/10.1016/j.jhazmat.2005.11.038

Zimbili, O., Salim, W., & Ndambuki, M. (2014). A Review on the Usage of Ceramic Wastes in Concrete Production. *International Scholarly and Scientific Research & Innovation*, *8*(1), 91–95.

Živica, V. (2000). Properties of blended sulfoaluminate belite cement. *Construction and Building Materials*, *14*(8), 433–437. https://doi.org/10.1016/S0950-0618(00)00050-7

APPENDICES

A. XRD Patterns

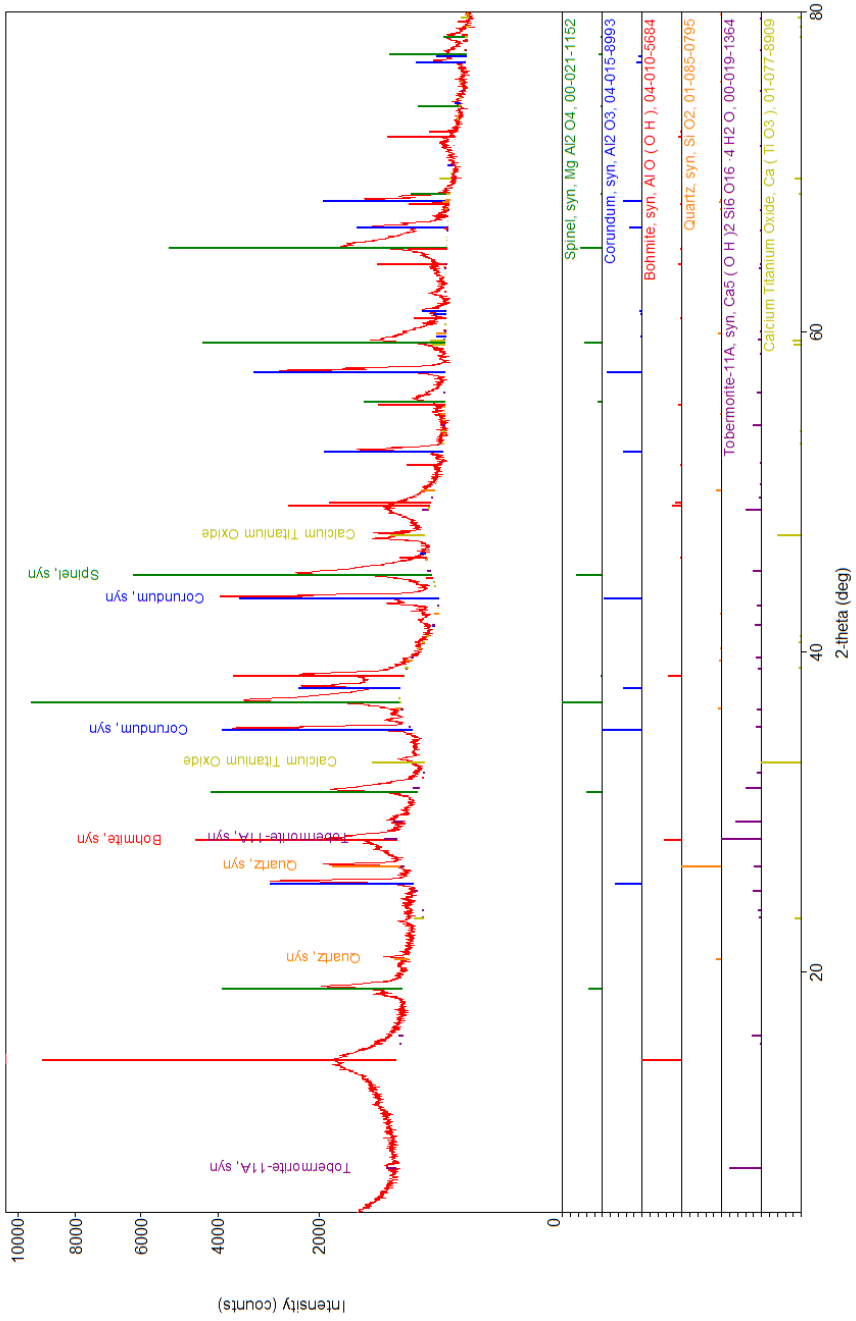

Figure A.1 XRD pattern of Serox

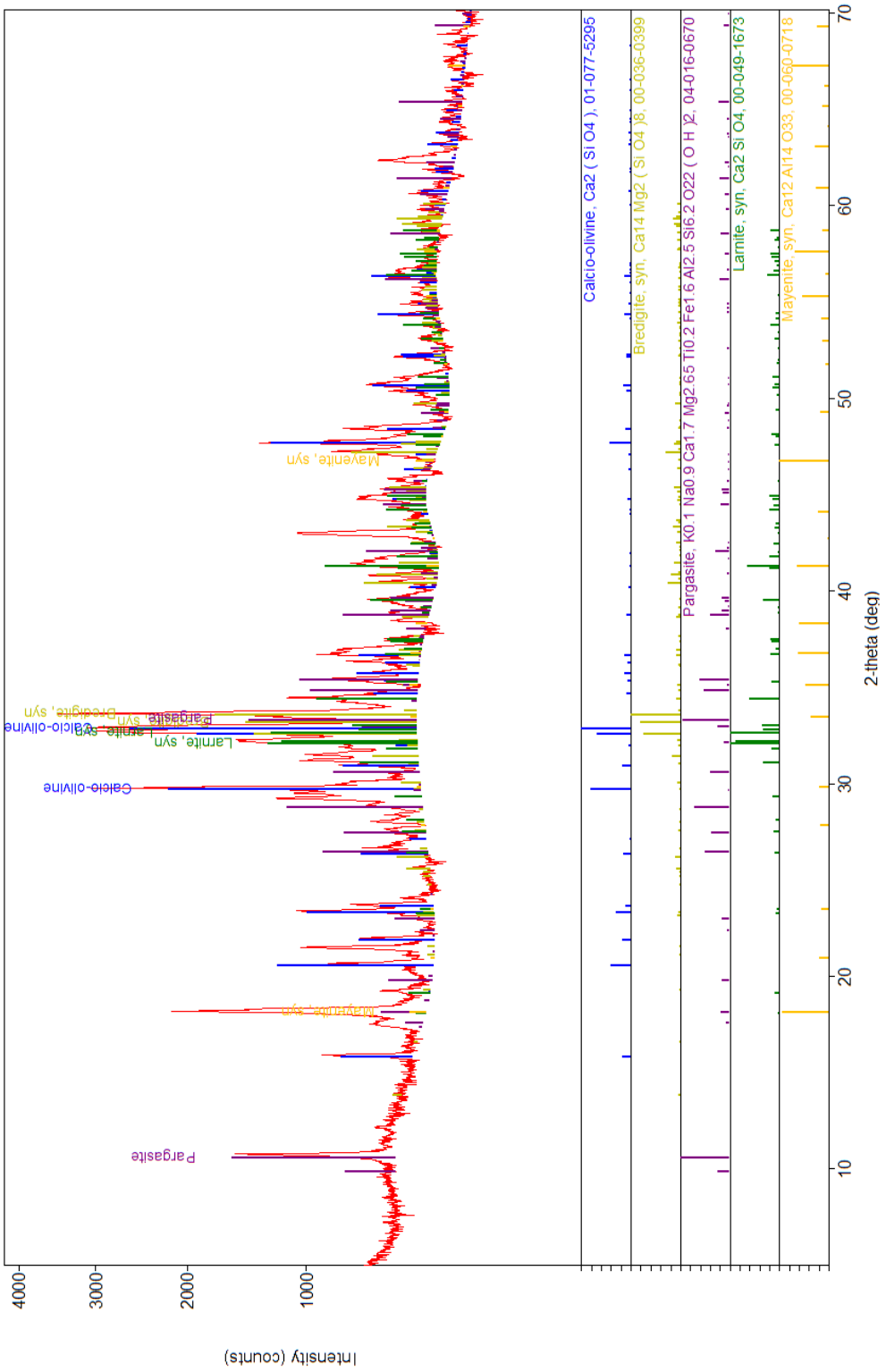

Figure A.2 XRD pattern of LFS

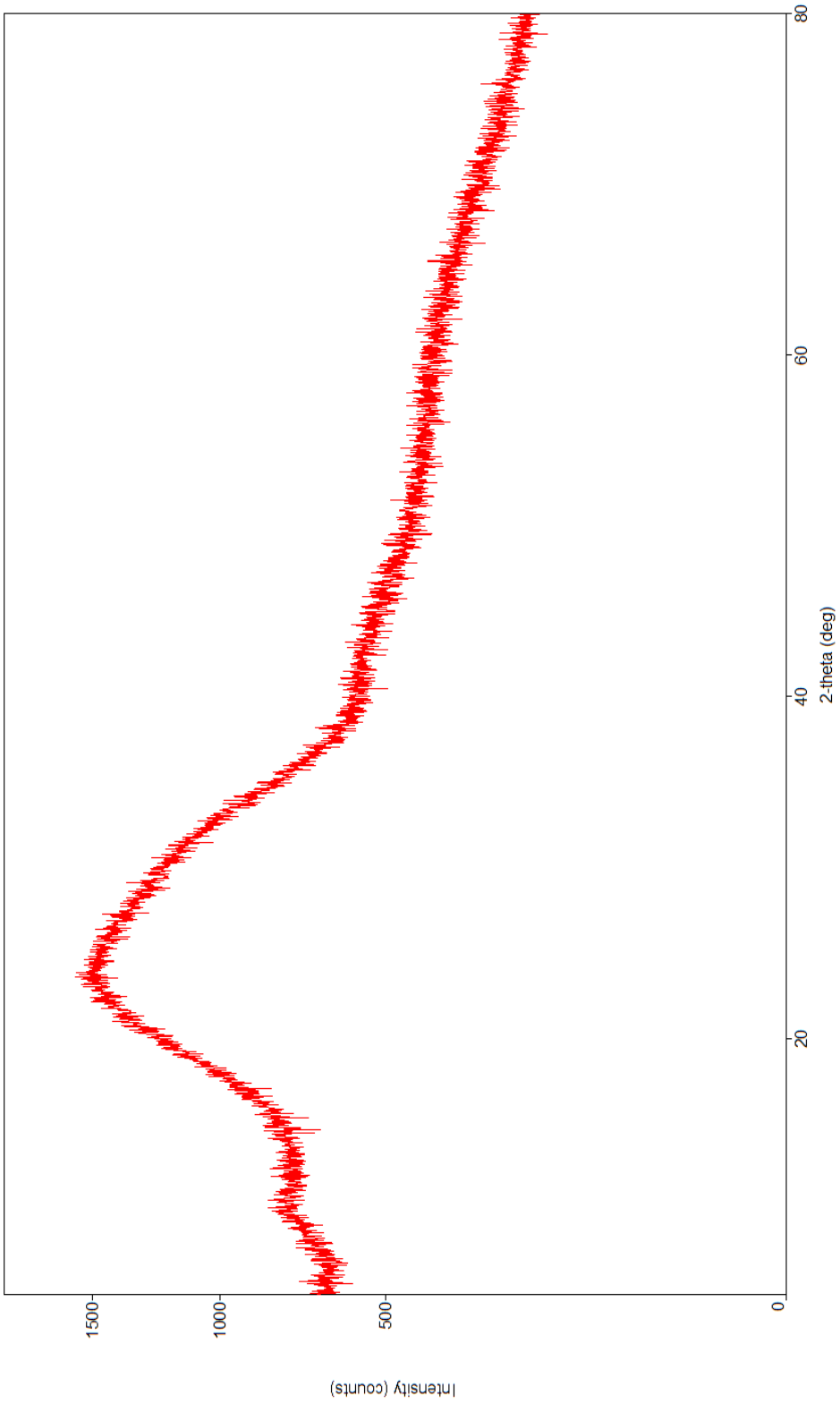

Figure A.3 XRD pattern of glass waste

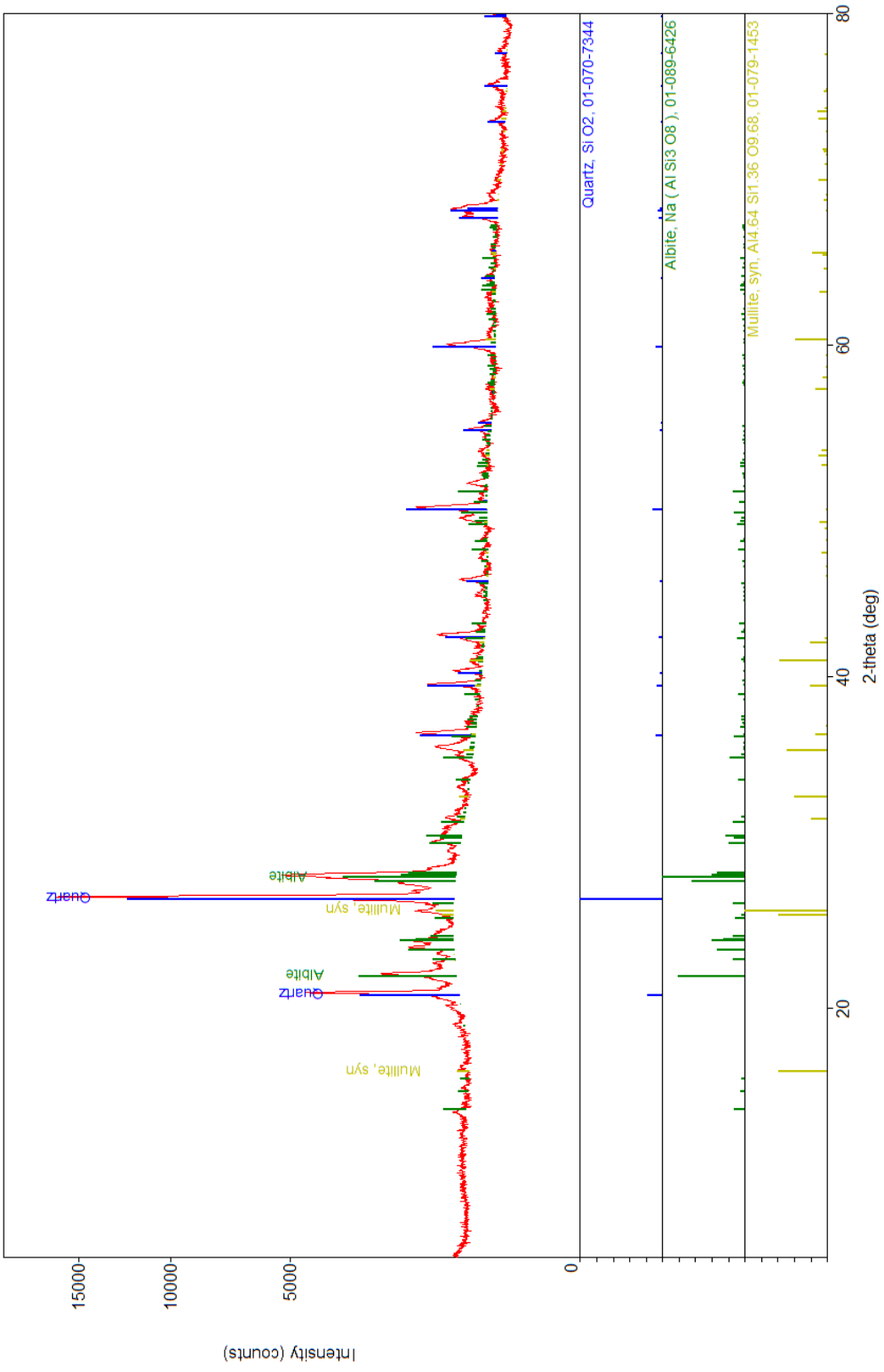

Figure A.4 XRD pattern of ceramic waste

CURRICULUM VITAE

Surname, Name: Tangüler Bayramtan, Meltem

EDUCATION

Degree	Institution	Year of Graduation
MS	METU Civil Engineering	2015
BS	Cukurova University Civil Engineering	2010
High School	Ismail Safa Ozler Anatolian High School, Adana	2005

FOREIGN LANGUAGES

Advanced English

PUBLICATIONS

Journal

1. Tanguler-Bayramtan M., Alam B, Sucu M., Delibas T. and Yaman I.O. "Cement and Hydroxyethyl Methyl Cellulose Interaction: The Performance of Cement-Based Adhesives", Materials and Structures, 55(3), 1-15 (2022)

2. Tanguler-Bayramtan M., Yaman I.O. "Calcium Sulfoaluminate Cement: State of the Art Review", Cement and Concrete World, 132, 72-78 (2018)

International Conferences

1. Tanguler M., Meral C. and Aslam I. "Early-Age Performance of Binary Fly Ash-Portland Cement Blends", Eurasia 2014 Waste Management Symposium, April 28-30 2014, Istanbul, Turkey

2. Tanguler M., Meral C. and Gursel P. "Merging Early Age Mechanical Performance of Turkish Fly Ash-Portland Cement Mortars to Their Environmental Performance", 11th International Congress on Advances in Civil Enginering (ACE), October 21-25 2014, Istanbul, Turkey

3. Seyedian Choubi S., Meral C., Akbas Y.S. and Tanguler-Bayramtan M. "A Comparative Study of Alkali-Activated Fly Ashes under Heat-Exposure", 4th International Conference on Sustainability Construction Materials and Technologies (SCMT 4), August 7-11 2016, Las Vegas, USA

4. Seyedian Choubi S., Meral C. and Tanguler-Bayramtan M. "Alkali-Activation Performance of Fly Ashes from Thermal Power Plants Utilizing Güney Ege Lignite Coal Reserve", 12th International Congress on Advances in Civil Enginering (ACE), September 21-23 2016, Istanbul, Turkey

5. Tanguler-Bayramtan M., Ustoglu C., Alam B., Sucu M. and Yaman I.O. "Effects of Different Cellulose Ethers on White Cement Based Ceramic Adhesives", 13th International Congress on Advances in Civil Enginering (ACE), September 12-14 2018, İzmir, Turkey

National Conferences

1. Tanguler M., Alam B. and Yaman I.O. "Farklı Kalıp Ayırıcılarının Beton Yüzey Özelliklerine Etkisi", Uluslararası Katılımlı Yapılarda Kimyasal Katkılar 4. Sempozyumu ve Sergisi, 24-25 Ekim 2013, Ankara, Turkey

2. Tanguler M., Gursel P. and Meral C. "Türkiye'de Uçucu Küllü Betonlar için Yaşam Döngüsü Analizi", 9. Ulusal Beton Kongresi, 16-18 Nisan 2015, Antalya, Turkey

Others

1. IMO Yapı Malzemeleri Komisyonu, Tanguler M. "Yapı Denetim Sistemi Kapsamında Elde Edilen Beton Basınç Dayanımı Sonuçlarına Dair Bir İrdeleme", Türkiye Mühendislik Haberleri, 480, 1 (2014)

2. IMO Yapı Malzemeleri Komisyonu, Tanguler M. "Yapı Denetim Sistemi Kapsamında Elde Edilen Çelik Çekme Deney Sonuçlarına Dair Bir İrdeleme", Türkiye Mühendislik Haberleri, 481, 2 (2014)